

# The consolidated European synthesis of CH<sub>4</sub> and N<sub>2</sub>O emissions for EU27 and UK: 1990-2019

Ana Maria Roxana Petrescu<sup>1</sup>, Chunjing Qiu<sup>2</sup>, Matthew J. McGrath<sup>2</sup>, Philippe Peylin<sup>2</sup>, Glen P. Peters<sup>3</sup>,  
Philippe Ciais<sup>2</sup>, Rona L. Thompson<sup>4</sup>, Aki Tsuruta<sup>5</sup>, Dominik Brunner<sup>6</sup>, Matthias Kuhnert<sup>7</sup>, Bradley  
Matthews<sup>8</sup>, Paul I. Palmer<sup>9</sup>, Oksana Tarasova<sup>10</sup>, Pierre Regnier<sup>11</sup>, Ronny Lauerwald<sup>12</sup>, David Bastviken<sup>13</sup>,  
Lena Höglund-Isaksson<sup>14</sup>, Wilfried Winiwarter<sup>14,15</sup>, Giuseppe Etiope<sup>16</sup>, Tuula Aalto<sup>5</sup>, Gianpaolo Balsamo<sup>17</sup>,  
Vladislav Bastrikov<sup>18</sup>, Antoine Berchet<sup>2</sup>, Patrick Brockmann<sup>2</sup>, Giancarlo Ciotoli<sup>19</sup>, Giulia Conchedda<sup>20</sup>,  
Monica Crippa<sup>21</sup>, Frank Dentener<sup>21</sup>, Christine D. Groot Zwaaftink<sup>4</sup>, Diego Guizzardi<sup>21</sup>, Dirk Günther<sup>22</sup>,  
Jean-Matthieu Haussaire<sup>6</sup>, Sander Houweling<sup>1</sup>, Greet Janssens-Maenhout<sup>21</sup>, Massae Kouyate<sup>2</sup>, Adrian  
Leip<sup>21,\*</sup>, Antti Leppänen<sup>23</sup>, Emanuele Lugato<sup>21</sup>, Manon Maisonnier<sup>11</sup>, Alistair J. Manning<sup>24</sup>, Tiina  
Markkanen<sup>5</sup>, Joe McNorton<sup>17</sup>, Marilena Muntean<sup>21</sup>, Gabriel D. Oreggioni<sup>(ex)21</sup>, Prabir K. Patra<sup>25</sup>, Lucia  
Perugini<sup>26</sup>, Isabelle Pison<sup>2</sup>, Maarit T. Raivonen<sup>23</sup>, Marielle Saunois<sup>2</sup>, Arjo J. Segers<sup>27</sup>, Pete Smith<sup>7</sup>, Efisio  
Solazzo<sup>(ex)21</sup>, Hanqin Tian<sup>28</sup>, Francesco N. Tubiello<sup>20</sup>, Timo Vesala<sup>23,29</sup>, Chris Wilson<sup>30,31</sup>, Sönke Zaehle<sup>32</sup>

<sup>1</sup>Department of Earth Sciences, Vrije Universiteit Amsterdam, 1081HV, Amsterdam, the Netherlands

<sup>2</sup>Laboratoire des Sciences du Climat et de l'Environnement, 91190 Gif-sur-Yvette, France

<sup>3</sup>CICERO Center for International Climate Research, Oslo, Norway

<sup>4</sup>Norwegian Institute for Air Research (NILU), Kjeller, Norway

<sup>5</sup>Finnish Meteorological Institute, P. O. Box 503, FI-00101 Helsinki, Finland

<sup>6</sup>Empa, Swiss Federal Laboratories for Materials Science and Technology, 8600 Dübendorf, Switzerland

<sup>7</sup>Institute of Biological and Environmental Sciences, University of Aberdeen, 23 St Machar Drive, Aberdeen, AB24 3UU, UK

<sup>8</sup>Umweltbundesamt GmbH, Climate change mitigation & emission inventories, 1090, Vienna, Austria

<sup>9</sup>School of GeoSciences, University of Edinburgh, Edinburgh, UK

<sup>10</sup>Science and Innovation Department, World Meteorological Organization (WMO), Geneva, Switzerland

<sup>11</sup>Biogeochemistry and Modeling of the Earth System, Université Libre de Bruxelles, 1050 Bruxelles, Belgium

<sup>12</sup>Université Paris-Saclay, INRAE, AgroParisTech, UMR ECOSYS, Thiverval-Grignon, France

<sup>13</sup>Department of Thematic Studies – Environmental Change, Linköping University, Sweden

<sup>14</sup>International Institute for Applied Systems Analysis (IIASA), 2361 Laxenburg, Austria

<sup>15</sup>Institute of Environmental Engineering, University of Zielona Góra, Zielona Góra, 65-417, Poland

<sup>16</sup>Istituto Nazionale di Geofisica e Vulcanologia, Sezione Roma 2, via V. Murata 605, Roma, Italy

<sup>17</sup>European Centre for Medium-Range Weather Forecasts (ECMWF), Reading, RG2 9AX, UK

<sup>18</sup>Science Partners, 75010 Paris, France

<sup>19</sup>Consiglio Nazionale delle Ricerche, Istituto di Geologia Ambientale e Geoingegneria, Via Salaria km 29300, 00015 Monterotondo, Rome, Italy

<sup>20</sup>Food and Agriculture Organization of the United Nations, Statistics Division. 00153 Rome, Italy

<sup>21</sup>European Commission, Joint Research Centre, 21027 Ispra (Va), Italy

\*now at: European Commission, DG Research and Innovation, 1050 Brussels, Belgium

<sup>22</sup>Umweltbundesamt (UBA), 14193 Berlin, Germany

<sup>23</sup>University of Helsinki, Institute for Atmospheric and Earth System Research/Physics, Faculty of Science, 00560 Helsinki, Finland<sup>24</sup>Hadley Centre, Met Office, Exeter, EX1 3PB, UK

<sup>25</sup>Research Institute for Global Change, JAMSTEC, Yokohama 2360001, Japan

<sup>26</sup>Centro Euro-Mediterraneo sui Cambiamenti Climatici (CMCC), Viterbo, Italy

<sup>27</sup>Department of Climate, Air and Sustainability, TNO, Princetonlaan 6, 3584 CB Utrecht, the Netherlands

<sup>28</sup>International Centre for Climate and Global Change, School of Forestry and Wildlife Sciences, Auburn University, Auburn, AL 36849, USA

<sup>29</sup>Institute for Atmospheric and Earth System Research/Forest Sciences, Faculty of Agriculture and Forestry, University of Helsinki, Helsinki, Finland

<sup>30</sup>Institute for Climate and Atmospheric Science, University of Leeds, Leeds, UK

<sup>31</sup>National Centre for Earth Observation, University of Leeds, Leeds, UK

<sup>32</sup>Max Planck Institute for Biogeochemistry (MPI-BGC), Jena, Germany

Correspondence to: A.M. Roxana Petrescu ([a.m.r.petrescu@vu.nl](mailto:a.m.r.petrescu@vu.nl))

## Abstract

Knowledge of the spatial distribution of the fluxes of greenhouse gases and their temporal variability as well as flux attribution to natural and anthropogenic processes is essential to monitoring the progress in mitigating anthropogenic emissions under the Paris Agreement and to inform its Global Stocktake. This study provides a consolidated synthesis of CH<sub>4</sub> and N<sub>2</sub>O emissions using bottom-up (BU) and top-down (TD) approaches for the European Union and UK (EU27+UK) and updates earlier syntheses (Petrescu et al., 2020, 2021). The work integrates updated emission inventory data, process-based model results, data-driven sector model results, inverse modelling estimates, and extends the previous period 1990-2017 to 2019. BU and TD products are compared with European National GHG Inventories (NGHGI) reported by Parties under the United Nations Framework Convention on Climate Change (UNFCCC) in 2021. Uncertainties in NGHGIs, as reported to the UNFCCC by the EU and its Member States are also included in the synthesis. Variation in estimates produced with other methods, such as atmospheric inversion models (TD) or spatially disaggregated inventory datasets (BU), arise from diverse sources including within-model uncertainty related to parameterization as well as structural differences between models. By comparing NGHGIs with other approaches, the activities included are a key source of bias between estimates e.g. anthropogenic and natural fluxes, which, in atmospheric inversions are sensitive to the prior geospatial distribution of emissions. **For CH<sub>4</sub> emissions**, over the updated 2015-2019 period, which covers a sufficiently robust number of overlapping estimates, and most importantly the NGHGIs, the anthropogenic BU approaches are directly comparable, accounting for mean emissions of 20.5 Tg CH<sub>4</sub> yr<sup>-1</sup> (EDGAR v6.0, last year 2018) and 18.4 Tg CH<sub>4</sub> yr<sup>-1</sup> (GAINS, 2015), close to the NGHGI estimates of 17.5 ± 2.1 Tg CH<sub>4</sub> yr<sup>-1</sup>. TD inversions estimates give higher emission estimates, as they also detect natural emissions. Over the same period, high resolution regional TD inversions report a mean emission of 34 Tg CH<sub>4</sub> yr<sup>-1</sup>. Coarser-resolution global-scale TD inversions result in emission estimates of 23 Tg CH<sub>4</sub> yr<sup>-1</sup> and 24 Tg CH<sub>4</sub> yr<sup>-1</sup> inferred from GOSAT and surface (SURF) network atmospheric measurements, respectively. The magnitude of natural peatland and mineral soils emissions from the JSBACH-HIMMELI model, natural rivers, lakes and reservoirs emissions, geological sources and biomass burning together could account for the gap between NGHGI and inversions and account for 8 Tg CH<sub>4</sub> yr<sup>-1</sup>. **For N<sub>2</sub>O emissions**, over the 2015-2019 period, both BU products (EDGAR v6.0 and GAINS) report a mean value of anthropogenic emissions of 0.9 Tg N<sub>2</sub>O yr<sup>-1</sup>, close to the NGHGI data (0.8 ± 55 % Tg N<sub>2</sub>O yr<sup>-1</sup>). Over the same period, the mean of TD global and regional inversions was 1.4 Tg N<sub>2</sub>O yr<sup>-1</sup> (excluding TOMCAT which reported no data). The TD and BU comparison method defined in this study can be ‘operationalized’ for future annual updates for the calculation of CH<sub>4</sub> and N<sub>2</sub>O budgets at the national and EU27+UK scales. Future comparability will be enhanced with further steps involving analysis at finer temporal resolutions and estimation of emissions over intra-annual timescales, of great importance for CH<sub>4</sub> and N<sub>2</sub>O, which may help identify sector contributions to divergence between prior and posterior estimates at the annual/inter-annual scale. Even if currently comparison between CH<sub>4</sub> and N<sub>2</sub>O inversions estimates and NGHGIs is highly uncertain because of the large spread in the inversion results, TD inversions inferred from atmospheric observations represent the most independent data against which inventory totals can be compared. With anticipated improvements in atmospheric modelling and observations, as well as modelling of natural fluxes, TD inversions may arguably emerge as the most powerful tool for verifying emissions inventories for CH<sub>4</sub>, N<sub>2</sub>O and other GHGs. The referenced datasets related to figures are

95 visualized at <https://doi.org/10.5281/zenodo.7553800> (Petrescu et al., 2023).

## 1. Introduction

100 Atmospheric concentrations of greenhouse gases (GHGs) reflect a balance between emissions from sources and removals by sinks, the former arising from both human activities and natural sources and the latter being found in the biosphere, oceans and atmospheric oxidation. Increasing levels of GHG in the atmosphere due to human activities have been the major driver of climate change since the pre-industrial period (pre-1750). In 2020, GHG mole fractions were record highs, with globally averaged mole fractions reaching  $1889 \pm 2$  parts per billion (ppb) for methane ( $\text{CH}_4$ ) and  $333.2 \pm 0.1$  ppb for nitrous oxide ( $\text{N}_2\text{O}$ ), representing 262% and 123% of respective pre-industrial levels (WMO, 2021). Since 2004, when  $\text{CH}_4$  registered a negative dip, the trend in the  $\text{CH}_4$  concentration in the atmosphere continues to increase (NOAA, atmospheric data: [https://www.esrl.noaa.gov/gmd/ccgg/trends\\_ch4/](https://www.esrl.noaa.gov/gmd/ccgg/trends_ch4/), last access May 2022). This increase was attributed to anthropogenic emissions from agriculture (livestock enteric fermentation and rice cultivation (12%) and fossil fuel related activities (17%)), combined with a contribution from natural tropical wetlands (Saunio et al., 2020, Thompson et al. 2018, Feng et al, 2022a,b). The increase in atmospheric  $\text{N}_2\text{O}$  also continues to rise with the highest annual increase ever recorded in 2020 ([https://gml.noaa.gov/ccgg/trends\\_n2o/](https://gml.noaa.gov/ccgg/trends_n2o/), last access: May 2022). The main sources remain linked to agriculture particularly the application of nitrogen fertilizers and livestock manure on agricultural land (FAO, 2020, 2015; IPCC, 2019b, Tian et al., 2020).

115 National GHG emission inventories (NGHGs) are prepared and reported on an annual basis by Annex I Parties<sup>1</sup> to the United Nations Framework Convention on Climate Change (UNFCCC). These inventories contain annual time series of each country's GHG emissions from the 1990 base year<sup>2</sup> until two years before the year of reporting and were originally set to track progress towards their reduction targets under the Kyoto Protocol (UNFCCC, 1997). Non-Annex I Parties<sup>3</sup> to the UNFCCC also provide emissions estimates in Biennial Update Reports (BURs) as well as through National Communications (NCs); however, non-Annex I emissions are neither reported for annually nor use harmonized formats due to the comparatively less-stringent reporting requirements. Annex I NGHGs are reported according to the Decision 24/CP.19 of the UNFCCC Conference of the Parties (COP) which states that the national inventories *shall* be compiled using the methodologies provided in the *IPCC Guidelines for National Greenhouse Gas Inventories* (IPCC, 2006). The 2006 IPCC Guidelines provide methodological guidance for estimating emissions for well-defined sectors using national activity and available emission factors. Decision trees

---

<sup>1</sup> Annex I Parties include the industrialized countries that were members of the OECD (Organization for Economic Co-operation and Development) in 1992 plus countries with economies in transition (the EIT Parties), including the Russian Federation, the Baltic States, and several central and eastern European states (UNFCCC, <https://unfccc.int/parties-observers>, last access: February 2022). Under the Paris agreement all countries are requested to report their emissions.

<sup>2</sup> For most Annex I Parties, the historical base year is 1990. However, parties included in Annex I with an economy in transition during the early 1990s (EIT Parties) were allowed to choose one year up to a few years before 1990 as reference because of a non-representative collapse during the breakup of the Soviet Union (e.g., Bulgaria, 1988, Hungary, 1985–1987, Poland, 1988, Romania, 1989, and Slovenia, 1986).

<sup>3</sup> Non-Annex I Parties are mostly developing countries. Certain groups of developing countries are recognized by the Convention as being especially vulnerable to the adverse impacts of climate change, including countries with low-lying coastal areas and those prone to desertification and drought. Others (such as countries that rely heavily on income from fossil fuel production and commerce) feel more vulnerable to the potential economic impacts of climate change response measures. The Convention emphasizes activities that promise to answer the special needs and concerns of these vulnerable countries, such as investment, insurance and technology transfer (UNFCCC, <https://unfccc.int/parties-observers>, last access: February 2022).

indicate the appropriate level of methodological sophistication (methodological *Tier*) based the absolute contribution of the sector to the national GHG balance (is the source or sink a *Key Category* or not) and the country's national circumstances (availability and resolution of national activity data and emission factors). Generally, Tier 1 methods are based on global or regional default emission factors that can be used with aggregated activity data, while Tier 2 methods rely on country-specific factors and/or activity data at a higher subsector resolution. Tier 3 methods are based on more detailed process-level modelling or even facility-level emission measurements. Annex I Parties are furthermore required to estimate and report uncertainties in emissions (95% confidence interval) following the 2006 IPCC guidelines using, as a minimum requirement, the Gaussian error propagation method (approach 1). Annex I Parties may use Monte-Carlo methods (approach 2) or a hybrid approach and are encouraged to do so.

Annex I NGHGs should follow principles of transparency, accuracy, consistency, completeness and comparability (TACCC) under the guidance of the UNFCCC (UNFCCC, 2014) and as mentioned above, shall be completed following the 2006 IPCC guidelines (IPCC, 2006). In addition, the IPCC 2019 Refinement (IPCC, 2019a), that may be used to complement the 2006 IPCC guidelines, has updated sectors with additional emission sources and provides guidance on the use of atmospheric data for independent verification of GHG inventories. Complementary to the NGHGs, research groups and international institutions produce estimates of national GHG emissions, with two kind of approaches: atmospheric inversions (top-down, TD) and GHG inventories based on the same principle as NGHGI but using activity and/or emissions factors from (partially) different sources (bottom-up, BU).

The two approaches (BU and TD) provide useful insights on emissions from two different point of view. First, TD approaches act as an additional quality control tool for BU and NGHGI approaches, and facilitates a deeper understanding of the processes driving changes in different elements of GHG budgets. Second, NGHGs cover regularly only a subset of countries (Annex I), and it is therefore necessary to construct BU estimates independently for all countries. Furthermore, while additional BU methods do not have prescribed standards like the IPCC Guidelines, independent BU methods can draw on different input data, or can provide estimates at higher-sectoral resolution, and therefore add complementary information to help quality control NGHGs and help inform climate mitigation policy processes. Additionally, BU estimates are needed as input for TD estimates. As there is no formal guideline to estimate uncertainties in TD or BU approaches, uncertainties are usually assessed from the spread of different estimates within the same approach, though some groups or institutions report uncertainties for their individual estimates using a variety of methods, for instance, by performing sensitivity tests (Monte Carlo approach) on input data parameters. However, this can be logistically and computationally difficult when dealing with complex process-based models.

Despite the important insights gained from complementary BU and TD emission estimates, it should be noted that comparisons with the official reported is not always straightforward. BU estimates often share common methodology and input data, and through harmonization, structural differences between BU estimates and NGHGs can be bridged. However, the use of common input data, albeit to varying extents, restricts the independence between the datasets and, from a verification perspective, may limit the conclusions drawn from the comparisons. On the other hand, TD estimates are constrained by independent atmospheric observations and can serve as an additional, almost-fully independent quality control for NGHGs. Nonetheless, structural differences between NGHGs (what sources

and sinks are included, and where and when emissions/removals occur) and the actual fluxes of GHGs to the atmosphere must be factored in to the comparison of estimates. While NGHGs go through a central QA/QC review process, the IPCC procedures do not incorporate mandatory large-scale observation-derived verification. Nevertheless, the individual countries may use atmospheric data and inverse modelling within their data quality control, quality assurance and verification processes, with expanded and updated guidance provided in chapter 6 of the 2019 Refinement of IPCC 2006 Guidelines (IPCC, 2019). So far, only a few countries (e.g. Switzerland, UK, New Zealand and Australia) have used atmospheric observations to constrain national emissions and documented these verification activities in their national inventory reports (Bergamaschi et al., 2018).

A key priority in the current policy process is to facilitate the 5 yearly Global Stocktakes (GSTs) of the Paris agreement, the first of which is in 2023, and to assess collective progress towards achieving the near- and long-term objectives, considering mitigation, adaptation and means of implementation. The GSTs are expected to create political momentum for enhancing commitments in Nationally Determined Contributions (NDCs) under the Paris Agreement. Though the modalities of the GSTs implementation are not clear, the key component of this process will be the NGHGI reporting by countries under the Enhanced transparency framework of the Paris Agreement. Under the framework, emissions reporting will move away from the differential Annex I and non-Annex I reporting requirements and become more harmonized across Parties. Non-Annex I parties will be required to follow the 2006 IPCC guidelines and provide regular (biennial) national GHG inventory reports to the UNFCCC, alongside developed countries, that will continue to submit their inventories on an annual basis. Some developing countries will face challenges to construct and subsequently update their NGHGs and meet the more-stringent reporting requirements.

The work presented in this paper covers dozens of distinct datasets and models, in addition to the individual country submissions to the UNFCCC of the EU Member States and the UK. As Annex I Parties, the NGHGs of the EU Member States and the UK are consistent with the general guidance laid out in IPCC (2006) yet still differ in specific approaches, models, and parameters, in addition to differences underlying activity datasets. A comprehensive investigation of detailed differences between all datasets is beyond the scope of this paper, though systematic analyses have been previously made for specific sectors (e.g. agriculture Petrescu et al., 2020) and by the Global Carbon Project CH<sub>4</sub> and N<sub>2</sub>O syntheses (Saunio et al., 2020 and Tian et al., 2020). The focus of this paper is on updates of the information from Petrescu et al., 2021a discussing whenever needed the changes in terms of emissions and trends. The data from Petrescu et al., 2021a is labeled as v2019, while the latest results are labeled v2021 respectively. Except for one on N<sub>2</sub>O, the global inversions did not provide an update for v2021, and, therefore, the earlier results are incorporated into this synthesis.

As Petrescu et al. (2021a) is the most comprehensive comparison of the NGHGI and research datasets (including both TD and BU approaches) for the EU27+UK to date, the focus of the current paper is on improvement of estimates in the most recent version in comparison with the previous one, including changes in the uncertainty estimates and identification of the knowledge gaps and added value for policy making. Such exercises of yearly updates are needed to improve the different respective approaches and furthermore can inform the development of formal verification systems. Official NGHGI emissions are compared with research datasets, including necessary harmonization of the latter on total emissions to ensure consistency. Differences and inconsistencies between emission

estimates were analyzed, and recommendations were made towards future evaluation of NGHGI data. It is important to remember that uncertainties provided by the NGHGIs are intended to be used in prioritization and decision-making (Volume 1, Chapter 3, IPCC, 2006) and not to enable comparisons between countries or other datasets. In addition, individual spatially disaggregated research emission datasets often lack quantification of uncertainty. Here, the focus is on the median and minimum/maximum (min/max) range of different research products of the same type to get a first estimate of uncertainty (see Sect. 2). For those datasets providing uncertainties, new uncertainty reduction maps are presented (see Section 3.1.5). For those models/inventories who did not provided an update for this study, the previously published timeseries are shown.

## 2. CH<sub>4</sub> and N<sub>2</sub>O data sources and estimation approaches

The CH<sub>4</sub> and N<sub>2</sub>O emissions in the EU27+UK from inversions and anthropogenic emissions inventories from various BU approaches covering specific sectors were analyzed. The data (Table 2) span the period from 1990 to 2019, with some of the data only available for shorter time periods or up until 2020. The estimates are available both from peer-reviewed literature and from unpublished research results from the VERIFY project (Table 1 and Appendix A) and in this work they are compared with NGHGIs reported in 2021 (time series for 1990-2019). Data sources are summarized in Table 2 with the detailed description of all products provided in Appendix A1-A3.

For both CH<sub>4</sub> and N<sub>2</sub>O BU approaches, inventories of anthropogenic emissions covering all sectors (EDGAR v6.0 and GAINS) and models and inventories limited to agriculture (CAPRI, FAOSTAT, DayCent, ECOSSE) were used. For CH<sub>4</sub> biogeochemical models of natural peatland emissions (JSBACH-HIMMELI), and lakes and reservoirs emissions (Lauerwald et al., 2019; Maisonnier et al., in prep.), as well as updated data for inland waters (rivers, lakes and reservoirs; Lauerwald et al., in rev. GBC) and updated data for total geological emissions (Etiope et al., 2019) were used. Emissions from gas hydrates and termites are not included as they are close to zero in the EU27+UK (Saunio et al., 2020). Anthropogenic NGHGI CH<sub>4</sub> emissions from the Land Use, Land Use Change and Forestry (LULUCF) sector are very small for EU27+UK (3 % in 2019 including biomass burning) (section 2.2).

TD approaches include both regional and global inversions, the latter having a coarser spatial resolution. These estimates are described in section 2.3.

For N<sub>2</sub>O emissions, the same global BU inventories as for CH<sub>4</sub>, natural emissions from inland waters (rivers, lakes and reservoirs) (RECCAP2 Lauerwald et al., in rev. GBC) were used, which did not change with respect to Petrescu et al., 2021a. In this study, about 66 % of the N<sub>2</sub>O emitted by Europe's natural rivers are considered anthropogenic indirect emissions, caused by leaching and run-off of N-fertilizers from the agriculture sector. One important update is the inclusion of estimates of natural N<sub>2</sub>O emissions from soils simulated with the O-CN model (Zaehle et al., 2011). These emissions are derived from model simulations in which land-use and atmospheric CO<sub>2</sub> remain constant, but climate varies through to 2020. These estimates are considered to be closer to what background natural N<sub>2</sub>O emissions would be present day, so they were used for subtraction from outputs of inversions (as it has a reasonable representation of the inter-annual variability (IAV)). The TD N<sub>2</sub>O inversions include one regional inversion FLEXINVERT and three global inversions (Friedlingstein et al., 2019; Tian et al., 2020; Patra et al., 2022).

Agricultural sector emissions of N<sub>2</sub>O were presented in detail by Petrescu et al., 2020. In this current study, CAPRI and ECOSSE models and FAO provided updated emissions, with the latter additionally covering non-CO<sub>2</sub> emissions from biomass burning as a contribution to LULUCF. Fossil fuel related emissions and industrial emissions were obtained from GAINS (see Appendix A1). Table A2 in Appendix A presents the methodological differences of the current study with respect to Petrescu et al., 2020 and Petrescu et al., 2021a.

*Table 1: Sectors included in this study and data sources providing estimates for these sectors.*

Anthropogenic (BU) <sup>4</sup> CH <sub>4</sub> and N <sub>2</sub> O	Natural (BU) <sup>5</sup> CH <sub>4</sub>	Natural** (BU) N <sub>2</sub> O	TD (CH <sub>4</sub> and N <sub>2</sub> O)
1. Energy (NGHGI, GAINS, EDGAR v6.0)	Peatlands, mineral soils (JSBACH-HIMMELI), inland waters fluxes (lakes, rivers and reservoirs and RECCAP2 estimate, Rosentreter et al, 2021), geological fluxes Etiope et al., 2019 with updated activity (this study) biomass burning (GFEDv4.1)	Inland water fluxes (lakes, rivers and reservoirs and RECCAP2 estimate, biomass burning (GFEDv4.1) pre-industrial natural soil emissions (O-CN)	No sectoral split – total emissions FLExKF (CAMSv19r); TM5-4DVAR; FLEXINVERT; CTE-CH <sub>4</sub> InGOS inversions GCP-CH <sub>4</sub> 2019 anthropogenic partition from inversions GCP-CH <sub>4</sub> 2019 Natural partition from inversions GN <sub>2</sub> OB 2019 InTEM NAME (only for UK) VERIFY Community Inversion Framework (CIF): CHIMERE, FLEXPARTv10.4 (NILU) and FELXPART (EMPA) (only CH <sub>4</sub> )
2. Industrial Products and Products in Use (IPPU) (NGHGI, GAINS, EDGAR v6.0)			
3. Agriculture* (NGHGI, CAPRI, GAINS, EDGAR v6.0, FAOSTAT, ECOSSE and DayCent (only for N <sub>2</sub> O))			
4. LULUCF total emissions (NGHGI Fig. 1,2,4,6, B1a for CH <sub>4</sub> and Fig. 10, 11, 14 and B1b for N <sub>2</sub> O)			
5. Waste (NGHGI, GAINS, EDGAR v6.0)			

\* Anthropogenic (managed) agricultural soils can also have a level of natural emissions.

\*\*Natural soils (unmanaged) can have both natural and anthropogenic emissions.

The units used in this paper are metric tonne (t) [1kt = 10<sup>9</sup> g; 1Mt = 10<sup>12</sup>g] of CH<sub>4</sub> and N<sub>2</sub>O. The referenced data used for the figures' replicability purposes are available for download at <https://doi.org/10.5281/zenodo.7553800> (Petrescu et al., 2023). Upon request, the codes necessary to plot the figures in the same style and layout can be provided. The focus is on EU27+UK emissions. In the VERIFY project, an additional web tool was developed which allows for the selection and display of all plots shown in this paper (as well as the companion paper on CO<sub>2</sub>), not only for the EU Member States and UK but for a total of 79 countries and groups of countries in Europe (Table A1,

<sup>4</sup> For consistency with the NGHGI, here we refer to the five reporting sectors as defined by the UNFCCC and the Paris Agreement decision (18/CMP.1), the IPCC Guidelines (IPCC, 2006), and their Refinement (IPCC, 2019a), with the only exception that the latest IPCC Refinement groups together Agriculture and LULUCF sectors in one sector (Agriculture, Forestry and Other land Use - AFOLU).

<sup>5</sup> The term natural refers here to unmanaged natural CH<sub>4</sub> emissions (peatlands, mineral soils, geological, inland waters and biomass burning) not reported under the UNFCCC LULUCF sector.

Appendix A). The data, located on the VERIFY project website: <http://webportals.ipsl.jussieu.fr/VERIFY/FactSheets/>, is free and can be accessed upon registration.

## 2.1. CH<sub>4</sub> and N<sub>2</sub>O anthropogenic emissions from NGHGI

Anthropogenic CH<sub>4</sub> emissions from the four UNFCCC sectors (excluding LULUCF) were grouped together. Anthropogenic CH<sub>4</sub> emissions in 2019 account for 17.1 Tg CH<sub>4</sub> yr<sup>-1</sup> and represent 10.5 % of the total EU27+UK emissions (in CO<sub>2</sub>e, GWP 100 years, IPCC AR4<sup>6</sup>). CH<sub>4</sub> emissions are predominantly related to agriculture (9.2 Tg CH<sub>4</sub> yr<sup>-1</sup> ± 0.8 Tg CH<sub>4</sub> yr<sup>-1</sup>) or 53.8 % in 2019 (52.5 % in 2018) of the total EU27+UK CH<sub>4</sub> emissions. Anthropogenic NGHGI CH<sub>4</sub> emissions from the LULUCF sector are very small for EU27+UK e.g. 0.5 Tg CH<sub>4</sub> yr<sup>-1</sup> or 3 % in 2019, including emissions from biomass burning.

Regarding CH<sub>4</sub> emissions from wetlands, following the recommendations of the 2013 IPCC Wetlands supplement (IPCC, 2014) only emissions from managed wetlands are reported by Parties. According to NGHGI data between 2008 and 2018, managed wetlands in the EU27+UK for which emissions were reported under LULUCF (CRF table 4(II) accessible for each EU27+UK country<sup>7</sup>) represent one fourth of the total wetland area in EU27+UK (G. Grassi, EC-JRC, pers. comm.) and their emissions summed up in 2019 to 0.1 Tg CH<sub>4</sub> yr<sup>-1</sup>.

Anthropogenic N<sub>2</sub>O emissions (excluding LULUCF) in 2019 account for 0.8 Tg N<sub>2</sub>O yr<sup>-1</sup> and represent 6.2 % of the total EU27+UK emissions in CO<sub>2</sub>eq. N<sub>2</sub>O emissions are predominantly related to agriculture (0.6 Tg N<sub>2</sub>O yr<sup>-1</sup> or 73.0 % in 2019 (73.5 % in 2018) of the total EU27+UK (including LULUCF+BB) N<sub>2</sub>O emissions) but are also found in the other sectors (Tian et al. 2020). In addition, N<sub>2</sub>O has natural sources, which are defined as the pre-industrial background emissions before the use of synthetic N-fertilizers and intensive agriculture, and derive from natural processes in soils but also in lakes, rivers and reservoirs (Lauerwald et al., in rev. GBC, Maavara et al., 2019; Lauerwald et al., 2019; Tian et al., 2020).

## 2.2. CH<sub>4</sub> and N<sub>2</sub>O anthropogenic and natural emissions from other bottom-up estimates

Data from five global data sets and models of CH<sub>4</sub> and N<sub>2</sub>O anthropogenic emissions inventories were used, namely: CAPRI, DayCent, ECOSSE, FAOSTAT, GAINS and EDGAR v6.0 (Table 3). These estimates are not completely independent from NGHGIs (see Figure 4 in Petrescu et al., 2020) as they integrate their own sectorial modelling with the UNFCCC data (e.g., common activity data and IPCC emission factors) when no other source of information is available. The CH<sub>4</sub> biomass and biofuel burning emissions are included in NGHGI under the UNFCCC LULUCF sector, although they are identified as a separate category by the Global Carbon Project CH<sub>4</sub> budget synthesis (Saunois et al., 2020). For both CH<sub>4</sub> and N<sub>2</sub>O, CAPRI (Britz and Witzke, 2014; Weiss and Leip, 2012) and FAOSTAT (FAO, 2021) report only agricultural emissions. DayCent and ECOSSE report only emissions for

<sup>6</sup> IPCC AR4 GWP 100 values are still used by the Member States in their NGHGI reporting to the UNFCCC.

<sup>7</sup> <https://unfccc.int/process-and-meetings/transparency-and-reporting/reporting-and-review-under-the-convention/greenhouse-gas-inventories-annex-i-parties/national-inventory-submissions-2019>



agriculture N<sub>2</sub>O. Out of all BU inventories, only CAPRI reported new uncertainties for 2014, 2016 and 2018, while values for EDGARv6.0 were the same (Solazzo et al., 2021) as those reported in Petrescu et al., 2021a.

285 In this study, natural CH<sub>4</sub> emissions are included under the category “peatlands” and “other natural emissions”, the latter including geological emissions, biomass burning emissions and two estimates of inland waters (rivers, lakes and reservoirs). One inland water estimate comes from “process-based models” and is based on the Rosentreter et al., (2021) with ranges from Bastviken et al., (2011) and Stanley et al., (2016) and the second represent an upscaled estimate for inland waters from the RECCAP2 project (Lauerwald et al., in rev. GBC).

290 For peatlands and mineral soils, the JSBACH-HIMMELI framework was used. Additionally, the ensemble of thirteen monthly gridded estimates of peatland emissions based on different land surface models as calculated for Saunio et al. (2020) were used as described in Appendix B2. Geological emissions were initially based on the global gridded emissions from Etiope et al. 2019 and previously estimated to be 1.3 Tg CH<sub>4</sub> yr<sup>-1</sup> (Petrescu et al., 2021a). For this study these emissions were recalculated, using more detailed input data related to the activity, i.e., a more precise  
295 estimate of the continental oil-gas field area (which determines the potential area of microseepage) and offshore seepage area (Appendix A2) and now account for 3.3 Tg CH<sub>4</sub> yr<sup>-1</sup> (0.9 Tg CH<sub>4</sub> yr<sup>-1</sup> from offshore marine seepage and 2.4 Tg CH<sub>4</sub> yr<sup>-1</sup> onshore). This rescaled geological source represent the second largest natural component accounting for 42 % of the total EU27+UK natural CH<sub>4</sub> emissions. The upscaled inland waters, (rivers, lakes, and reservoirs, based on Lauerwald et al., in rev. GBC) are the largest component of natural emissions (3.3 Tg CH<sub>4</sub> yr<sup>-1</sup>  
300 and ranging from 2.7 Tg CH<sub>4</sub> yr<sup>-1</sup> to 4.3 Tg CH<sub>4</sub> yr<sup>-1</sup>) and account for 44 %. The remaining 14 % emissions are attributed to peatlands, mineral soils and biomass burning. Overall, in EU27+UK the natural emissions thus accounted for 8 Tg CH<sub>4</sub> yr<sup>-1</sup>. Finally, It should be noted that, to a small extent, the CH<sub>4</sub> natural emissions from waters are also due to an anthropogenic component, namely eutrophication following N-fertilizer leaching to inland waters. Globally, the contribution of eutrophication is estimated to lead to a further increase in lake and reservoir emission by 30 to 90%  
305 over the 21<sup>st</sup> century, which would be the result of a ~3 times higher nutrient loading to lakes and reservoirs (Beaulieu et al., 2019), similar to the review by Li et al. 2021 who gathered a lot of prove that eutrophication significantly increase CH<sub>4</sub> emissions. In temperate Europe, eutrophication contributes significantly to the overall increase natural emissions and Rinta et al., 2017 found that eutrophic, central European lakes show CH<sub>4</sub> emission rates which are about one order of magnitude higher than those of oligotrophic boreal lakes and this study’s model results are consistent  
310 with it.

The N<sub>2</sub>O anthropogenic emissions from inventory datasets belong predominantly to agriculture and are associated to two main categories: 1) direct emissions from the agricultural sector where synthetic fertilizers and manure were applied, and from manure management, and 2) indirect emissions on non-agricultural land and water receiving anthropogenic N through atmospheric N deposition, leaching and run-off (also from agricultural land).  
315 Additional anthropogenic emissions result from industrial processes, in particular, adipic and nitric acid production, which are declining owing to the implementation of emission abatement technologies. Other N<sub>2</sub>O emissions come from the wastewater treatment activities and fossil fuel combustion.

In this study, “natural” N<sub>2</sub>O fluxes refer to emissions from inland waters (lakes, rivers and reservoirs, Maavara et al., 2019; Lauerwald et al., 2019, Lauerwald et al., in rev. GBC) which include also lakes with dams. The

other component is the natural N<sub>2</sub>O emissions from soils simulated with the O-CN model (Zaehle et al., 2011). Regarding the inland water emissions, more than half of the emissions (56 % globally, Tian et al., 2020, and 66 % for Europe this study) are due to enhanced N inputs from fertilizers, manure, sewage and, to a smaller extent, atmospheric N deposition. However, emissions from natural soils in this study are considered as “anthropogenic” because, according to the country specific National Inventory Reports (NIRs), all land in EU27+UK is considered to be managed

For both CH<sub>4</sub> and N<sub>2</sub>O the natural biomass burning emissions from GFEDv4.1 (van der Werf et al., 2017) are included in Figs. 1, 4b, 5b, 9 and 13, while for CH<sub>4</sub> only, biomass burning emissions from the GCP 2020 (Saunois et al., 2020) are included in Fig 6.

### 2.3. CH<sub>4</sub> and N<sub>2</sub>O emission data from inversions

Atmospheric inversions optimize prior estimates of emissions and sinks through modeling frameworks that utilizes atmospheric observations as a constraint on fluxes. Emission estimates from inversions depend on the data set of atmospheric measurements and the choice of the atmospheric model, as well as on other inputs (e.g., prior emissions and their uncertainties). Inversion results were taken from original publications without evaluation of their performance through specific metrics (e.g., fit to independent cross validation atmospheric measurements (Bergamaschi et al., 2013, 2018; Patra et al., 2016)). Some of the inversions allow for explicit attribution to different sectors, while others optimize all fluxes in each grid cell and then attribute emissions to sectors using prior grid-cell fractions (see details in Saunois et al. 2020 for global inversions).

For CH<sub>4</sub>, the same set of nine regional inversions and 22 global inversions as listed in Table 3 and presented in Petrescu et al., 2021a was used. While many different inversions exist, it should be stressed that the variants are not completely independent of one another. Table B4, Appendix B in Petrescu et al., 2021a illustrates this by documenting to what extent the transport models, priors and atmospheric measurement data vary between the inversion datasets”. The subset of InGOS inversions (Bergamaschi et al., 2018a) belongs to a project where all models used the same atmospheric data over Europe covering the period 2006-2012. The global inversions from Saunois et al. 2020 were not updated for this work and cover a period until 2017.

The regional inversions generally use both higher-resolution prior data and higher-resolution transport models, and e.g. TM5-JRC runs simultaneously over the global domain at coarse resolution and over the European domain at higher resolution, with atmospheric CH<sub>4</sub> concentration boundary conditions taken from global fields. For CH<sub>4</sub>, 11 global inversions use GOSAT for the period 2010-2017, eight global inversions use surface stations (SURF) from 2000 to 2017, two global models use SURF since from 2010-2017 and one SURF from 2003-2017 (see “Appendix 4 Table” in Saunois et al. 2020). All regional inversions use observations from SURF stations as a base of their emission calculation.

Table 2: Data sources for CH<sub>4</sub> and N<sub>2</sub>O emissions used in this study:

Name	CH <sub>4</sub>	N <sub>2</sub> O	Contact / lab	References	Status compared to Petrescu et al., 2021a

CH <sub>4</sub> and N <sub>2</sub> O Bottom-up anthropogenic					
UNFCCC NGHGI (2021) CRFs	CH <sub>4</sub> emissions 1990-2019	N <sub>2</sub> O emissions 1990-2019	MS inventory agencies  Yearly uncertainties provided by the EU GHG inventory team	UNFCCC CRFs  <a href="https://unfccc.int/process-and-meetings/transparency-and-reporting/reporting-and-review-under-the-convention/greenhouse-gas-inventories-annex-i-parties/national-inventory-submissions-2019">https://unfccc.int/process-and-meetings/transparency-and-reporting/reporting-and-review-under-the-convention/greenhouse-gas-inventories-annex-i-parties/national-inventory-submissions-2019</a>	updated
EDGAR v6.0	CH <sub>4</sub> sectoral emissions 1990-2018	N <sub>2</sub> O sectoral emissions 1990-2018	EC-JRC	Crippa et al., 2019a  Crippa et al., 2019 EU REPORT  Janssens-Maenhout et al., 2019  Solazzo et al., 2020 (in review ACP)	Updated
CAPRI	CH <sub>4</sub> agricultural emissions 1990-2014 and 2016, 2018	N <sub>2</sub> O agricultural emissions 1990-2014 and 2016, 2018	EC-JRC	Britz and Witzke, 2014  Weiss and Leip, 2012	Updated
GAINS	CH <sub>4</sub> sectoral emissions 1990-2015	N <sub>2</sub> O sectoral emissions 1990-2015  (every five years)	IIASA	Höglund-Isaksson, L. 2017  Höglund-Isaksson, L. et al., 2020  Winiwarter et al., 2018	Not updated
FAOSTAT	CH <sub>4</sub> agriculture and land use emissions 1990-2019	N <sub>2</sub> O agricultural emissions 1990-2019	FAO	Tubiello et al. 2013  FAO, 2015, 2020  Tubiello, 2019	Updated
ECOSSE		Direct N <sub>2</sub> O emissions from agricultural soils  2000-2020	UNIABD N	Bradbury et al., 1993  Coleman., 1996  Jenkinson., 1977, 1987  Smith et al., 1996, 2010a,b	Updated
DayCent		N <sub>2</sub> O emissions from direct agricultural soils	EC-JRC	Orgiazzi et al., 2018  Lugato et al., 2018, 2017	Updated

		avg. 2015-2019		Quemada et al., 2020	
<b>CH<sub>4</sub> and N<sub>2</sub>O natural</b>					
JSBACH-HIMMELI	CH <sub>4</sub> emissions from peatlands and mineral soils  2005-2020		FMI	Raivonen et al., 2017  Susiluoto et al., 2018	Updated
Non-wetland inland waters	One average value for CH <sub>4</sub> fluxes from rivers, lakes and reservoirs with uncertainty  2010-2019  One median upscaled value from RECCAP2 analysis  1990-2019	One median N <sub>2</sub> O value for emissions from lakes, rivers, reservoirs from the RECCAP2 analysis  1990-2019	ULB	Maisonnier et al., in prep., after Maavara et al., 2017, 2019 and Lauerwald et al., 2019  Bastviken et al., 2011  Stanley et al. 2016  Rosentreter et al., 2021  Lauerwald et al., rev. GBC	Updated
Geological emissions, (onshore and offshore)	Global grid geological CH <sub>4</sub> emission model (2019)		Istituto Nazionale di Geofisica e Vulcanologia (INGV)	Etioppe et al., 2019 and this work (updated activity data)	updated
GFED4.1	Biomass burning emissions  2000-2020	Biomass burning emissions  2000-2020	VU Amsterdam	van der Werf et al., 2017	new
O-CN		Background natural N <sub>2</sub> O emissions from soils (model simulations in which land-use and atm. CO <sub>2</sub> remain constant, but climate varies through to 2020)	MPI-BGC	Zaehle et al., 2011  Zaehle & Friend, 2010	new
<b>CH<sub>4</sub> and N<sub>2</sub>O inversions</b>					
<b>Regional inversions over Europe (high transport model resolution)</b>					

FLExKF-CAMsv19r	Total CH <sub>4</sub> emissions from inversions with uncertainty 2005-2019		EMPA	Brunner et al., 2012 Brunner et al., 2017 Background concentrations from CAMsv19r (Arjo Segers)	Updated
TM5-4DVAR	CH <sub>4</sub> emissions from inversions, split into total, anthropogenic and natural 2005-2018		EC-JRC	Bergamaschi et al., 2018a	Not updated
FLEXINVERT	CH <sub>4</sub> total emissions from inversions 2005-2018	N <sub>2</sub> O total emissions, 2005-2019	NILU	Thompson and Stohl, 2014	Updated for N <sub>2</sub> O
CTE-CH <sub>4</sub>	Total CH <sub>4</sub> emissions from inversions for Europe with uncertainty 2005-2018		FMI	Brühl et al., 2014 Houweling et al., 2014 Giglio et al., 2013 Ito et al., 2012 Janssens-Maenhout et al., 2013 Krol et al., 2005 Peters et al., 2005 Saunois et al., 2020 Stocker et al., 2014 Tsuruta et al., 2017	Not updated
InGOS inversions	Total CH <sub>4</sub> emissions from inversions 2006-2012		EC-JRC and InGOS project partners	Bergamaschi et al., 2018a TM5-4DVAR: Meirink et al., 2008; Bergamaschi et al. 2010; 2015 TM5-CTE: Tsuruta et al., 2017 LMDZ-4DVAR: Hourdin and Armengaud, 1999; Hourdin et al., 2006 TM3-STILT: Trusilova et al., 2010; Gerbig et al., 2003; Lin et al., 2003; Heimann and Koerner, 2003 NAME: Manning et al. 2011; Bergamaschi et al., 2015 CHIMERE: Berchet et al. 2015a; 2015b; Menut et al., 2013; Bousquet et al., 2011\	Not updated

				COMET: Eisma et al., 1995; Vermeulen et al., 1999; Vermeulen et al., 2006	
VERIFY Community Inversion Framework (CIF): CHIMERE, FLEXPARTv10.4 (NILU) and FELXPART (EMPA) (only CH <sub>4</sub> )	Total CH <sub>4</sub> emissions from inversions  2006-2017	Total N <sub>2</sub> O emissions from inversions  2005-2018	LSCE, NILU and EMAP	Berchet et al., 2021  Fortems-Cheiney et al., 2021	New datasets
<b>Global inversions from the Global Carbon Project CH<sub>4</sub> and N<sub>2</sub>O budgets (Saunois et al. 2020, Tian et al., 2020)</b>					
GCP-CH <sub>4</sub> 2019 anthropogenic partition from inversions	22 models for CH <sub>4</sub> inversions, both <i>SURF and GOSAT</i>  2000-2017		LSCE and GCP-CH <sub>4</sub> contributo rs	Saunois et al., 2020 and model specific references in Appendix B, Table B4	Not updated
GCP-CH <sub>4</sub> 2019 Natural partition from inversions	22 models with optimized wetland CH <sub>4</sub> emissions  2000-2017		LSCE	Saunois et al., 2020 and model specific references in Appendix B, Table B3	Not updated
GN <sub>2</sub> OB 2019		Inverse N <sub>2</sub> O emissions - 3 Inversions PYVAR (CAMS-N <sub>2</sub> O)  TOMCAT  MIROC4-ACTM  1998-2016	GN <sub>2</sub> OB 2019 and contributo rs	Thompson et al., 2019  Tian et al., 2020	Not updated

355 For N<sub>2</sub>O, one regional inversion (FLEXINVERT) for the 2005-2019 period and three global inversions for the period 1998-2016 from Tian et al., (2020) and Thompson et al. (2019) were used as listed in Table 3. These estimates were not updated for this paper. These inversions are not completely independent from each other since most of them use the same input information (Appendix B3). The regional inversion uses a higher resolution atmospheric transport model for Europe, with atmospheric N<sub>2</sub>O concentration boundary conditions taken from global model fields. As all inversions produced total rather than anthropogenic emissions, emissions from soils (O-CN) and inland waters (lakes, rivers and reservoirs) estimated by Lauerwald et al., in rev. GBC were subtracted from the total emissions. Note that inland water emissions include anthropogenic emissions from N-fertilizer leaching accounting for 66 % of the inland water emissions in EU27+UK. In 2019, emissions from inland waters represented 1.4 % of the total UNFCCC NGHGI (2021) N<sub>2</sub>O emissions.

365 The largest share of N<sub>2</sub>O emissions comes from agricultural soils (direct and indirect emissions from the applications of fertilizers, whether synthetic or manure) contributing in 2019 79 % of the total N<sub>2</sub>O emissions (excluding LULUCF) in EU27+UK. In Petrescu et al., 2021a, “Table B1c, Appendix B1” presented the allocation of

emissions by activity type covering all agricultural activities and natural emissions, following the IPCC (2006) sector classification scheme. Each data product has its own particular way of grouping emissions, and does not necessarily cover all emissions activities. The main inconsistencies between process-based models and inventories are observed regarding activity allocation in the two models, ECOSSE and DayCent. ECOSSE only estimates direct N<sub>2</sub>O emissions, and does not estimate downstream emissions of N<sub>2</sub>O, for example indirect emissions from nitrate leached into water courses, which also contributes to an underestimation of total N<sub>2</sub>O emissions. Field burning emissions are also not included by most of the data sources.

### 3. Results and discussion

#### 3.1. Comparing CH<sub>4</sub> emission estimates from different approaches

##### 3.1.1. *Estimates of European and regional total CH<sub>4</sub> fluxes*

Total CH<sub>4</sub> fluxes from EU27+UK and five main regions in Europe: North, West, Central, East (non-EU) and South are presented in the paper. The countries included in these regions, which include countries outside the EU27+UK bloc, are all Annex I Parties to UNFCCC and are listed in Appendix A, Table A. Figure 1 shows the total CH<sub>4</sub> fluxes from the NGHGs for base year 1990, as well as five-year mean values for the 2011-2015 and 2015-2019 periods. The five-year periods are informing on emission trends and what could be achieved by the GST process. Given that the GST is only repeated every five years, a five-year average is clearly of interest even if, in this current study 2021 estimates are not available. The total NGHGI estimates include emissions from all sectors (excluding LULUCF) and are plotted and compared to fluxes from global datasets, BU models and inversions. There is a good agreement noted in absolute total values between inventories, as well as between regional and global inversion ensembles, but uncertainties (min/max ranges) are large. This match can be explained by interdependencies in input data (AD and EFs) for the BU estimates (Petrescu et al., 2020) and similar prior information used by inversions (Petrescu et al., 2021a). In Figure 1, hatched transparent bars represent the 2011-2015 mean while colour-filled bars represent the new updated 2015-2019 mean values. For GAINS and some inversions that do not have annual estimates for all five years, only the average of available years is calculated (e.g., 2015 for GAINS).

For all study regions, 2019 CH<sub>4</sub> emissions decreased by 24 % (Southern Europe) to 57 % (Eastern Europe), with respect to NGHGI 1990 values; and for EU27+UK emissions decreased by 39 %. The decrease in CH<sub>4</sub> emissions is mainly due to the EU legislation policies and strategies starting with the implementation in the early 90s of European and country-specific emission reduction policies on agriculture and the environment, as well as socioeconomic changes in the sector resulting in overall lower agricultural livestock and lower emissions from managed waste disposal on land and from agricultural soils. After 2005, these trends maintain their decreasing trajectory, even if, at a lower intensity. For the Central and Eastern Europe, reductions were abrupt and mainly due to the dissolution of the Soviet Union (1989–1991) and the consequent structural changes in the economy of the former eastern European communist centralized economy block (Petrescu et al., 2020). This is encouraging in the context of meeting EU total GHG commitments under the Paris Agreement (55% decrease in 2030 compared to 1990 levels and reaching carbon

neutrality by 2050). This reduction will need to be achieved by strong reductions in top emitter sectors (e.g. Agriculture) and compensated by sinks in the LULUCF sector. It also shows that not only at EU27+UK level, but also at regional European level, the emissions from BU (anthropogenic and natural) and TD estimates agree in magnitude with reported NGHGI data despite the high uncertainty associated with the TD estimates. This uncertainty is represented here by the variability in the model ensembles and denotes the range (min and max) of estimates within each model ensemble. The comparison of TD to anthropogenic estimates (Fig. 1), suggests that the total  $\text{CH}_4$  flux is dominated by natural emissions (i.e., Northern Europe) although comparison with EDGAR v6.0 would indicate that anthropogenic emissions are dominant (e.g. Northern, Central and Western Europe).

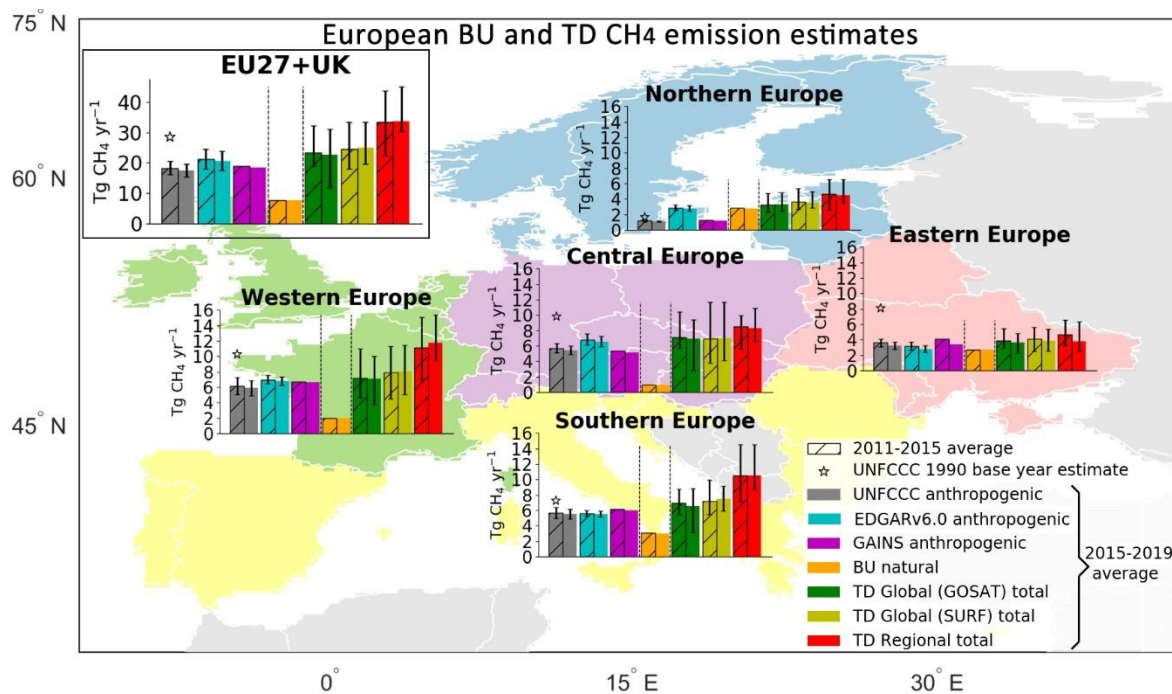


Figure 1: Five-year means (2011-2015, hashed bars and 2015-2019 full bars) in total  $\text{CH}_4$  emission estimates (excluding LULUCF) for EU27+UK and five European regions (North, West, Central, South and East non-EU). Eastern European region does not include European Russia. Northern Europe includes Norway. Central Europe includes Switzerland. The data comes from UNFCCC NGHGI (2021) submissions (grey), which are plotted with respective base year 1990 (black star) estimates, two inventories (GAINS and EDGAR v6.0), natural unmanaged emissions (sum of peatland, geological, inland waters (RECCAP2) and GFEDv4.1 biomass burning emissions) and three inversion estimates: one regional European inversion (excluding InGOS unavailable for 2013-2015) and GOSAT and SURF ensemble estimates from global inverse models. The relative error on the UNFCCC value represents the NGHGI (2021) reported uncertainties computed with the error propagation method (95% confidence interval) and gap-filled to provide respective estimates for each year. Uncertainty for EDGAR v6.0 was calculated for 2015 based on the 95 % confidence interval of a lognormal distribution (Solazzo et al., 2021).



The EDGAR v6.0 updated estimates for Northern Europe remain two-times higher than NGHGI and GAINS ones. The EDGAR approach is to use a globally harmonised methods and sources of data, which means that country-specific detail is often replaced with global averages. In some countries and for some sectors or gases, these assumptions lead to huge differences. For example, fugitive emissions of methane in the oil and gas sector are estimated based on the level of production of oil and gas. In the case of Norway this ignores the substantial effects of regulation on reducing such fugitive emissions. Instead, EDGAR's methane emissions estimates for Norway follow the pattern of its total production of oil and gas (Olhoff et al., 2022). For Eastern Europe we note that all estimates decreased compared to the previous five year mean and the BU anthropogenic estimates remain similar in magnitude to the TD estimates of total CH<sub>4</sub> emissions. One possible explanation is that for TD estimates (i.e. using atmospheric inversions) the fluxes are better constrained by a larger number of observations. Where there are fewer or no observations, like in Eastern Europe, the fluxes in the inversion will stay close to the prior estimates, since there is little or no information to adjust them.

In line with Bergamaschi et al., 2018a the potentially significant contribution from natural unmanaged sources (peatlands, mineral soils, geological and inland waters (RECCAP2)), which for EU27+UK accounted in 2019 for 8 Tg CH<sub>4</sub> yr<sup>-1</sup> (Figure 1) can be highlighted. Taking into account these natural unmanaged CH<sub>4</sub> emissions, and adding it to the range of the BU anthropogenic estimates (22 Tg CH<sub>4</sub> yr<sup>-1</sup> (NGHGI) – 26 Tg CH<sub>4</sub> yr<sup>-1</sup> (EDGARv6.0)) improves agreement with the TD estimates. BU estimates become consistent with the lower range of the regional total TD estimates (32 Tg CH<sub>4</sub> yr<sup>-1</sup> (TM5\_JRC)– 41 Tg CH<sub>4</sub> yr<sup>-1</sup> (FLEXINVERT)) and show even better agreement in absolute values with the global median SURF (24 Tg CH<sub>4</sub> yr<sup>-1</sup>) and GOSAT (23 Tg CH<sub>4</sub> yr<sup>-1</sup>) inversions. The broad consistency between the TD and BU estimates could be interpreted in two ways: 1) BU and TD regional estimates are similar given the large uncertainties and spread in TD results, or 2) regional TD higher estimates potentially indicate shortcomings of BU inventories, the latter interpretation being more consistent with the general atmospheric developments (WMO, 2021).

Is it notable to highlight that the regional TD total is considerably higher for all regions and EU27+UK total and by considering this estimate the best to date total estimate for the whole Europe, including all sources and sinks, this would infer a missing of 20 to 30 % of CH<sub>4</sub> emissions from the other BU approaches.

### ***3.1.2. NGHGI sectoral emissions and decadal changes***

According to the UNFCCC (2021) NGHGI estimates, in 2019 the EU27+UK emitted GHGs totaling 3.7 Gt CO<sub>2</sub>e (including LULUCF), of this total, CH<sub>4</sub> emissions accounted for 11.8 % (0.4 Gt CO<sub>2</sub>e or 17.5 Tg CH<sub>4</sub> yr<sup>-1</sup> ± 2.2 Tg CH<sub>4</sub> yr<sup>-1</sup>) (Appendix, B2, Figure B2a) with France, UK and Germany together contributing 37 % of total CH<sub>4</sub> emissions.

The data in Figure 2 shows anthropogenic CH<sub>4</sub> emissions and their change from one decade to the next, from UNFCCC NGHGI (2021), with the split between the different sectors. In 2019, NGHGI report CH<sub>4</sub> from agricultural activities to be 52.4 % (± 8.7 %) of the total EU27+UK CH<sub>4</sub> emissions, followed by emissions from waste, 27.5 % (± 22.5 %). The large share of agriculture in total anthropogenic CH<sub>4</sub> emissions also holds at global level (IPCC Special Report on Climate Change and Land (SRCCL), 2019). Between the 1990s and the 2000s, the net 17.6 % reduction

originates largely from the energy and waste sectors, with only negligible contributions to emission trends and levels from IPPU (metal and chemical industry) and LULUCF. Between the 2000s and 2010-2019, a further reduction by 16.5 % is observed with the waste sector as the largest contributor to this reduction. The two largest sectors contributing to total EU27+UK emission are agriculture and waste, but energy and waste are showing the higher reductions over the last decade.

The reduction observed in the waste sector coincide with the adoption of the first EU methane strategy published in 1996 (COM(96) 557, 1996). EU legislation addressing emissions in the waste sector may have been successful to trigger the largest reductions. Directive 1999/31/ EC on the landfill (also referred to as the Landfill Directive) required the Member States to separate waste, minimizing the amount of biodegradable waste disposed untreated in landfills and to install landfill gas recovery at all new sites. Based on the 1999 Directive, the new 2018/1999 EU Regulation on the Governance of the Energy Union requires the European Commission to propose a strategic plan for methane, which will become an integral part of the EU's long-term strategy. In the waste sector, the key proposal included the adoption of EU legislation requiring the installation of methane recovery and use systems at new and existing landfills. Other suggested actions included measures aimed at the minimization, separate collection and material recovery of organic waste (Olczak and Piebalgs, 2019).

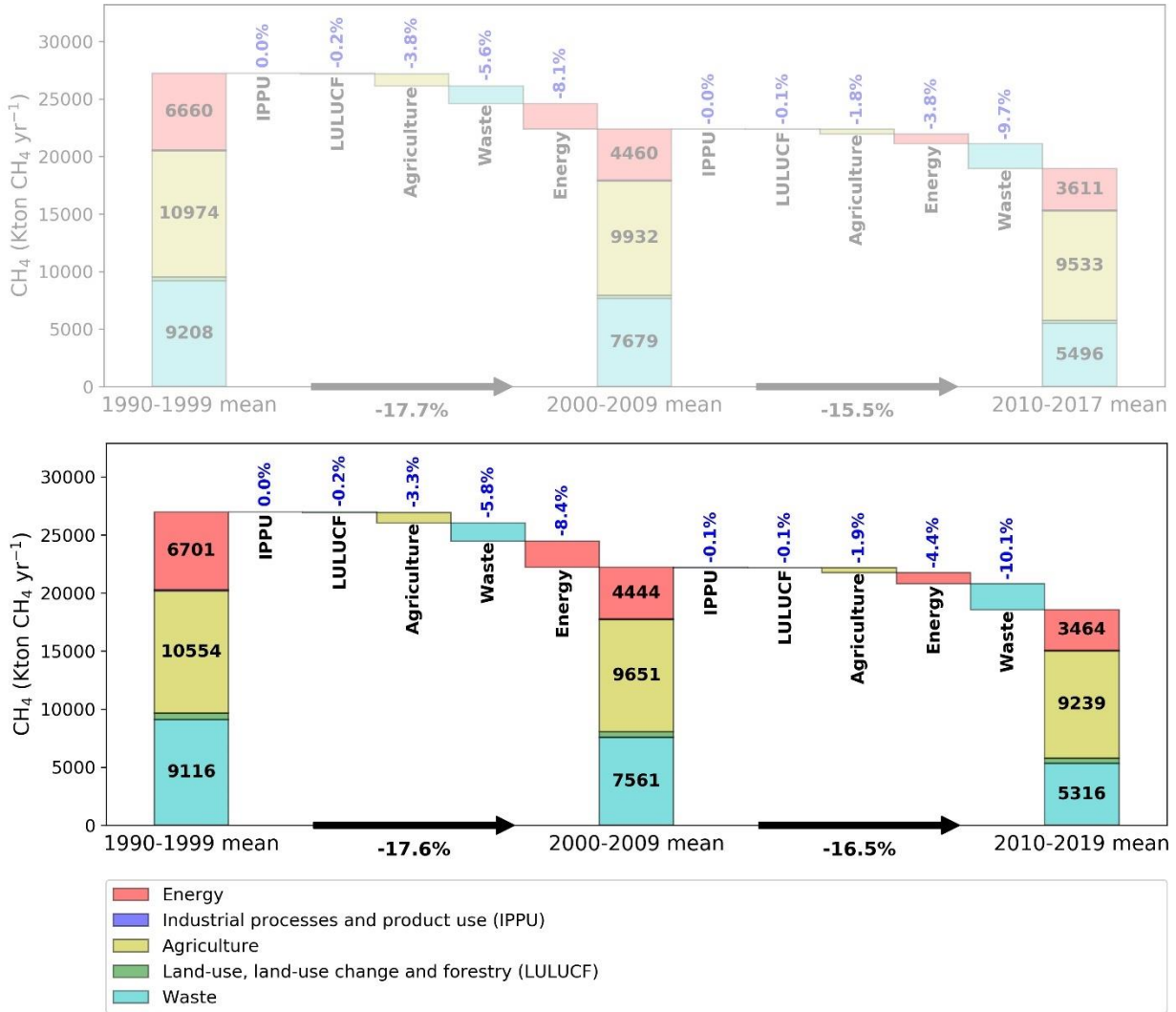


Figure 2: The contribution of changes (%) in CH<sub>4</sub> anthropogenic emissions in the five sectors to the overall change in decadal mean for the EU27+UK, as reported to UNFCCC. The top plot shows the previous NGHGI data from Petrescu et al., 2021a and bottom plot illustrates data from UNFCCC NGHGI (2021). The three stacked columns represent the average CH<sub>4</sub> emissions from each sector during three periods (1990-1999, 2000-2009 and 2010-2019) and percentages represent the contribution of each sector to the total reduction percentages (black arrows) between periods.

### 3.1.3. NGHGI estimates compared with bottom-up inventories

The data in Figure 3 presents the total anthropogenic CH<sub>4</sub> emissions from four BU inventories and UNFCCC NGHGI (2021) submissions excluding emissions from LULUCF, which was identified to a non-significant contributor (Figure 2). According to NGHGI, in 2019 anthropogenic CH<sub>4</sub> emissions from the four sectors (Table 1, excluding LULUCF) amounted to 17.1 Tg CH<sub>4</sub> yr<sup>-1</sup>, representing 10.5 % of the total EU27+UK GHG emissions in CO<sub>2</sub>eq.. Figure 3a shows EDGARv6.0 and GAINS trends being consistent with the ones of NGHGI (excluding LULUCF), although while GAINS and NGHGI agree in terms of emissions levels. EDGARv6.0 estimates are consistently higher

estimates (~19 %) than NGHGI. In contrast to the previous version, EDGAR v4.3.2, which was found by Petrescu et al. 2020 to be consistent with NGHGI (2018) data, EDGAR v6.0 reports higher estimates than EDGARv5.0 (~8% higher) and falls outside the 9.6 % UNFCCC uncertainty range. Over the 1990-2019 period, the trends in emissions agree well between the two BU data sets and NGHGI, showing linear trend reductions of 40 % for EDGAR v6.0 and 36 % for GAINS and NGHGI. The average yearly reduction trend was 2 % yr<sup>-1</sup> for all three data sources .

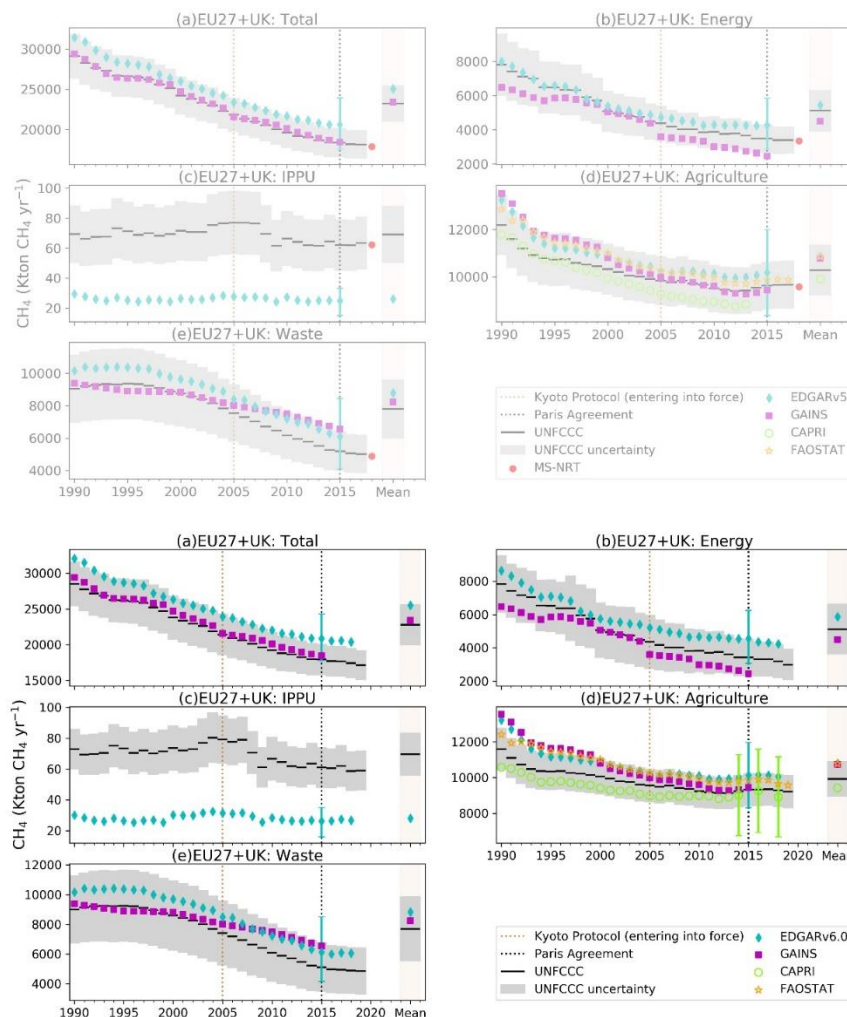


Figure 3: Total annual anthropogenic CH<sub>4</sub> emissions (excluding LULUCF) for the EU27+UK over time. The top plot presents previous data synthesized in Petrescu et al., 2021a while bottom plot data synthesized by the current study: a) EU27+UK and total sectoral emissions from: b) Energy, c) Industry and Products in Use (IPPU), d) Agriculture and e) Waste from UNFCCC NGHGI (2021) submissions compared to global bottom-up inventory models for agriculture (CAPRI, FAOSTAT) and all sectors excl. LULUCF (EDGAR v6.0, GAINS). CAPRI reports one estimate for Belgium and Luxembourg. The relative error on the UNFCCC value represents the UNFCCC NGHGI (2021) Member States reported uncertainties computed with the error propagation method (95% confidence interval) that were gap-filled and provided for every year. The uncertainty for EDGARv6.0 is the same as that of v5.0 and calculated for 2015 as min/max values for the total and each sector (Solazzo et al., 2021) and represents the 95 % confidence

interval of a lognormal distribution. The mean column represents the common overlapping periods between datasets: 1990-2015 for Total EU27+UK, Energy, Agriculture and Waste, 1990-2018 for IPPU and 1990-2014 for CAPRI. Last years of the time series of the respective datasets are 2018 (EDGAR v6.0, CAPRI) 2019 (FAOSTAT, UNFCCC) and 2015 (GAINS). After 2014 CAPRI delivered estimates for two additional years, 2016 and 2018 as well as uncertainties for 2014 and 2018 (25.1 %) and 2016 (25.2 %).

Sectoral time series of anthropogenic CH<sub>4</sub> emissions (excluding LULUCF) and their means are shown in Figures 3b,c,d and e. For the energy sector (Figure 3b), both EDGAR v6.0 and GAINS agree in trends with the NGHGI thanks to updated methodology that derives emission factors and accounts for country-specific information about associated petroleum gas generation and recovery, venting and flaring (Höglund-Isaksson, 2017). After 2005, GAINS reports consistently lower emissions than UNFCCC due to a phase-down of hard coal production in Czech Republic, Germany, Poland and the UK, a decline in oil production in particular in the UK, and declining emission factors reflecting reduced leakage from gas distribution networks as old town gas networks are replaced. A difference in tiers is also one reason for the differences (Petrescu et al., 2020).

The consistently higher estimates (+6 % compared to the UNFCCC mean) of EDGAR v6.0 might be due to the use of default emission factors for oil and gas production based on data from the US (Janssens-Maenhout et al. (2019)). There are several other reasons that could be the cause for the differences, including the use of Tier 1 emission factors for coal mines, assumptions for material in the pipelines (in the case of gas transport) and the activity data). Also EDGAR v6.0, similar to the previous estimates from EDGARv5.0 uses the gas pipeline length as a proxy for the activity data however this may not be appropriate for the case of the official data, which could consider the total amount of gas being transported or both methods according to the countries. Using pipeline length may overestimate the emissions because the pipeline is not always at 100% capacity thus a larger amount of methane is assumed to be leaked (Rutherford et al., 2021). For coal mining, emissions are a function of the different types of processes being modelled.

The IPPU sector (Figure 3c), which has only a small share of the total emissions, is not included in GAINS, while EDGAR v6.0 estimates are less than half of the emissions reported by NGHGI 2021 in this sector. The discrepancy for this sector has negligible impact on discrepancy for the total CH<sub>4</sub> emission. However, we identified that the low bias of EDGAR v6.0 could be explained by fewer activities included in EDGAR v6.0 (e.g. missing solvent, electronics and other manufacturing goods) accounting for 5.5 % of the total IPPU emissions in 2015 reported to UNFCCC. The reason for the remaining difference could be explained by the allocation of emissions from auto-producers<sup>8</sup> in EDGAR v6.0 to the Energy sector (following the 1996 IPCC guidelines), while in NGHGI they are reported under the IPPU sector (following the 2006 IPCC guidelines).

As CAPRI and FAOSTAT report only emissions from agriculture, they are included only in Fig. 3d. The data (EDGAR v6.0, GAINS, CAPRI and FAOSTAT) shows good agreement, with CAPRI at the lower range of emissions (Petrescu et al., 2020) and on average 3% lower than that of NGHGI, and EDGAR v6.0 at the upper range. The reason for EDGAR v6.0 having the highest estimate (contrary to Petrescu et al., 2020 where NGHGI were the highest and

---

<sup>8</sup> auto-producers of electricity and heat: cogeneration by industries and companies for housing management (central heating and other services) (Olivier et al., 2017 PBL report)

EDGAR v4.3.2 was the second highest) is likely due to the activity data updates in EDGAR v6.0 based on FAOSTAT values, compared to EDGAR v4.3.2. When looking at the time series mean, EDGAR v6.0, GAINS and FAOSTAT show 5 % higher emissions than that of NGHGI. The three BU estimates and NGHGI estimates show similar mean values likely due to the use of similar activity data and emission factors (EFs) (i.e. Figure 4 in Petrescu et al., 2020). The updates submitted by CAPRI, for the years 2014, 2016 and 2018 match the NGHGI emission estimates and have uncertainties of 21 %. Compared to the previous version of CAPRI used in Petrescu et al., 2021a, the new runs report lower CH<sub>4</sub> emissions. Compared to previous results, in the last version some changes have been implemented in the last version (e.g. introduction of slope and altitude limits based on LUCAS<sup>9</sup>, improved distribution of grazing livestock etc.). The main activity triggering the differences was the emissions from enteric fermentation. Statistical information on most agricultural data required for the estimation of CH<sub>4</sub> and N<sub>2</sub>O emissions are not available at high spatial (regional) and temporal (annual since 1990) resolution. Therefore, the CAPRI model features a module that provides generic data at regional level (CAPREG) and additionally a module that also estimates feed distribution and GHG emissions at the required resolution for VERIFY (CAPINV). As indicated in an internal VERIFY report (Leip et al., 2019), the results of the CAPINV module were scrutinized and shortcomings were identified. These concern mainly the distribution of feed, which is one of the most important parameter for CH<sub>4</sub> emissions from enteric fermentation, and manure excretion and subsequent GHG emissions. Other updates included addition of some regional input data (sources: FAOSTAT and EUROSTAT).

For the waste sector (Figure 3e) EDGAR v6.0 shows consistently higher estimates compared to the NGHGI data, while GAINS has higher emissions than the NGHGI after 2000 (mean 1990-2015 value 6% higher than NGHGI emissions). The two inventories, EDGAR v6.0 in its 2020 update for landfills, and GAINS used an approach based on the decomposition of waste into different biodegradable streams, with the aim of applying the methodology described in the 2019 Refinement of the 2006 IPCC guidelines and the IPCC waste model (IPCC, 2019) using the First-Order-Decay (FOD) method. The main differences between the two datasets come from i) sources for total waste generated per person, ii) assumption for the fraction composted and iii) the oxidation. The two inventories may have used different strategies to complete the waste database when inconsistencies were observed in the EUROSTAT database or in the waste emissions trends in NGHGI.

### ***3.1.4. NGHGI estimates compared to atmospheric inversions***

#### ***European estimates from regional inversions***

Figure 4 compares TD regional estimates, NGHGI anthropogenic data for CH<sub>4</sub> emissions and natural BU emissions. Figure 4a presents TD estimates of total emissions (anthropogenic and natural) from Petrescu et al., 2021a while Fig. 4b shows the current study with updated total TD estimates. Figs. 4c and 4d show estimates of anthropogenic emissions (Petrescu et al., 2021a and current study) calculated by subtracting the total natural emissions from the total TD emissions.

---

<sup>9</sup> <https://ec.europa.eu/eurostat/web/lucas>

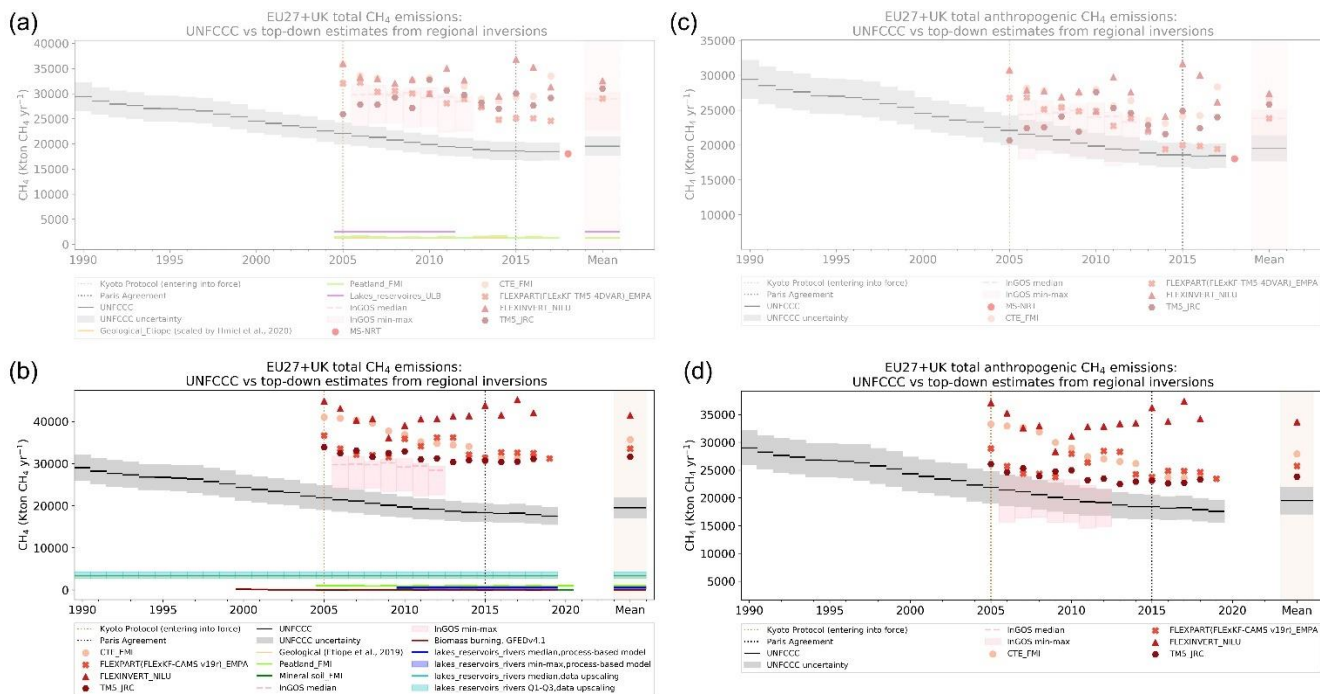


Figure 4: a) and b) Comparison of total  $\text{CH}_4$  emissions for EU27+UK from four top-down regional inversions with UNFCCC NGHGI (grey) data and two estimates for inland waters (lakes\_rivers\_reservoirs process-based models, blue and upscaled emissions, cyan), peatlands and mineral soils (from JSBACH-HIMMELI, light green and dark green), geological emissions (orange) and biomass burning, (from GFEDv4.1, brown) as following: a) shows previous data from Petrescu et al., 2021a and b) current study; c) and d) comparison of anthropogenic  $\text{CH}_4$  emissions from four top-down regional inversions with UNFCCC NGHGI (grey) data as following: c) previous data from Petrescu et al., 2021a and d) current study. Anthropogenic emissions from these inversions are obtained by removing natural emissions and biomass burning from total TD  $\text{CH}_4$  emissions shown in Figure 4a,b. UNFCCC NGHGI (2021) reported uncertainties computed with the error propagation method (95% confidence interval) were calculated for each year of the time series and represents the gap-filled harmonized Member States reported uncertainty for all sectors (including LULUCF). The time series mean was computed for the common period 2005-2018 between datasets (excluding InGOS).

The TD estimates of European  $\text{CH}_4$  emissions in Figure 4b use four European regional models for 2005-2018 period and an ensemble of five different inverse models (InGOS, Bergamaschi et al., 2015) for 2006-2012. For the 2005-2018 period (excluding InGOS), the four regional inversions give a total  $\text{CH}_4$  emissions mean of 36 (32-42)  $\text{Tg CH}_4 \text{ yr}^{-1}$  compared to anthropogenic total of 20  $\text{Tg CH}_4 \text{ yr}^{-1}$  in NGHGI (Fig. 4b). The large positive difference between TD and NGHGI suggests a potentially significant contribution from BU natural sources, represented separate in Figure B1c, Appendix B (peatlands, geological sources, inland waters and biomass burning), which for the same period are estimated at 8  $\text{Tg CH}_4 \text{ yr}^{-1}$ . However, it needs to be emphasized that natural wetland emission estimates have large uncertainties and show large variability in the spatial (seasonal) distribution of  $\text{CH}_4$  emissions but for



Europe their inter-annual variability is not very strong (mean of 14 years from JSBACH-HIMMELI peatland emissions is  $1.0 \text{ Tg CH}_4 \text{ yr}^{-1}$ ). Overall, they do represent an important source, and could dominate the budget assessments in some regions such as Northern Europe (Figure 1). That TD and NGHGI diverged in terms of both emissions levels and trends is certainly significant and potentially has implications for bottom-up and NGHGI estimates of  $\text{CH}_4$  emissions, if the discrepancies cannot be explained by natural fluxes alone.

The differences between inversion results in current study and Petrescu et al., 2021a can be summarized as following: for the version used in this study, FLE<sub>x</sub>KF-CAMsv19r\_EMPA, the background mole fraction was taken from a global CAMS v19r assimilation run with assimilation of surface observations of  $\text{CH}_4$  only (no satellite data) where the domain was cut out following the two-step approach of Rödenbeck et al. (2009). Background concentrations from CAMS v19r are on average about 5 ppb lower than those of the TM5-4DVAR system used previously, which results in somewhat higher emission estimates over Europe compared to Petrescu et al. (2021a). The major differences to previous CTE-FMI run are the prior fluxes, except for biomass-burning which remained GFED. The new VERIFY\_S5 (core) run uses fluxes as described in Thompson et al., 2021. The new VERIFY\_S5 (core) run uses fluxes as described in Thomson et al., 2021. Lake & geological emissions were not included in Petrescu et al., 2021a synthesis, but are included in the current CTE-FMI simulation, which probably also contributes to higher total emissions. On top of this, the assimilated data (i.e. observation network) contributes to the differences (enlarged observation network, more sites (five core sites for  $\text{CH}_4$  located in Spain, France and UK were added). The FLEXINVERT version used in this study updated the atmospheric observation network (more sites were added) as well as the prior emissions. The background mole fraction was also coupled with that from CAMS v19r assimilation run, which, similar to FLE<sub>x</sub>KF model, might imply higher emissions. Regarding decreasing trends seen for the current inversion  $\text{CH}_4$  results, for FLE<sub>x</sub>KF model the trend in  $\text{CH}_4$  emission was slightly negative over 2005-2019, at  $-0.48\%$  per year, which is lower than the decrease in the prior of  $-0.8\%$  per year. For the other models, based on Thompson et al., 2021, the differences in trends might be due to regional vs. global inversion differences.

The geological emissions were recalculated based on the global grid model of Etiope et al (2019), using more precise “activity” data for EU27+UK (details in Appendix A2): the emission resulted to be  $3.3 \text{ Tg CH}_4 \text{ yr}^{-1}$ , i.e. 42 % of the total natural  $\text{CH}_4$  emissions in EU27+UK. Geological emissions are an important component of the EU27+UK emissions budget, but their temporal variability is unknown (Etiope and Schwietzke, 2019) and so their impact on climate warming cannot be predicted.

The other natural sources of  $\text{CH}_4$  contribute as following: natural emissions from inland waters (based on Lauerwald et al., in rev. GBC, see Appendix A2) contribute  $3.4 \text{ Tg CH}_4 \text{ yr}^{-1}$ , or 43 % of the total natural  $\text{CH}_4$  emissions; peatlands and mineral soils (Raivonen et al. 2017 and Susiluoto et al. 2018) account for  $1.0 \text{ Tg CH}_4 \text{ yr}^{-1}$ , i.e. 13.4 % of the total natural  $\text{CH}_4$  emissions while biomass burning contributes only 0.6 % to the total  $\text{CH}_4$  natural emissions. Similar to peatlands, inland water emissions also remain highly uncertain. The compilation of emission estimates lead to a total flux that is  $3.3 \text{ Tg CH}_4 \text{ yr}^{-1}$  (min  $2.7 \text{ Tg CH}_4 \text{ yr}^{-1}$  and max  $4.3 \text{ Tg CH}_4 \text{ yr}^{-1}$ ) and about five times larger than the process-based model estimates for lakes+reservoirs and the spatially resolved flux for rivers ( $0.6 \text{ Tg CH}_4 \text{ yr}^{-1}$  with min 0.2 and max  $0.8 \text{ Tg CH}_4 \text{ yr}^{-1}$ ) and about 25 % larger than the previous budget in Petrescu et al., 2021a ( $2.5 \text{ Tg CH}_4 \text{ yr}^{-1}$ ), which ignored the contribution of rivers and relied on one observation-based estimate (extrapolation from



late-summer data reported in Rinta et al. 2017) and four semi-empirical model assessments (Petrescu et al., 2021a). Interestingly, the new process-based estimate for natural lake+reservoirs CH<sub>4</sub> emissions matches well the data-driven assessment by Rinta et al. (2017) for the late summer season, with a relative difference smaller than 5 %. The first approach synthesizes 15 average annual CH<sub>4</sub> emissions fluxes for Europe that were rescaled to a consistent set of inland water surface area (Lauerwald et al., in rev. GBC) and corrected for the effect of seasonal ice cover.

Model results however also reveal a strong seasonal variability in CH<sub>4</sub> emissions, with much lower fluxes during winter. This seasonality is driven by physical factors (changing ice cover and bottom-water temperature) and biogeochemical factors (autotrophic primary production) that are well established drivers of the temporal variability in lake CH<sub>4</sub> emissions (Del Sontro et al., 2018; Jansen et al., 2022). This finding provides a likely explanation as to why the spatio-temporally resolved model results lead to significantly lower estimates than observation-based methods that do not capture well the temporal variability in lake CH<sub>4</sub> emissions.

According to the IPCC 2006 guidelines (IPCC, 2006) CH<sub>4</sub> emissions from wetlands are reported by the Member States to the NGHGI under the LULUCF sector and considered anthropogenic, if the wetlands in question are considered managed land. They are included in the total LULUCF values (Figure 1, 2, 4 and 6) and in 2019 reported CH<sub>4</sub> emissions from wetlands accounted for 0.1 Tg CH<sub>4</sub> yr<sup>-1</sup>.

To quantify the anthropogenic CH<sub>4</sub> component in the European TD estimates, the BU peatland emissions from the regional JSBACH-HIMMELI model and those from geological, inland water sources and biomass burning were subtracted from the total TD emissions (Fig. 4d). It remains however uncertain to perform these corrections due to the prior inventory data allocation of emissions to different sectors (e.g. anthropogenic or natural) used in inversions, which can induce uncertainty of up to 100 % if for example an inventory allocates all emissions to natural emissions and the correction is made by subtracting the natural emissions. All regional inversion anthropogenic estimates are higher compared to the UNFCCC NGHGI (2021), mean of 28 Tg CH<sub>4</sub> yr<sup>-1</sup> from inversions compared to 20 Tg CH<sub>4</sub> yr<sup>-1</sup> from the NGHGIs.. Regarding trends, TD are stable except for CTE showing a linear decreasing trend up to 2015 followed by an increase over the next three years, while NGHGIs and BU trends are declining. From this attempt we find that not many of the inversions showed the clear decline reported by the NGHGIs. As NGHGI emissions are dominated by anthropogenic fluxes and decline by almost 30% compared to 1990, a similar decline was expected in the corrected anthropogenic inversions. Further investigation into how well the NGHGIs reflect reality or how well the TD estimates capture the trends is clearly needed. Currently, in the UK NIR (<https://unfccc.int/documents/273439>) the national inversion system produced similar recent UK CH<sub>4</sub> emission levels, but did not validate the large declining trend since 1990 that is estimated by the UK inventory.

#### ***Spatial distribution of CH<sub>4</sub> emissions from regional inversions***

A novelty in this study is represented by the new top-down estimates of CH<sub>4</sub> fluxes were also calculated in this reporting period using the Community Inversion Framework (CIF) (Berchet et al. 2021). For CH<sub>4</sub> (Figure 5), inversions using three atmospheric transport models (or model variants) were performed with the CIF, there were: i) the regional non-hydrostatic Eulerian model, CHIMERE (Fortems-Cheiney et al., 2021) used by LSCE, ii) the

Lagrangian particle dispersion model, FLEXPART used by EMPA (from hereon, FLEXPART-EMPA), and iii) FLEXPART used by NILU (from hereon, FLEXPART-NILU).

The spatial distribution of  $\text{CH}_4$  fluxes are similar for the three inversions with higher emissions in the Netherlands and Belgium, western France and southern UK. However, FLEXPART-NILU inversions show some spurious areas of very low fluxes in Italy, Switzerland and southern France, which are presumably owing to the positive bias in the prior modelling mixing ratios at mountain sites, which will be corrected in future simulations. The patterns of differences, however, are quite different between the CHIMERE and the two FLEXPART inversions. All inversions find positive increments (posterior high than prior) over northern Netherlands, but FLEXPART-EMPA finds negative increments over southern Netherlands and both FLEXPART inversions find negative increments over northern Italy, which is not the case in CHIMERE (Figure 5, top). The total mean emissions for EU27+UK over 2006-2017 (Figure 5) were 26, 22 and 24  $\text{Tg CH}_4 \text{ yr}^{-1}$ , for CHIMERE, FLEXPART-NILU and FLEXPART-EMPA, respectively. FLEXPART-EMPA is the same model as used in the comparison shown in Figure 4 (FLEXPART(FLExKF-CAMSv19r)) but in those inversions the total mean emissions for EU27+UK were higher at 33  $\text{Tg yr}^{-1}$ . This difference is likely owing to the different dataset used for determining the background mixing ratios and farther analysis is ongoing.

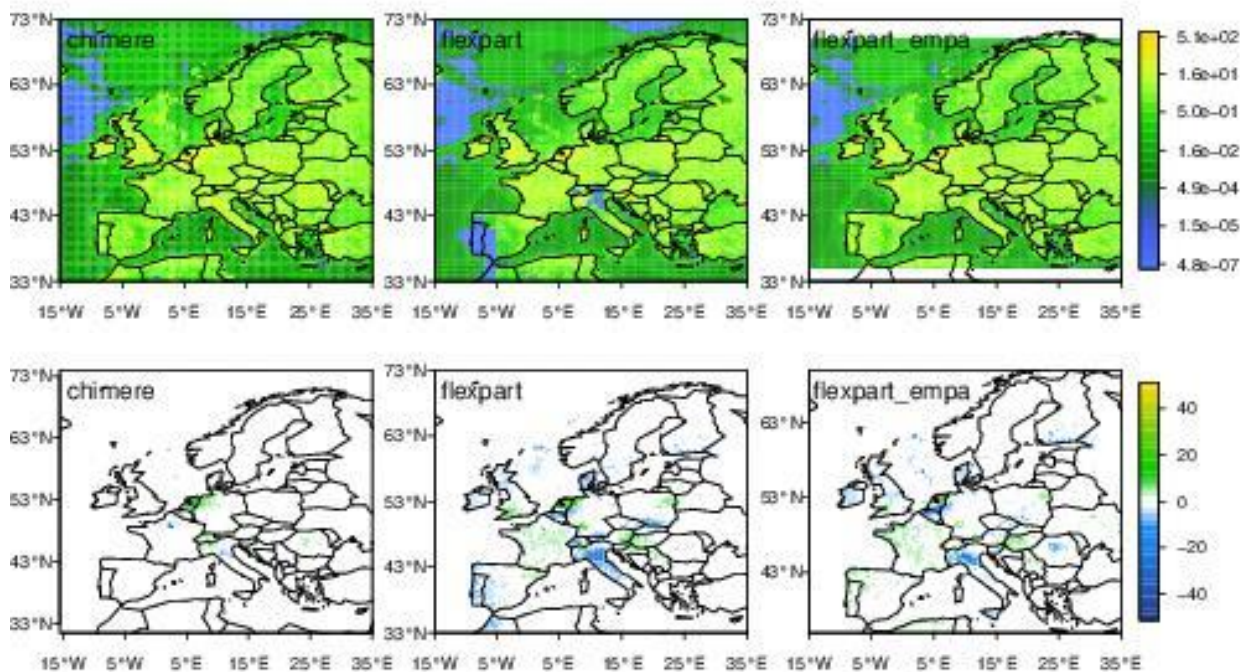


Figure 5: Posterior  $\text{CH}_4$  fluxes averaged over 2006-2017 ( $\text{g CH}_4 \text{ m}^{-2} \text{ yr}^{-1}$ ) from three regional inversions, CHIMERE (LSCE), FELXPART (NILU) and FLEXPART (EMPA) shown with a log base 2 color scale (top) and the flux increments (posterior-prior) ( $\text{g CH}_4 \text{ m}^{-2} \text{ yr}^{-1}$ ) shown on a linear color scale (bottom).

### European estimates from global inversions

Figures 6 compares TD global estimates, with NGHGI data and provides information about the wetland emissions from global wetland inversions (Saunois et al., 2020). Figure 6a presents TD estimates of total emissions

(anthropogenic and natural) from Petrescu et al., 2021a while Fig. 6b shows the current study with updated total TD estimates. Figs. 6c and 6d show estimates of anthropogenic emissions (Petrescu et al., 2021a and current study) calculated by subtracting the total natural emissions from the global total TD emissions.

700 The global inversion models were split according to the type of observations used, 11 of them using satellites (GOSAT) and 11 using surface stations (SURF). Each of these 22 global inversions provided as well wetlands emissions used by the Global Methane Budget (Saunois et al., 2020) and are post-processed with prior ratios estimates for wetlands CH<sub>4</sub> emissions (Appendix B2, Table B2.4).

705 For the common period between datasets (2010-2016), the two ensembles of regional and global models give a total CH<sub>4</sub> emission mean (Figure 6a) of 23 Tg CH<sub>4</sub> yr<sup>-1</sup> (GOSAT) and 24 Tg CH<sub>4</sub> yr<sup>-1</sup> (SURF) for the EU27+UK compared to 19 Tg CH<sub>4</sub> yr<sup>-1</sup> ± 2.3 Tg CH<sub>4</sub> yr<sup>-1</sup> of NGHGI (Figure 6a). The mean of the natural wetland emissions from the global inversions is 1.3 Tg CH<sub>4</sub> yr<sup>-1</sup> and partly explains the positive difference between total emissions from inversions and NGHGI anthropogenic emissions.

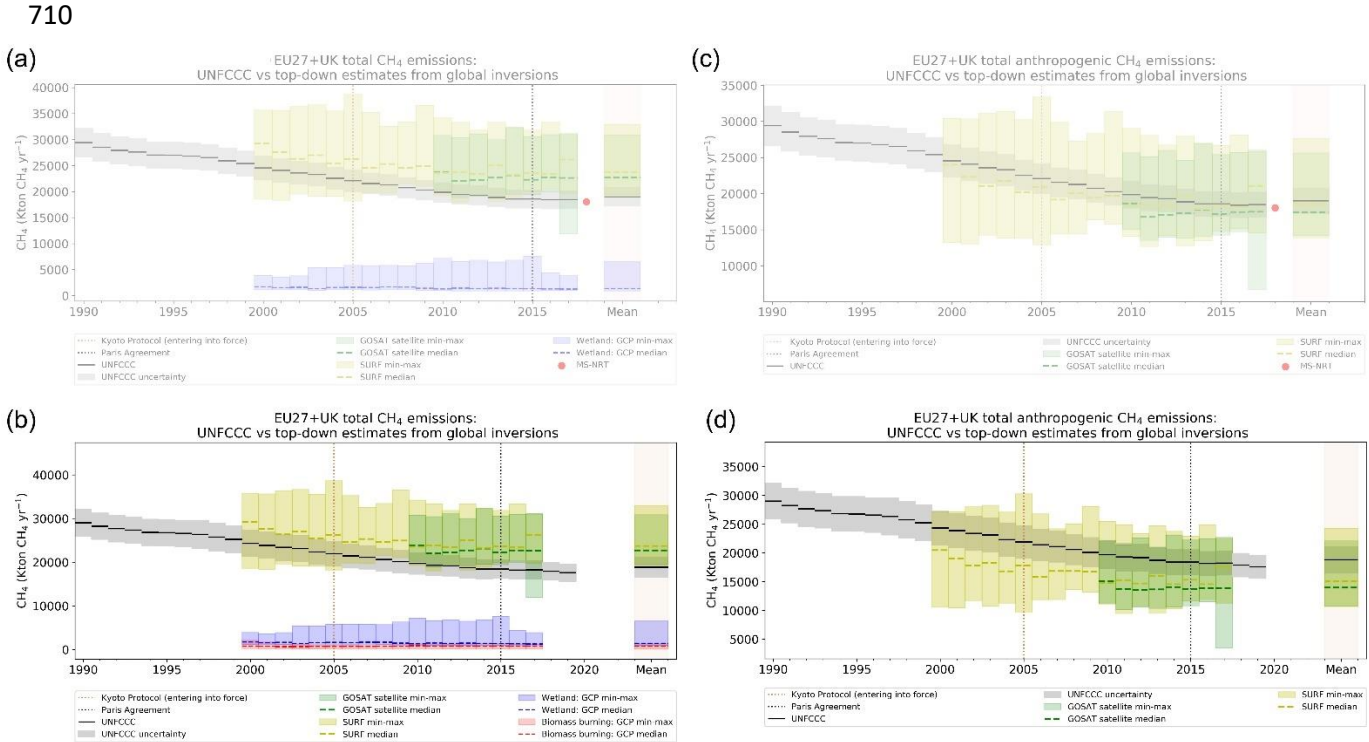


Figure 6: a) and b) Total CH<sub>4</sub> emissions from TD global ensembles based on surface stations data (SURF) (yellow) and satellite concentration observations (GOSAT) (green) from 22 global models compared with UNFCCC NGHGI (grey) data (including LULUCF) as following: a) represents previous data from Petrescu et al., 2021a and b) the current study; c) and d) Anthropogenic CH<sub>4</sub> emissions from top-down global inversions based on surface stations (SURF) (yellow) and on satellite concentration observations (GOSAT) (green) from different estimates as following: c) previous data from Petrescu et al., 2021a and d) the current study. Anthropogenic emissions from these inversions were obtained by removing the sum of the natural emissions (global wetland GCP emissions (blue), the inland waters and geological fluxes as shown in figure 4a) from the total estimates. The biomass burning emissions included in each

inversion results was removed as well. UNFCCC NGHGI (2021) Member States reported uncertainty computed with the error propagation method (95% confidence interval) was gap-filled and provided for every year for all sectors (including LULUCF). The time series mean was computed for the common period 2010-2016. Two out of 11 SURF products (GELCA-SURF\_NIES, TOMCAT-SURF\_UOL) were not available for 2016.

To quantify the European TD anthropogenic CH<sub>4</sub> component, the GCP inversions wetlands emissions and those from geological, inland water sources and biomass burning emissions (reported by the global inversions) were subtracted from the total CH<sub>4</sub> emissions (Fig. 6d).

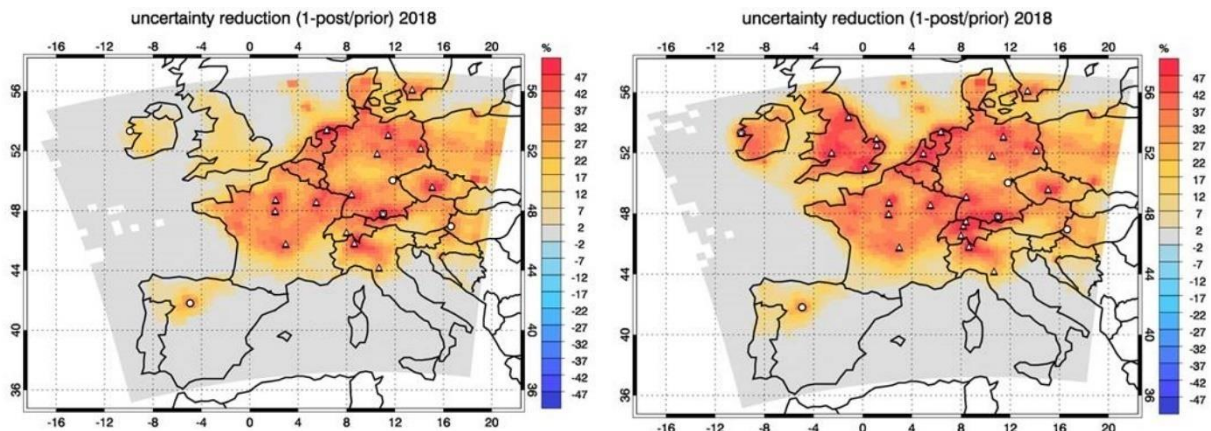
For the 2010-2016 common period, the two ensembles of global models give an anthropogenic CH<sub>4</sub> emission median (Figure 6b) of 13 Tg CH<sub>4</sub> yr<sup>-1</sup> with min and max values of 10 and 21 Tg CH<sub>4</sub> yr<sup>-1</sup> (GOSAT) and 14 Tg CH<sub>4</sub> yr<sup>-1</sup> with min and max values of 9 and 22 Tg CH<sub>4</sub> yr<sup>-1</sup> (SURF) compared to 19 ± 2.3 Tg CH<sub>4</sub> yr<sup>-1</sup> for NGHGI. The TD ensemble that produced the closest anthropogenic estimate (Figure 6d) to the UNFCCC NGHGI (2021) is SURF, with the median of SURF inversions falling just below the uncertainty range of the NGHGI.

Between 2010-2016, total TD CH<sub>4</sub> emissions (Figure 6b) from the SURF and GOSAT ensemble decreased by 0.5% and 4.6%, respectively. For anthropogenic CH<sub>4</sub> emissions (Figure 6d), the SURF and GOSAT ensembles show a decrease of 1.1 % and 6.3%, respectively, compared to the 7.7 % decrease for the NGHGI.

### 3.1.5 CH<sub>4</sub> uncertainty reduction maps

Bergamaschi et al (2010) used TM5 4DVAR to analyze the sensitivity of the modelling system to observations, for further interpretation of the derived emissions, in particular in the context of verification of BU inventories. For this purpose, Bergamaschi et al., 2010 calculated uncertainty reduction maps, as a measure of the sensitivity of the observational network used for the reference inversion. This reduction in uncertainty is calculated as the ratio between a posterior and a prior uncertainty with the formula  $(1 - \Delta_{\text{post}}/\Delta_{\text{prior}})$ , where  $\Delta_{\text{post}}$  represents the posterior uncertainties and  $\Delta_{\text{prior}}$  the prior uncertainties of the inversion system. The same methodology was applied to two VERIFY regional inversions systems, CTE-CH<sub>4</sub> and FLExKF (Brunner et al., 2022).

The first inversion system, FLExKF, calculated the uncertainty reduction maps for CH<sub>4</sub> for the year 2018 with two different sets of observation stations (Figure 7). Maps of uncertainty reduction can be really informative and





the results below (Figure 7) present the uncertainty reductions for two different sets of stations, which show the value of only considering ICOS sites (left figure) and when adding also other stations in the U.K. and Switzerland (right figure). However, the larger the prior uncertainties, the stronger potential for uncertainty reduction is, therefore given that the prior uncertainty varies, the uncertainty reduction is not a direct indication of the information provided by observations.

Figure 7: FLExKF uncertainty reduction maps computed as  $(1 - \Delta_{\text{post}}/\Delta_{\text{prior}})$  for the same year, 2018, but with two different sets of observation stations (white dots).

The second inversion system, CTE-CH4 (Tsuruta et al., 2017) calculated the uncertainty reduction maps from surface inversions (SURF) for 2006 and 2018, as those used in Thompson et al., (2021), referred to here as VERIFY\_S5 ("core" inversion) (Figure 8). The system included two sets of inversions with different observation sets assimilated. However, the degrees of freedom in the state of the system was low, and therefore, the uncertainty estimates may not differ much between the two. The data from CTE-CH4 includes uncertainties (standard deviations) and fluxes for 2006 and 2018. The differences in the simulations are observation sets and underlying prior covariance structure. "VERIFY\_S5" uses data from only those sites that have long-term measurements assimilated i.e. there is little differences in the assimilated sites between the years. From the two panels of the Fig.8, higher uncertainty reductions are seen in 2018 compared to 2006 in E Poland, N Italy and Spain.

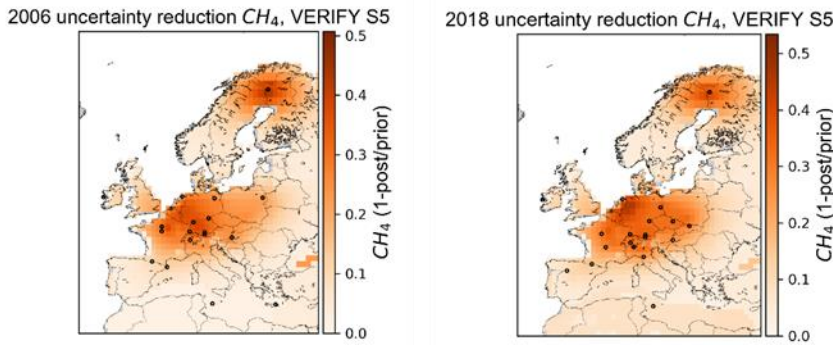


Figure 8: VERIFY\_S5 (core) inversion run, uncertainty reduction maps computed as  $(1 - \Delta_{\text{post}}/\Delta_{\text{prior}})$  for 2006 (left) and 2018 (right) with different sets of observation stations.

The differences between the two years are mostly due to changes in the amount of observational data, although additional observation stations in certain locations may produce only a limited reduction in uncertainty. This can occur if: i) uncertainty assigned to the observations (i.e. how much weight/trust we put on it) are comparatively high, ii) prior emissions and/or their uncertainties around the sites are simply very small, and therefore the inversion does not change fluxes much; and/or iii) the location is not very sensitive to emissions in the surrounding area (e.g. mountain sites) due to the atmospheric transport to the observation site. Generally, sites that contribute to a larger uncertainty reduction should be included in the inversions and located closer to emission sources and/or sink areas.

CTE-CH<sub>4</sub> was also used to estimate fluxes utilizing prior information from GOSAT data, for 2010 and 2017. Figure 9 presents the associated uncertainty reduction maps. Because of the different inversion system set-up (e.g. resolution, spatial correlation) compared to previous results, where prior data was coming from observation networks, it is difficult to conclude on the effects satellites have on posterior emissions from the two years. However, it is interesting to note how satellite data assimilation infers changes on a regional scale. Unlike surface stations, satellite data have more power to constrain northern European emissions than central European emissions.

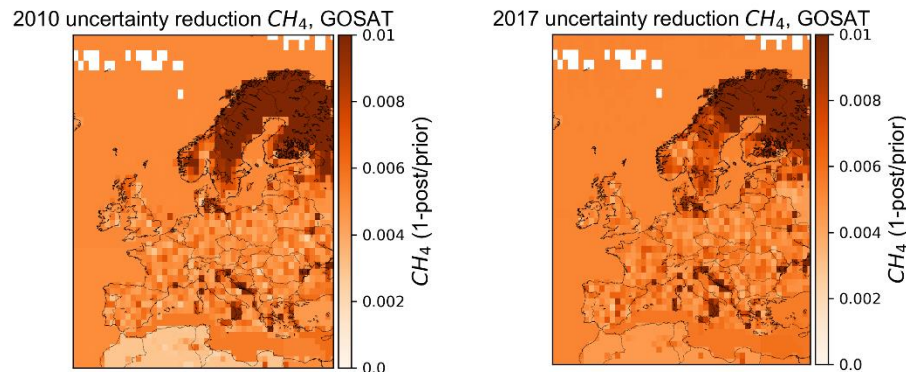


Figure 9: CTE-CH<sub>4</sub> GOSAT inversion run, uncertainty reduction maps computed as  $(1-\Delta_{\text{post}}/\Delta_{\text{prior}})$  for 2010 (left) and 2017 (right).

## 3.2 Comparing N<sub>2</sub>O emission estimates from different approaches

### 3.2.1. Estimates of European and regional total N<sub>2</sub>O fluxes

Total N<sub>2</sub>O fluxes from EU27+UK and five main regions in Europe are presented in a similar fashion as the CH<sub>4</sub>. Figure 10 summarizes the total N<sub>2</sub>O fluxes from NGHGI 2021 (excluding LULUCF) for the base year 1990 as well as mean annual emissions for the 2011-2015 and 2015-2019 five-year periods.

The total UNFCCC estimates that include emissions from all sectors are compared with the fluxes from global datasets, BU models and TD inversions. Relative to 1990, N<sub>2</sub>O emissions in 2019 decreased by a minimum of 26 % (Eastern Europe) up to a maximum of 46 % (Western Europe) and by 39 % for EU27+UK. At European level, the emissions from BU estimates (anthropogenic NGHGI plus the sum of all natural, 991 kton N<sub>2</sub>O) and TD total (including natural) regional estimate (1443 kton N<sub>2</sub>O) averaged over 2015-2019, roughly agree within the uncertainty reported by UNFCCC ( $\pm 59\%$ ). The TD uncertainty is represented as the variability in the model ensembles and denotes the range between the minimum and maximum estimates within each model ensemble. There is significant uncertainty in Northern Europe, where the TD average estimates indicate sources yet the ensemble ranges from a net sink to a net source (Figure 10). The current observation network is sparse, which currently limits the capability of inverse models to quantify N<sub>2</sub>O emissions at country or regional scale.

For all other regions, the BU anthropogenic emissions agree in absolute values with the NGHGI given uncertainties, though consistently higher estimates are produced by TD regional and global models. The difference is still too high to be attributed to the sum of the natural emission, which ranges for all five regions in 2019 between a minimum of 13 kton N<sub>2</sub>O yr<sup>-1</sup> (Northern Europe) to a maximum of 113 kton N<sub>2</sub>O yr<sup>-1</sup> (Southern Europe), while the EU27+UK total natural emission is estimated at 178 kton N<sub>2</sub>O yr<sup>-1</sup>.

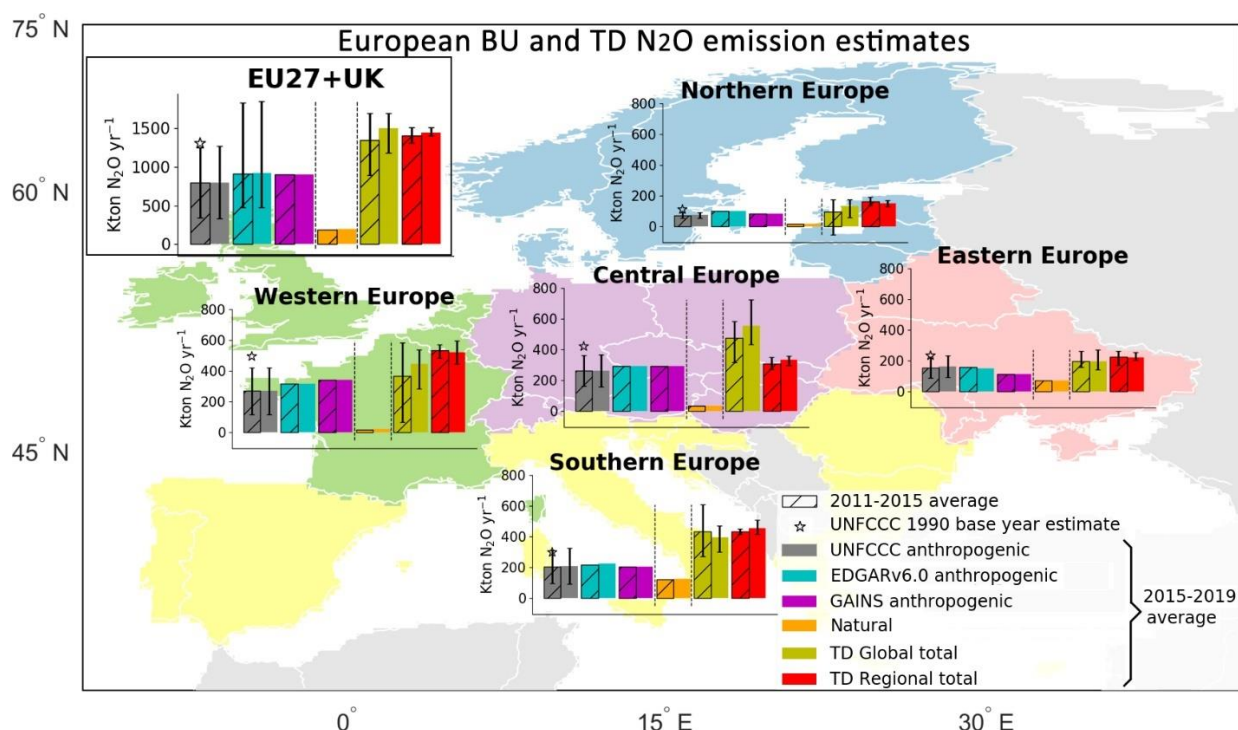


Figure 10: Five-yearly means (2011-2015 hashed bars and 2015-2019 full bars) in total N<sub>2</sub>O emission estimates (excluding LULUCF) for EU27+UK and five European regions (Northern, Western Central, Southern and Eastern non-EU). The Eastern European region does not include European Russia, Northern Europe includes Norway and Central Europe includes Switzerland. The data are from the UNFCCC NGHGI (2021) submissions (grey), which are plotted with respective base year 1990 (black star) estimates, two inventories (GAINS and EDGAR v6.0), natural unmanaged emissions (lakes\_rivers\_reservoirs emissions from RECCAP2 and natural N<sub>2</sub>O from O-CN) and two inversion total estimates (one regional European inversions (FLEXINVERT) and average of three global inverse models from GN<sub>2</sub>OB, Tian et al. 2020). The relative error on the UNFCCC value represents the NGHGI (2021) reported uncertainties computed with the error propagation method (95% confidence interval) and gap-filled to provide respective estimates for each year. (see Appendix A); For Easter Europe non-EU the uncertainty value of 42.3 % was calculated from the NIRs. Northern Europe Tier 1 uncertainty for Norway was not available.

### 3.2.2. NGHGI sectoral emissions and decadal changes

According to the UNFCCC NGHGI (2021) estimates for 2019, the EU27+UK emitted GHGs totaling 3.7 Gt CO<sub>2</sub>e (including LULUCF, using a GWP 100, IPCC AR4) (Appendix B1, Figure B1b), of which N<sub>2</sub>O emissions

accounted for ~7 % (254 Mt CO<sub>2</sub>e or 854 kton N<sub>2</sub>O yr<sup>-1</sup>) (Figure 11). France, Germany and UK together contributed 40 % of total N<sub>2</sub>O emissions (338 kton N<sub>2</sub>O yr<sup>-1</sup>). For 2019, NGHGI reported anthropogenic emissions from the EU27+UK for the four activity sectors (excluding LULUCF) (Table 1), to be 793 kton N<sub>2</sub>O yr<sup>-1</sup>. Agricultural N<sub>2</sub>O emissions accounted for 79 % (± 72.5 %) of total EU27+UK emissions in 2019, followed by emissions from the energy sector with 12 % (± 30 %).

Figure 11 shows anthropogenic N<sub>2</sub>O emissions from UNFCCC NGHGI (2021) and their changes from one decade to the next, with the respective contributions from different sectors also illustrated.

Between the 1990s and the 2000s, the net reduction of 17.9 % originates mainly from IPPU (-13.2 %), with a smaller contribution from agriculture (-4.4 %). For the period between the 2000s and 2010-2019, the net reduction of 15.4 % was again mainly attributed to the IPPU sector (14.1 %), despite very small increases from the LULUCF (0.2 %) and waste sectors (0.2 %).

By 2019, emissions from the IPPU sector were only 36 kton N<sub>2</sub>O yr<sup>-1</sup>, a 91 % decrease compared to 1990. Although the IPPU sector contributes in only 4% to 2019 total N<sub>2</sub>O emissions, it is the sector associated with the largest emissions reduction. IPPU sector emissions are mainly linked to the production of nitric acid (e.g. used in fertilizer production) and adipic acid (e.g. used in nylon production). In the late 1990's and early 2000's the five European adipic acid plants were equipped with efficient abatement technology, cutting emissions by 95-99 %, largely through voluntary agreements of the companies. Much of the remaining IPPU emissions, from nitric acid plants, were cut in a similar manner around 2010, a development that has been connected with the introduction of the European Emission Trading System that made it economically attractive for companies to apply emission abatement technologies (catalytic reduction of N<sub>2</sub>O in the flue gas) to reduce their emissions.



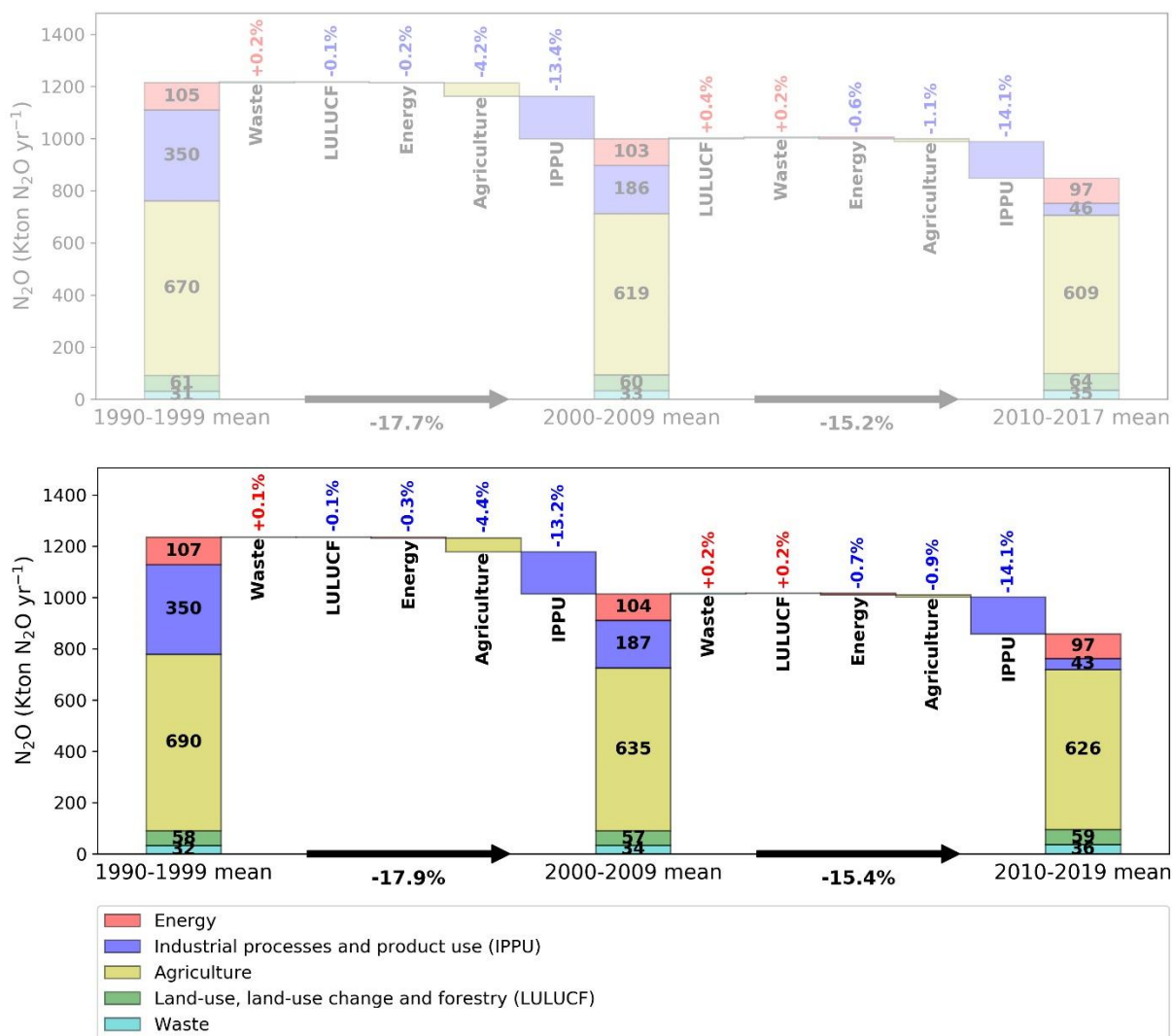


Figure 11: The contribution of changes (%) in  $N_2O$  anthropogenic emissions in the five sectors to the overall change in decadal mean for the EU27+UK as reported to UNFCCC. The top plot shows the previous NGHGI data in Petrescu et al., 2021a and bottom plot depicts data from UNFCCC NGHGI (2021). The three stacked columns represent the average  $N_2O$  emissions from each sector during three periods (1990-1999, 2000-2009 and 2010-2019) and percentages represent the contribution of each sector to the total reduction percentages between periods.

### 3.2.3. NGHGI estimates compared with bottom-up inventories

Figure 12 compares the six bottom-up inventories with UNFCCC NGHGI (2021) data, and shows that all of them are around the NGHGI estimates (Figure 12a), noting that GAINS only provides emissions every five years. The BU estimates show good agreement with one another and with the NGHGI estimates until 2005. After 2005 the slightly increasing trend is influenced by the IPPU (Figure 12c) and Waste (Figure 12e) sectors, with estimates of both EDGAR v6.0 and GAINS for total anthropogenic  $N_2O$  emissions in the year 2018 being 9 % and 13 % higher than the respective UNFCCC NGHGI (2021) estimates. Except for agriculture (Figure 12d), where four of the five models/inventories

show good match in absolute mean values with the NGHGI and over 1990-2018 and have similar linear trends of -0.18, -0.17, -0.15 and -0.11 % yr<sup>-1</sup> in NGHGI, EDGAR v6.0, GAINS and FAOSTAT respectively, for the other sectors the trends differ. The match in agriculture trends reflects that the sources rely on the same basic activity data from FAOSTAT and follow the IPCC EF Tier 1 or 2 approach (Petrescu et al., 2020). However, the high reported uncertainty range from the NGHGIs contradicts the match of the BU estimate absolute values and represents an important research question to be further investigated. In contrast, ECOSSE shows lower estimates because it does not use the FAO fertilizer application rate data base, but instead calculates ideal fertilizer application rates from the nitrogen demand of the crops. ECOSSE uses fertilizer data derived by Mueller et al. (2012) and simulates only for winter wheat. It is very likely that the assumed fertilizer application rates are lower than those used in FAO for the country specific average, which could explain the lower estimates. This means that it may severely under-estimate the applied fertilizer amounts for some areas (e.g. Netherlands, Denmark or North-West Germany), and the results are more indicative of emissions under idealized fertilizer application rates. Additionally, as mentioned above, the model simulates only the direct emissions.

870

875

880

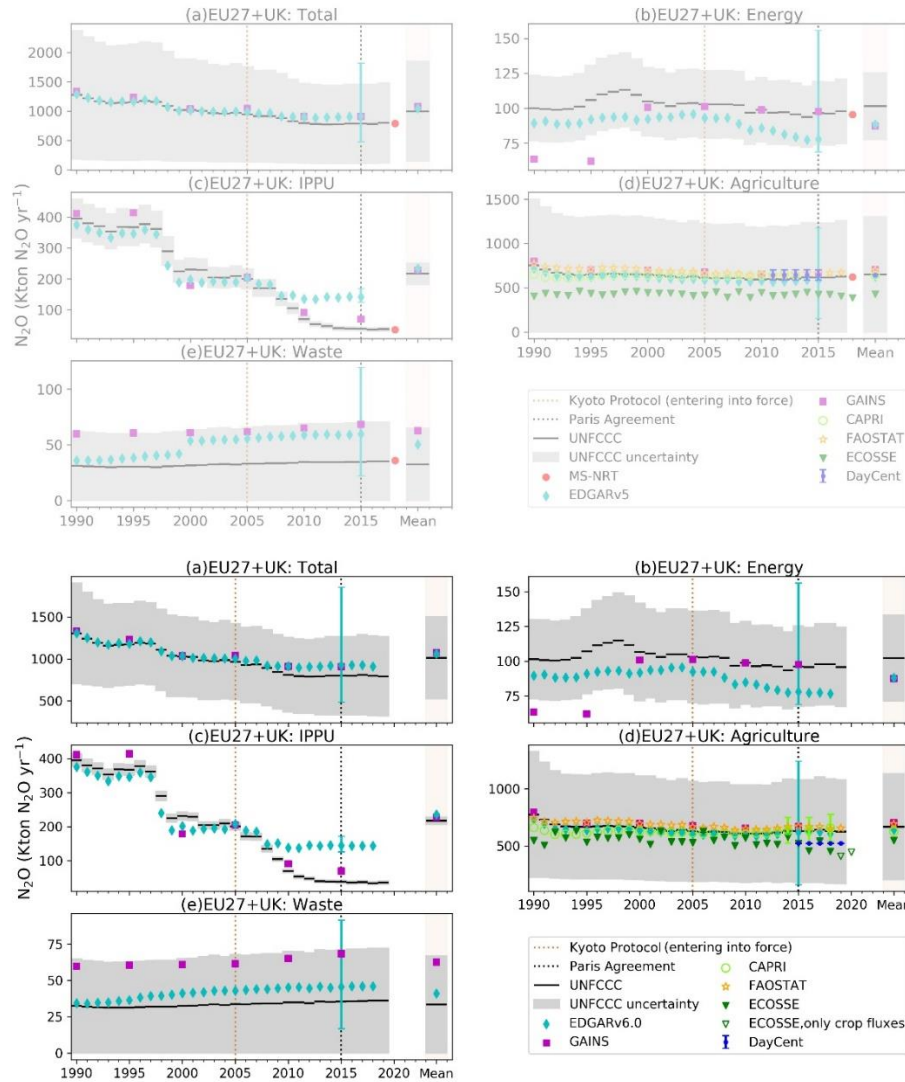


Figure 12: a) Total annual anthropogenic  $N_2O$  emissions (excluding LULUCF) for the EU27+UK over time. The top plot presents previous data synthesized in Petrescu et al., 2021a while the bottom plot depicts data synthesized by the current study: a) EU27+UK and total sectoral emissions from: b) Energy, c) IPPU, d) Agriculture, e) Waste from UNFCCC NGHGI (2021) submissions compared to global BU inventories for agriculture (CAPRI, ECOSSE, FAOSTAT, DayCent) and all sectors excl. LULUCF (EDGAR v6.0, GAINS). CAPRI reports one value for Belgium and Luxembourg. The relative error on the UNFCCC value represents the UNFCCC NGHGI (2021) Member States reported uncertainties computed with the error propagation method (95% confidence interval) that were gap-filled and provided for every year. The uncertainty for EDGARv6.0 is the same as that of v5.0 and calculated for 2015 as min/max values for the total and each sector (Solazzo et al., 2021) and represents the 95 % confidence interval of a lognormal distribution. CAPRI reports uncertainties for the last three years as following: 2014 and 2016 (17.6 %) and 2018 (17.8 %). The mean column represents the common overlapping period 1990-2018 between datasets Last years of the time series of the respective datasets are 2019 (UNFCCC and FAOSTAT), 2018 (EDGAR v6.0, CAPRI),

2015 (GAINS every five years), 2015-2019 (DayCent) and 2020 ECOSSE, with last two years reporting only crop emissions.

In the NGHGI (2021) submissions, for 2019, the EU27+UK Tier 1 total uncertainty for the waste sector (based on the IPCC chapter 3 error propagation method described in detail by Petrescu et al., 2020) and the gap-filling method described in Appendix A, was 360 %. The sectoral activity responsible for this high uncertainty is the wastewater treatment and discharge (462%) and this remains one of the most uncertain sources of N<sub>2</sub>O having the highest emissions in the waste sector. Emissions are known to vary markedly in space and time even within a single wastewater treatment plant (Gruber et al., 2020), a fact that only recently has been properly accounted for in the inventory guidelines (IPCC, 2019a). However, the total emissions from the waste sector account for only 4.2 % of the total EU27+UK 2019 N<sub>2</sub>O emissions (excl. LULUCF).

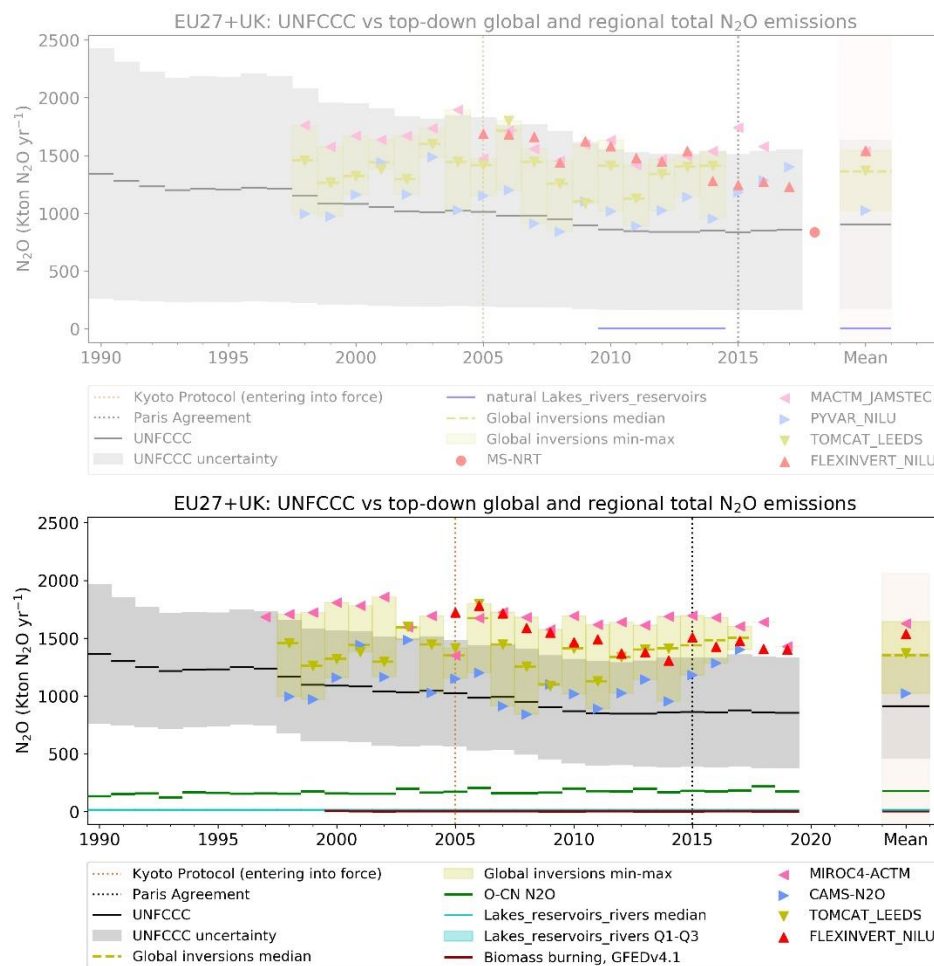
### 3.3.4. NGHGI estimates compared to atmospheric inversions

Figure 13 compares inversion estimates of total N<sub>2</sub>O emissions, including natural, from regional (FLEXINVERT) and global (three models) N<sub>2</sub>O inversions with the UNFCCC NGHGI (2021) estimates. The min-max range of all inversions is within the 2-sigma uncertainty of NGHGI, with the median of global inversions being on average 42 % or 0.4 Tg N<sub>2</sub>O yr<sup>-1</sup> higher than that of NGHGI. Over the period 2005-2019, the regional FLEXINVERT is almost double that of UNFCCC NGHGI (2021). From the three global inversions, MIROC4-ACTM shows consistently higher estimates until 2019, when it registers a drop in the estimated emission level (similar to FLEXINVERT). Similar reduction of emissions are seen for 2003 and 2005. In all these years, Europe registered record breaking heatwaves. One plausible explanation for the low N<sub>2</sub>O is that high temperature accompanied with lesser soil moisture reduces N<sub>2</sub>O emission, as seen in the tropics (Patra et al., 2022).

The other two global inverse models, TOMCAT and CAMS-N<sub>2</sub>O register high estimates as well as very high variability. Regarding trends, FLEXINVERT shows a similar decreasing trend of 18 % over 2005-2019, compared to 16 % for UNFCCC NGHGI (2021). The global CAMS-N<sub>2</sub>O inversion agrees the best in its absolute mean value (1.0 Tg N<sub>2</sub>O yr<sup>-1</sup>) with the NGHGI estimate (0.9 Tg N<sub>2</sub>O yr<sup>-1</sup>) but not in its trend. In this updated synthesis, natural pre-industrial soil emissions of N<sub>2</sub>O from the O-CN model, were included, but these are not considered in NGHGI reporting, and therefore cannot explain the gap between inventories and TD estimates. In addition, the emission factors used in NGHGI reporting are regarded to be very uncertain (up to 300% for direct agricultural emissions) which, based on the comparison with TD estimates, could imply that inventories underestimate N<sub>2</sub>O emissions. The uncertainty reported by the NGHGIs in 2019 was 59% compared to 86% in 2017 (Petrescu et al., 2021a).

Regarding the natural N<sub>2</sub>O emissions, the median natural flux from inland waters, is very low (12.7 kton N<sub>2</sub>O yr<sup>-1</sup>) and part of the inland water natural estimate is considered anthropogenic in Europe and is due to the leaching of N-fertilizers from agriculture. The anthropogenic share accounts for 66 % of the total inland waters emissions (Petrescu et al., 2021a). In the current study more natural N<sub>2</sub>O estimates have been added. The soil natural background emissions are estimated at 177 kton N<sub>2</sub>O yr<sup>-1</sup> averaged over 2005-2014 (the common overlapping period of all data

930 sources), while the biomass burning emissions account for only 1.6 kton N<sub>2</sub>O yr<sup>-1</sup> for the same period. In the lower plot, the NGHGI uncertainty was recalculated to 56 % compared to 86% in Petrescu et al., (2021a) (upper plot).



935 Figure 13: Comparison of total N<sub>2</sub>O emissions for EU27+UK from one top-down regional inversion (FLEXINVERT) and three inversions (TOMCAT, CAMS-N<sub>2</sub>O and MIROC4-ACTM) with UNFCCC NGHGI (grey) data and natural N<sub>2</sub>O emissions (lakes\_reservoirs\_rivers from RECCAP2, natural pre-industrial soil emissions from the O-CN model and biomass burning from GFEDv4.1) as following: the top plot shows the previous synthesized data in Petrescu et al., 2021a and the bottom plot depicts data synthesized by the current study. The relative error on the UNFCCC value represents the UNFCCC NGHGI (2021) Member States reported uncertainties computed with the error propagation method (95% confidence interval) that were gap-filled and provided for every year (including LULUCF). Last years of the time series of the respective datasets are 2014 (TOMCAT), 2017 CAMS-N<sub>2</sub>O, 2019 (UNFCCC, FLEXINVERT and MIROC4-ACTM). The mean column represents the common overlapping period (2005-2014) between datasets MACTM-JAMSTEC is the same with MIROC4-ACTM and PYVAR\_NILU with CAMS-N<sub>2</sub>O.

940 For the N<sub>2</sub>O results (FLEXINVERT in Figure 13), after updating the last runs, both the magnitude and trends of the N<sub>2</sub>O emissions changed. This new decreasing trend is confirming the UNFCCC trend but shows a larger average

source after correcting for the estimate of natural emissions. Future work should strongly focus on establishing the uncertainty and variability in the natural emissions of N<sub>2</sub>O so that the results of inversion could be more directly compared to emission inventories.

950 *Spatial distribution of N<sub>2</sub>O emissions from regional inversions*

New top-down estimates of N<sub>2</sub>O fluxes were produced using the CIF (Berchet et al. 2021). For N<sub>2</sub>O, inversions were performed by LSCE using three CHIMERE and by NILU using FLEXPART(v10.4). For the CIF inversions, the prior fluxes and observations of N<sub>2</sub>O were the same as those used in the Figure 13, and the background  
955 mixing ratios were calculated using the CAMSv19r products for N<sub>2</sub>O (Segers, 2020) (based on the global TM5-4DVAR assimilation run (Bergamaschi et al. 2018a, Rödenbeck et al. (2009))).

For N<sub>2</sub>O, the FLEXPART inversion resulted in slightly larger fluxes over Europe compared to the CHIMERE inversion, especially over the Netherlands, Belgium, northern France and England. In these regions, FLEXPART also results in larger fluxes compared to the prior. FLEXPART estimated smaller fluxes compared to the prior and to  
960 CHIMERE in northeastern Germany. CHIMERE, on the other hand remained close to the prior estimates. The total mean emission for EU27+UK for the period 2005-2018 was 1538 kton N<sub>2</sub>O and 1680 kton N<sub>2</sub>O yr<sup>-1</sup> for CHIMERE and FLEXPART, respectively, compared to the estimate of 1513 kton N<sub>2</sub>O yr<sup>-1</sup> from FLEXPART (Figure 13). Both

inversions also found a decreasing trend over 2005-2018 with decreases of 157 kton N<sub>2</sub>O yr<sup>-1</sup> and 298 kton N<sub>2</sub>O yr<sup>-1</sup> per year for CHIMERE and FLEXPART, respectively, which was not seen in the prior estimates.

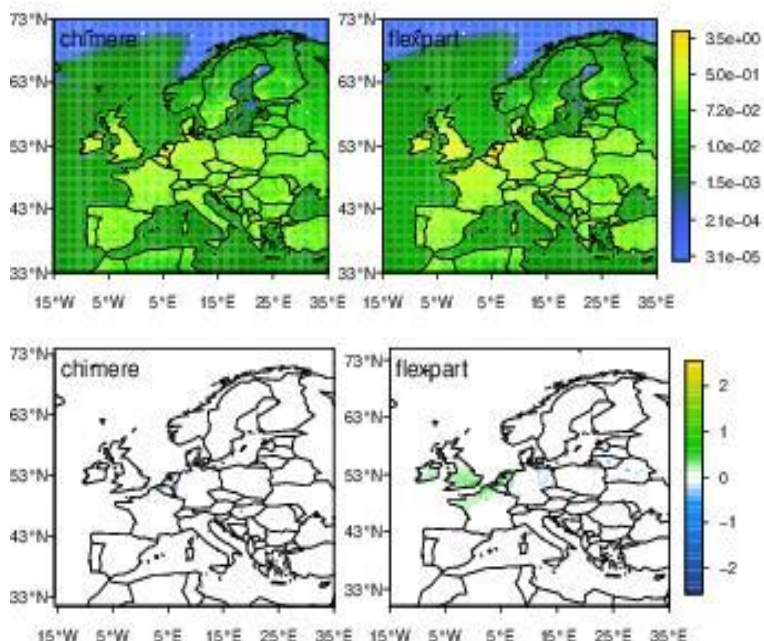


Figure 14. Posterior N<sub>2</sub>O fluxes averaged over 2005-2018 (g N<sub>2</sub>O m<sup>-2</sup> yr<sup>-1</sup>) from two regional inversions CHIMERE (LSCE) and FLEXPART (NILU) shown with a log base 2 color scale (top) and the flux increments (posterior-prior) (g N<sub>2</sub>O m<sup>-2</sup> yr<sup>-1</sup>) shown on a linear color scale.

Similar to CH<sub>4</sub>, the differences might be owing to the different dataset used for determining the background mixing ratios. Farther analysis is ongoing.

#### 4. Data availability

Data files reported in this work which were used for calculations and figures are available for public download at <https://doi.org/10.5281/zenodo.7553800> (Petrescu et al., 2023). The data are reachable with one click (without the need for entering login and password), with a second click to download the data, consistent with the two click access principle for data published in ESSD (Carlson and Oda, 2018). The data and the DOI number are subject to future updates and only refers to this version of the paper. The raw gridded data, according to the VERIFY consortium governing document, will be made publicly available 12 months after its publication in ESSD.

#### 5. Summary and concluding remarks

This study is an update of the first comprehensive synthesis of European CH<sub>4</sub> and N<sub>2</sub>O emission estimates (Petrescu et al., (2021a), that compares total and sectoral European CH<sub>4</sub> and N<sub>2</sub>O from BU (anthropogenic and natural) with TD estimates to assess their use for quality control and verification of UNFCCC NGHGI reporting. Using the most recent data, differences between TD and BU estimates were compared and comparisons were made with the previous synthesis, Petrescu et al., (2021a). Identification of source specific uncertainty is key in understanding these

differences and can lead to a reduction of the overall uncertainty in GHG inventories. Furthermore, the results have been synthesized in a way that would be compatible with the methodological framework of the first 2023 Global Stocktake of the Paris Agreement. Five-year means of CH<sub>4</sub> (Figure 1) and N<sub>2</sub>O (Figure 10) emissions for the periods 2011-2015 and 2015-2019 from the different BU and TD datasets have been calculated for the EU27+UK bloc, as well as for five regions in Europe. These estimates are then compared with respective NGHGI emissions for the same periods and the 1990 base year.

Inconsistencies between CH<sub>4</sub> BU estimates and NGHGI data at EU27+UK level (Figure 3), are mainly caused by different methodologies in calculating emissions as highlighted in Petrescu et al. (2020, 2021a). Both BU inventories and the NGHGI use similar activity data and, to varying extents, the default EFs reported in the IPCC 2006 guidelines meaning that the estimates are predestinated to agree rather well. Thus, the spread in all BU estimates may not be indicative of the uncertainty. For global consistency purposes, EDGAR v6.0 and FAOSTAT mostly uses Tier 1 approaches in calculating emissions (and uncertainties), a fact which triggers differences with other data sources using Tier 2 or 3 methods (GAINS for all sectors and CAPRI for agriculture). Within the UNFCCC reporting process, the agriculture sector was the highest contributor to the CH<sub>4</sub> emissions, followed by energy and waste (Figure 1).

A reason for the small inconsistencies between datasets is the allocation of emissions to different sectors and that some data sources use updated methods and emission factors from different versions of the IPCC guidelines (e.g. 1996 versus 2006 or 2019 Refinements to the 2006 (i.e. EDGAR v6.0)).

For N<sub>2</sub>O anthropogenic emissions, all BU data sources show good agreement with the UNFCCC NGHGI (2021) data in both trends and means (Figure 12), agriculture remaining the largest emitter (e.g. soil emissions due to fertilizer additions), within the reported uncertainties. As with CH<sub>4</sub>, the different BU estimates share some common elements such as activity data and emissions factors, and the agreement between estimates may not be relevant to the underlying uncertainties.

An important improvement compared to Petrescu et al., 2021a, was the harmonization of UNFCCC Member States uncertainty estimates, which were gap-filled and calculated for each year of the time series. VERIFY interaction with the EU inventory team has helped improve the uncertainty estimations on the EU GHG emissions reported under UNFCCC. For both CH<sub>4</sub> and N<sub>2</sub>O the uncertainties reported by NGHGI are large and underline the need for further improvement in the inventories of these two GHGs.

Regarding the TD estimates, this analysis shows that comparison between CH<sub>4</sub> inversions estimates and NGHGIs is highly uncertain because of the large spread in the inversion results. Nevertheless, in contrast to BU methods, TD inversions inferred from atmospheric observations represent the most independent data against which CH<sub>4</sub> inventory totals can be compared. With anticipated improvements in atmospheric modelling and observations, as well as modelling of natural fluxes, TD inversions may arguably emerge as the most powerful tool for verifying emissions inventories for CH<sub>4</sub> and other GHGs.

As TD inversions do not fully distinguish between all emission sectors used by NGHGI and report either total emissions or a coarse sectorial partitioning, their comparison to NGHGI is only possible for total emissions. It is also necessary to make an adjustment for natural emissions, which are included in TD inversions but not reported by the NGHGIs. A future improvement for the natural CH<sub>4</sub> emissions are the consistent time series of measurements to



make clear statements about how wetland and lake fluxes change over time. For lakes there is virtually no long-term monitoring, while for wetlands variability (e.g. area) is a key uncertainty but Fronzek et al., (2018) have shown that model ensembles work well in simulating highly uncertain variables. In general regional inversions show less spread than the global inversions as they used recent updates of transport models and simulate atmospheric transport at higher resolutions.

The global models use fewer observations for Europe compared to the included regional inversions, and thus are expected to have larger uncertainties for the European fluxes. In addition, the global models are at coarser resolution, and thus likely have larger model representation errors compared to the regional ones, which may contribute to further systematic uncertainty for the European fluxes. Currently, for Europe the regional TD total is considerably higher than the global estimates (Figure 1). If the regional TD estimate for whole EU27+UK including all sources and sinks is considered to be the best total estimate in place, and if the natural fluxes are assumed to have been accurately subtracted from the optimized net flux, then NGHGI and BU approaches may be underestimating total EU27+UK CH<sub>4</sub> emissions by approximately 20-30%. For N<sub>2</sub>O, the TD estimates fall within the large range of the NGHGI uncertainties, and, in fact, the spread in the regional ensembles is much smaller than the inventory uncertainty range (Figure 13). Compared to Petrescu et al., 2021a, the natural emissions consisting of pre-industrial natural soil emissions and biomass burning emissions were included, however, for N<sub>2</sub>O natural emissions do not explain the 415 kton N<sub>2</sub>O difference between NGHGI (and BU) estimates and the average TD estimate. More research is thus needed to identify the source of discrepancies.

A key challenge for the inversion CH<sub>4</sub> community remains the separation of emissions in specific source sectors, as derived total emissions may also include natural emissions (or removals). In the case of N<sub>2</sub>O this won't be possible since the anthropogenic emissions due to agriculture are caused by a perturbation to microbial processes (i.e., nitrification and denitrification) and cannot be cleanly separated from "natural" emissions (defined as the level of emission in the pre-industrial period, i.e., before perturbation by anthropogenic N-inputs). However, some TD quantification of industrial emissions should be possible in high-resolution inversions. In any case, TD inversions for estimating N<sub>2</sub>O emissions should mainly focus on the trends. Furthermore, the accuracy of derived emissions and the spatial scales at which emissions can be estimated depend on the quality and density of measurements and the quality of the atmospheric models (Bergamaschi et al., 2018b). Significant further developments of the global observations system and the top-down methods would be required to support the implementation of the Paris Agreement.

The exercise of presenting uncertainty reduction maps illustrated the effect on uncertainty reductions with removing/adding ground-based observation stations. This is one of the elements informing policy makers on the need for further investing into a denser and efficient surface observation network used by inverse systems to calibrate their estimates and better inform climate policy with respect to emissions verification. This might serve to monitor and build more accurate budget of country estimates as well as provide data for inferring subnational (e.g. city-scale) emissions.

This synthesis makes use and brings together state-of-the-art BU and TD estimates from different sources and compares these data with the official NGHGI estimates reported to UNFCCC. The exercise underlines the uncertainties in the emissions of these important GHGs and illustrates the importance of regional consistent analyses

and synthesis of available estimates for informing climate policy. Specifically, the approach demonstrated here could form the basis of the Multilateral Facilitative Consideration of Progress under the enhanced transparency framework of the Paris Agreement. The implementation of the Paris Agreement requires accurate quantification of GHG emissions in order to track the progress of all parties with their "Nationally Determined Contributions" and to assess collective progress towards achieving the purpose of this Agreement and its long-term goals (GST). As this will be mainly achieved and built upon BU methodologies developed by the IPCC, we need to take into consideration the potential to quantify GHG emissions by using "top-down" methods ("inverse modelling") (Bergamaschi et al., 2018b). One advantage of the inverse estimate is that it provides total emission estimates inferred from atmospheric GHG measurements. Therefore, the capability to quantify anthropogenic emissions depends on the magnitude of natural sources and sinks and the capability to quantify them and subtract them from the TD estimates.

As stated in the introduction, the main aim was to explore and discuss the issues causing differences between NGHGI, BU and TD approaches. Such an exercise can help to improve the different respective approaches and furthermore can inform the development of formal verification systems. Some differences in BU and NGHGI estimates were observed and were traced back to factors such as the variations activity data, emission factors and sectoral allocation of emissions (CH<sub>4</sub>). Nevertheless, BU and NGHGI estimates generally converged at the total emission level for the EU27+UK bloc and the five European regions. The overall agreement is generally due to similar sources of input activity data and emission factors (albeit with some aforementioned variations) and is not indicative of the true uncertainties in the respective CH<sub>4</sub> and N<sub>2</sub>O inventories. Indeed, NGHGI report CH<sub>4</sub> and N<sub>2</sub>O emissions with large uncertainties and, furthermore, NGHGI estimates generally diverged from the respective TD fluxes. Despite the significant spread in the inversion estimates (due to e.g. use of different transport models and/or observation datasets, while priors might be the same (Table B2.4)), TD estimates were generally higher than NGHGI, even when accounting for the (albeit uncertain) natural fluxes.

The analysis done here generally compared estimates in terms of long-term trends and averages over five or more years, and thus provides a working example of how such syntheses could inform future Global Stocktakes under the Paris Agreement. A further step could involve analysis at finer temporal resolutions. While NGHGI are reported at annual scales, analyzing emissions over intra-annual timescales, of great importance for CH<sub>4</sub> (wetland emission estimates have large uncertainties and show large variability in space and between seasons) and N<sub>2</sub>O (agricultural fertilizer application), may help to identify sector contributions to divergence between prior and posterior estimates at the annual/inter-annual scale. To do this, however requires expanded in-situ monitoring so that such dynamics can be better represented in the temporally-resolved prior estimates that feed into the top-down inversions.

## 6. Appendices

### Appendix A: Data sources, methodology and uncertainty descriptions

The country specific plots are found at: <http://webportals.ipsl.jussieu.fr/VERIFY/FactSheets/v1.28>

## VERIFY project

VERIFY's primary aim was to develop scientifically robust methods to assess the accuracy and potential biases in national inventories reported by the parties through an independent pre-operational framework. The main concept is to provide observation-based estimates of anthropogenic and natural GHG emissions and sinks as well as associated uncertainties. The proposed approach is based on the integration of atmospheric measurements, improved emission inventories, ecosystem data, and satellite observations, and on an understanding of processes controlling GHG fluxes (ecosystem models, GHG emission models).

Two complementary approaches relying on observational data-streams were combined in VERIFY to quantify GHG fluxes:

1) atmospheric GHG concentrations from satellites and ground-based networks (top-down atmospheric inversion models) and

2) bottom-up activity data (e.g. fuel use and emission factors) and ecosystem measurements (bottom-up models).

For CH<sub>4</sub> and N<sub>2</sub>O, agricultural emissions were separated from fossil fuel and industrial emissions. Finally, trends in the budget of the three GHGs were analyzed in the context of NDC targets.

The objectives of VERIFY were:

**Objective 1.** Integrate the efforts between the research community, national inventory compilers, operational centres in Europe, and international organizations towards the definition of future international standards for the verification of GHG emissions and sinks based on independent observation.

**Objective 2.** Enhance the current observation and modelling ability to accurately and transparently quantify the sinks and sources of GHGs in the land-use sector for the tracking of land-based mitigation activities.

**Objective 3.** Develop new research approaches to monitor anthropogenic GHG emissions in support of the EU commitment to reduce its GHG emissions by 40% by 2030 compared to the year 1990.

**Objective 4.** Produce periodic scientific syntheses of observation-based GHG balance of EU countries and practical policy-oriented assessments of GHG emission trends, and apply these methodologies to other countries.

For more information on project team and products/results check <https://verify.lsce.ipsl.fr/>.

Table A1: *Country grouping used for reconciliation purposes between BU and TD estimates. The countries and groups of countries in italic are not directly used by this study but their figures and data is available on the VERIFY project web portal at: <http://webportals.ipsl.jussieu.fr/VERIFY/FactSheets/>.*

Country name – geographical Europe	BU-ISO3	Aggregation from TD-ISO3
Luxembourg	LUX	
Belgium	BEL	BENELUX
Netherlands	NLD	BNL
Bulgaria	BGR	BGR
Switzerland	CHE	
<i>Lichtenstein</i>	<i>LIE</i>	<i>CHL</i>

Czech Republic	CZE	Former Czechoslovakia
Slovakia	SVK	CSK
Austria	AUT	AUT
Slovenia	SVN	North Adriatic countries
Croatia	HRV	NAC
Romania	ROU	ROU
Hungary	HUN	HUN
Estonia	EST	
Lithuania	LTU	Baltic countries
Latvia	LVA	BLT
Norway	NOR	NOR
Denmark	DNK	
Sweden	SWE	
Finland	FIN	DSF
Iceland	ISL	ISL
Malta	MLT	MLT
Cyprus	CYP	CYP
France (Corsica incl.)	FRA	FRA
<i>Monaco</i>	<i>MCO</i>	
<i>Andorra</i>	<i>AND</i>	
Italy (Sardinia, Vatican incl.)	ITA	ITA
<i>San Marino</i>	<i>SMR</i>	
United Kingdom (Great Britain + N Ireland)	GBR	UK
<i>Isle of Man</i>	<i>IMN</i>	
Iceland		
Ireland	IRL	IRL
Germany	DEU	DEU
Spain	ESP	IBERIA
Portugal	PRT	IBE
Greece	GRC	GRC
<i>Russia (European part)</i>	<i>RUS European</i>	
<i>Georgia</i>	<i>GEO</i>	<i>RUS European+GEO</i>

<i>Russian Federation</i>	<i>RUS</i>	<i>RUS</i>
Poland	POL	POL
<i>Turkey</i>	<i>TUR</i>	<i>TUR</i>
EU27+UK (Austria, Belgium, Bulgaria, Cyprus, Czech Republic, Germany, Denmark, Spain, Estonia, Finland, France, Greece, Croatia, Hungary, Ireland, Italy, Lithuania, Latvia, Luxembourg, Malta, Netherlands, Poland, Portugal, Romania, Slovakia, Slovenia, Sweden, United Kingdom)	AUT, BEL, BGR, CYP, CZE, DEU, DNK, ESP, EST, FIN, FRA, GRC, HRV, HUN, IRL, ITA, LTU, LVA, LUX, MLT, NDL, POL, PRT, ROU, SVN, SVK, SWE, GBR	E28
Western Europe (Belgium, France, United Kingdom, Ireland, Luxembourg, Netherlands)	BEL, FRA, UK, IRL, LUX, NDL	WEE
Central Europe (Austria, Switzerland, Czech Republic, Germany, Hungary, Poland, Slovakia)	AUT, CHE, CZE, DEU, HUN, POL, SVK	CEE
Northern Europe (Denmark, Estonia, Finland, Lithuania, Latvia, Norway, Sweden)	DNK, EST, FIN, LTU, LVA, NOR, SWE	NOE
<i>South-Western Europe (Spain, Italy, Malta, Portugal)</i>	<i>ESP, ITA, MLT, PRT</i>	<i>SWN</i>
<i>South-Eastern Europe (all) (Albania, Bulgaria, Bosnia and Herzegovina, Cyprus, Georgia, Greece, Croatia, Macedonia, the former Yugoslav, Montenegro, Romania, Serbia, Slovenia, Turkey)</i>	<i>ALB, BGR, BIH, CYP, GEO, GRC, HRV, MKD, MNE, ROU, SRB, SVN, TUR</i>	<i>SEE</i>
<i>South-Eastern Europe (non-EU) (Albania, Bosnia and Herzegovina, Macedonia, the former Yugoslav, Georgia, Turkey, Montenegro, Serbia)</i>	<i>ALB, BIH, MKD, MNE, SRB, GEO, TUR</i>	<i>SEA</i>
<i>South-Eastern Europe (EU) (Bulgaria, Cyprus, Greece, Croatia, Romania, Slovenia)</i>	<i>BGR, CYP, GRC, HRV, ROU, SVN</i>	<i>SEZ</i>
<i>Southern Europe (all) (SOE) (Albania, Bulgaria, Bosnia and Herzegovina, Cyprus, Georgia, Greece, Croatia, Macedonia, the former Yugoslav, Montenegro, Romania, Serbia, Slovenia, Turkey, Italy, Malta, Portugal, Spain)</i>	<i>ALB, BGR, BIH, CYP, GEO, GRC, HRV, MKD, MNE, ROU, SRB, SVN, TUR, ITA, MLT, PRT, ESP</i>	<i>SOE</i>
<i>Southern Europe (non-EU) (SOY) Albania, Bosnia and Herzegovina, Georgia,</i>	<i>ALB, BIH, GEO, MKD, MNE, SRB, TUR,</i>	<i>SOY</i>

<i>Macedonia, the former Yugoslav, Montenegro, Serbia, Turkey)</i>		
Southern Europe (EU) (SOZ) (Bulgaria, Cyprus, Greece, Croatia, Romania, Slovenia, Italy, Malta, Portugal, Spain)	BGR, CYP, GRC, HRV, ROU, SVN, ITA, MLT, PRT, ESP	SOZ
Eastern Europe (non-EU) (Belarus, Moldova, Republic of, Russian Federation, Ukraine)	BLR, MDA, RUS, UKR	EAE
<i>EU-15 (Austria, Belgium, Germany, Denmark, Spain, Finland, France, United Kingdom, Greece, Ireland, Italy, Luxembourg, Netherlands, Portugal, Sweden)</i>	<i>AUT, BEL, DEU, DNK, ESP, FIN, FRA, GBR, GRC, IRL, ITA, LUX, NDL, PRT, SWE</i>	<i>E15</i>
<i>EU-27 (Austria, Belgium, Bulgaria, Cyprus, Czech Republic, Germany, Denmark, Spain, Estonia, Finland, France, Greece, Croatia, Hungary, Ireland, Italy, Lithuania, Latvia, Luxembourg, Malta, Netherlands, Poland, Portugal, Romania, Slovakia, Slovenia, Sweden)</i>	<i>AUT, BEL, BGR, CYP, CZE, DEU, DNK, ESP, EST, FIN, FRA, GRC, HRV, HUN, IRL, ITA, LTU, LVA, LUX, MLT, NDL, POL, PRT, ROU, SVN, SVK, SWE</i>	<i>E27</i>
<i>All Europe (Aaland Islands, Albania, Andorra, Austria, Belgium, Bulgaria, Bosnia and Herzegovina, Belarus, Switzerland, Cyprus, Czech Republic, Germany, Denmark, Spain, Estonia, Finland, France, Faroe Islands, United Kingdom, Guernsey, Greece, Croatia, Hungary, Isle of Man, Ireland, Iceland, Italy, Jersey, Liechtenstein, Lithuania, Luxembourg, Latvia, Moldova, Republic of, Macedonia, the former Yugoslav, Malta, Montenegro, Netherlands, Norway, Poland, Portugal, Romania, Russian Federation, Svalbard and Jan Mayen, San Marino, Serbia, Slovakia, Slovenia, Sweden, Turkey, Ukraine)</i>	<i>ALA, ALB, AND, AUT, BEL, BGR, BIH, BLR, CHE, CYP, CZE, DEU, DNK, ESP, EST, FIN, FRA, FRO, GBR, GGY, GRC, HRV, HUN, IMN, IRL, ISL, ITA, JEY, LIE, LTU, LUX, LVA, MDA, MKD, MLT, MNE, NDL, NOR, POL, PRT, ROU, RUS, SJM, SMR, SRB, SVK, SVN, SWE, TUR, UKR</i>	<i>EUR</i>

\*countries highlighted in *italic* are not discussed in the current synthesis mostly because unavailability of NGHGI data (non-Annex I countries<sup>10</sup>) but are present on the web-portal: <http://webportals.ipsl.jussieu.fr/VERIFY/FactSheets/>. Results of Annex I countries (NOR, CHE, ISL) and non-EU EAE countries/groups are represented in Figures 1 and 9.

<sup>10</sup>Non-Annex I countries are mostly developing countries. The reporting to UNFCCC is implemented through national communications (NCs) and biennial update reports (BURs): <https://unfccc.int/national-reports-from-non-annex-i-parties>.

1140 *Table A2: Main methodological changes (**in bold**) of current study with respect to Petrescu et al., 2020 and 2021a; n/a cells mean that there is no data available.*

Publication year	Gas	Bottom-up anthropogenic CH <sub>4</sub> / N <sub>2</sub> O emissions			Bottom-up natural CH <sub>4</sub> / N <sub>2</sub> O emissions	Top-down CH <sub>4</sub> / N <sub>2</sub> O emissions		Uncertainty and other changes
		Inventories	Global databases	Emission models	Emission models	Regional models	Global models	
Petrescu et al., 2020	CH <sub>4</sub>	National emissions from UNFCCC (2018)  1990-2016  <i>AFOLU sector (Agriculture and LULUCF)</i> EU28 data for four years (1990, 2005, 2010 and 2016)	EGDAR v4.3.2 1990-2012  EDGAR FT2017 1990-2016  FAOSTAT 1990-2016  <i>Agriculture sector EU28 data for four years (1990, 2005, 2010 and last reported year)</i>	CAPRI 1990-2013  GAINS 1990-2015  <i>Agriculture sector EU28 data for four years (1990, 2005, 2010 and last reported year)</i>	Natural (wetlands) CH <sub>4</sub> emissions model ensemble GCP (2018) Poulter et al. (2017)  Time series 1990-2017	n/a	n/a	UNFCCC (2018) uncertainty estimates for 2016 (error propagation 95% interval method)  EDGAR v.4.3.2. reports only for 2012
	N <sub>2</sub> O	National emissions from UNFCCC (2018)  1990-2016  <i>Agriculture sector EU28 data for four years (1990, 2005, 2010 and 2016)</i>	EGDAR v4.3.2 1990-2012  EDGAR FT2017 1990-2016  FAOSTAT 1990-2016  <i>Agriculture sector EU28 data for four years (1990, 2005, 2010 and last reported year)</i>	CAPRI 1990-2013  GAINS 1990-2015  <i>Agriculture sector EU28 data for four years (1990, 2005, 2010 and last reported year)</i>	n/a	n/a	n/a	UNFCCC (2018) uncertainty estimates for 2016  EDGAR v.4.3.2. reports only for 2012
Petrescu et al., 2021a	CH <sub>4</sub>	National emissions from UNFCCC (2019)	EGDAR v 5.0 1990-2015	CAPRI 1990-2013	Non-wetland inland waters	Total CH <sub>4</sub> column  Time series 2005-2017:	Anthropogenic and natural partitions	UNFCCC (2018) uncertainty estimates for 2016 (error



		1990-2017  All UNFCCC sectors  EU27+UK time series  and 2018 MS-NRT estimate (EEA, 2019)  Regional EU27+UK totals (incl. NOR, CHE, UKR, MLD and BLR)	FAOSTAT (only agriculture) 1990-2017  Anthropogenic EU27+UK time series (excl. LULUCF)  Regional EU27+UK totals (incl. NOR, CHE, UKR, MLD and BLR)  Excl. LULUCF	GAINS 1990-2015  Agriculture sector EU27+UK  Times series	Average 2005-2011  Geological fluxes  Total pre-industrial era  JSBACH-HIMMELI 2005-2017	FLEXPART - FLExKF  TM5-4DVAR  FLEXINVERT_NILU  CTE-FMI  InTEM-NAME Only for UK  InGOS inversions 2006-2012	GCP-GCB 2019 2000-2017	propagation 95% interval method)  EDGAR v.4.3.2. reports only for 2015  For model ensembles reported as variability in extremes (min/max)
	N <sub>2</sub> O	National emissions from UNFCCC (2019) 1990-2017  All UNFCCC sectors  EU27+UK time series  and 2018 MS-NRT estimate (EEA, 2019)  Regional EU27+UK totals (incl. NOR, CHE, UKR, MLD and BLR)	EGDAR v 5.0 1990-2015 (excl. LULUCF) FAOSTAT (only agriculture) 1990-2017 Anthropogenic EU27+UK time series  Regional EU27+UK totals (incl. NOR, CHE, UKR, MLD and BLR)  Excl. LULUCF	Agriculture CAPRI 1990-2013  ECOSSE 1990-2018	N <sub>2</sub> O missions from lakes, rivers, reservoirs  Average 2010-2014	Total N <sub>2</sub> O column Time series  FLEXINVERT_NILU 2005-2017	Total N <sub>2</sub> O column Time series  GCP - GN <sub>2</sub> OB 2019 CAMS-N <sub>2</sub> O TOMCAT MIROC4-ACTM 1998-2016	UNFCCC (2018) uncertainty estimates for 2016 (error propagation 95% interval method)  EDGAR v.4.3.2. reports only for 2015  For model ensembles reported as variability in extremes (min/max)
Current study	CH <sub>4</sub>	National emissions from UNFCCC (2021) 1990-2019  All UNFCCC sectors	EGDAR v6.0 1990-2018  FAOSTAT (only agriculture) 1990-2020	CAPRI 1990-2014 and 2016 and 2018  GAINS	One median value from process-based models for non-wetland inland waters (lakes, rivers, reservoirs) 2010-2019	Total CH <sub>4</sub> column Time series 2005-2018: FLEXPART - FLExKF	Anthropogenic and natural partitions  GCP-GCB 2000-2017	UNFCCC (2021) uncertainty estimates for 2019 (error propagation 95% interval method) and yearly uncertainties provided by the EU GHG inventory team  EDGAR reports only for 2015 values from v6.0

		<p>EU27+UK time series</p> <p>Regional EU27+UK totals (incl. NOR, CHE, UKR, MLD and BLR) excl. LULUCF</p> <p>Two means: 2011-2015 <b>2015-2019</b></p>	<p>Anthropogenic EU27+UK time series (excl. LULUCF)</p> <p>Regional EU27+UK totals (incl. NOR, CHE, UKR, MLD and BLR) excl. LULUCF</p>	<p>1990-2015</p> <p>Agriculture sector EU27+UK</p> <p>Times series</p>	<p><b>One median value from upscaled results in RECCAP2</b></p> <p><b>1990-2019</b></p> <p>Geological fluxes</p> <p>Total pre-industrial era <b>updates for EU27+UK</b></p> <p>JSBACH-HIMMELI <b>peatlands and mineral soils</b></p> <p><b>2005-2020</b></p> <p><b>Biomass burning GFEDv4.1 emissions</b></p>	<p>TM5-4DVAR</p> <p>CTE-FMI</p> <p>FLEXINVERT_NILU</p> <p><b>1990-2019</b></p> <p>InGOS inversions</p> <p>2006-2012 <b>not included anymore in the mean</b></p> <p>InTEM-NAME (only for UK plots on the VERIFY website)</p> <p><b>VERIFY Community Inversion Framework (CIF): CHIMERE, FLEXPARTv10.4 (NILU) and FELXPART (EMPA)</b></p> <p><b>2006-2017</b></p>		<p>For model ensembles reported as variability in extremes (min/max)</p> <p><b>CAPRI uncertainties for 2014, 2016 and 2018</b></p>
	N <sub>2</sub> O	<p>National emissions from UNFCCC (<b>2021</b>)</p> <p><b>1990-2019</b></p> <p>All UNFCCC sectors</p> <p>EU27+UK time series</p> <p>Regional EU27+UK totals (incl. NOR, CHE, UKR, MLD and BLR) <b>excl. LULUCF</b></p> <p>Two means: 2011-2015 <b>2015-2019</b></p>	<p><b>EGDAR v 6.0</b></p> <p><b>1990-2018</b></p> <p>FAOSTAT (<b>v2021</b>) (only agriculture)</p> <p><b>1990-2020</b></p> <p>Anthropogenic EU27+UK time series (excl. LULUCF)</p> <p>Regional EU27+UK totals (incl. NOR, CHE, UKR, MLD and BLR) excl. LULUCF</p>	<p>CAPRI</p> <p><b>1990-2014 and 2016 and 2018</b></p> <p>GAINS</p> <p>1990-2015</p> <p>Agriculture sector EU27+UK</p> <p>Times series</p> <p>ECOSSE</p> <p><b>1990-2020</b></p>	<p><b>One N<sub>2</sub>O median value for emissions from lakes, rivers, reservoirs (RECCAP2)</b></p> <p>Average <b>1990-2019</b></p> <p><b>Natural N<sub>2</sub>O pre-industrial emissions from O-CN model</b></p> <p><b>1990-2020</b></p> <p><b>Biomass burning GFEDv4.1 emissions</b></p> <p><b>2000-2019</b></p>	<p>Total N<sub>2</sub>O column</p> <p>Time series</p> <p>FLEXINVERT_NILU</p> <p><b>2005-2019</b></p> <p><b>VERIFY Community Inversion Framework (CIF): CHIMERE, FLEXPARTv10.4 (NILU)</b></p> <p><b>2005-2018</b></p>	<p>Total N<sub>2</sub>O column</p> <p>Time series</p> <p>CAMS-N<sub>2</sub>O</p> <p>1998-2017</p> <p>TOMCAT</p> <p>1998-2014</p> <p><b>MIROC4-ACTM</b></p> <p><b>1997-2019</b></p> <p><b>FELXINVERT</b></p> <p><b>2005-2019</b></p>	<p>UNFCCC (<b>2021</b>) uncertainty estimates for <b>2019</b> (error propagation 95% interval method) <b>and yearly uncertainties provided by the EU GHG inventory team</b></p> <p>EDGAR reports only for 2015 values from v6.0</p> <p>For model ensembles reported as variability in extremes (min/max)</p> <p><b>CAPRI uncertainties for 2014, 2016 and 2018</b></p>

## **A1: Anthropogenic CH<sub>4</sub> emissions (sectors Energy, IPPU, Agriculture, LULUCF and Waste)**

### ***Bottom-up CH<sub>4</sub> emissions estimates***

#### ***UNFCCC NGHGI (2021)***

Under the UNFCCC and its Kyoto Protocol national greenhouse gas (GHG) inventories are the most important source of information to track progress and assess climate protection measures by countries. In order to build mutual trust in the reliability of GHG emission information provided, national GHG inventories are subject to standardized reporting requirements, which have been continuously developed by the Conference of the Parties (COP)<sup>11</sup>. The calculation methods for the estimation of greenhouse gases in the respective sectors is determined by the methods provided by the 2006 IPCC Guidelines for National Greenhouse Gas Inventories (IPCC, 2006). These Guidelines provide detailed methodological descriptions to estimate emissions and removals, as well as provide recommendations to collect the activity data needed. As a general overall requirement, the UNFCCC reporting guidelines stipulate that reporting under the Convention and the Kyoto Protocol follow the five key principles of transparency, accuracy, completeness, consistency and comparability (TACCC).

The reporting under UNFCCC should meet the TACCC principles. The three main GHGs are reported in time series from 1990 up to two years before the due date of the reporting. The reporting is strictly source category based and is done under the Common Reporting Format tables (CRF), downloadable from the UNFCCC official submission portal: <https://unfccc.int/ghg-inventories-annex-i-parties/2021>.

The UNFCCC NGHGI anthropogenic CH<sub>4</sub> and N<sub>2</sub>O emissions analyzed in this study include estimates from 4 key sectors for the EU27+UK: 1 Energy, 2 Industrial processes and product use (IPPU), 3 Agriculture and 5 Waste. The methodological tiers a country applies depends on the source contribution to the national total (*Key Category* or not), on the national circumstances and the individual conditions of the land, which explains the variability of uncertainties among the sector itself as well as among EU countries. The LULUCF CH<sub>4</sub> and N<sub>2</sub>O emissions are very small but are included in some figures (see Table 1).

#### **Gap-filling harmonization procedure for NGHGI uncertainties**

The presented uncertainties in the emission levels of the individual countries and the EU27+UK bloc were calculated by using the methods and data used to compile the official GHG emission uncertainties that are reported by the EU under the UNFCCC (NIRs, 2022). The EU uncertainty analysis reported in the bloc's National Inventory Report (NIR) is based on country-level, Approach 1 uncertainty estimates (IPPC, 2006, Vol. 1, Chap. 3) that are reported by EU Member States, Iceland and United Kingdom under Article 7(1)(p) of Regulation (EU) 525/2013. These country-level uncertainty estimates are typically reported at beginning of a submission cycle and are not always revised with updated CRF submissions later in the submission cycle. Furthermore, the compiled uncertainties of some countries are incomplete (e.g. uncertainties not estimated for LULUCF and/or indirect CO<sub>2</sub> emissions, certain

---

<sup>11</sup> The last revision has been made by COP 19 in 2013 (UNFCCC, 2013)

subsector emissions are confidential) and the sector and gas resolution at which uncertainties are provided varies between the countries. The EU inventory team therefore implements a procedure to harmonise and gap-fill these uncertainty estimates. A processing routine reads the individual country uncertainty files that are pre-formatted manually to assign consistent sector and gas labels to the respective estimates of emissions/removals and uncertainties. The uncertainty values are then aggregated to a common sector resolution, at which the emissions and removals reported in the uncertainty tables of the countries are then replaced with the respective values from the final CRF tables of the countries. Due to the issue of incompleteness mentioned above, the country-level data are then screened to identify residual GHG emissions and removals for which no uncertainty estimates have been provided. Where sectors are partially complete, the residual net emission is quantified in CO<sub>2</sub> equivalents and incorporated. An uncertainty is then estimated, by calculating the overall sector uncertainty of the sources and sinks that were included in that country's reported uncertainties estimates and assigning this percentage average to the residual net emission. In cases where for certain sectors no uncertainties have been provided at all (e.g. indirect CO<sub>2</sub> emissions, LULUCF), an average (median) sector uncertainty in percent is calculated from all the countries for which complete sectoral emissions and uncertainties were reported, and this average uncertainty is assigned to the country's sector GHG total reported in its final CRF tables.

The country-level uncertainties presented in this paper were provided by the EU GHG inventory team and have been compiled using this same processing routine and using the uncertainties and CRF data reported by the countries in the 2021 submission. However, for the purpose of this synthesis work, the method has been expanded to gap-fill at the individual greenhouse gas level (CH<sub>4</sub> and N<sub>2</sub>O emissions only) rather than at the aggregate GHG level. Furthermore, the expanded method here assigns the sub-sectoral uncertainties to the emissions and removals of the entire time series (1990-2019), rather than just the base year and latest year of the respective time series. This allows uncertainties to be sensitive to the sub-sectoral contributions to sectoral and national total emissions, which of course change over time. For each year of the time series, uncertainties in the total and sectoral CH<sub>4</sub> and N<sub>2</sub>O emissions are calculated using Gaussian error propagation, by summing the respective sub-sectoral uncertainties (expressed in kton CH<sub>4</sub> and N<sub>2</sub>O) in quadrature and assuming no error correlation. In contrast, for the EU27+UK bloc, uncertainties in the total and sectoral CH<sub>4</sub> and N<sub>2</sub>O emissions were calculated to take into account error correlations between the respective country estimates at the subsector level. This was done by applying the same methods and assumptions described in the 2022 EU NIR (UNFCCC NIR, 2022). The subsector resolution applied for gap-filling allows the routine to access respective data on emission factors from CRF Table *Summary 3* and apply correlation coefficients ( $r$ ) when aggregating the uncertainties. For a given subsector, it is assumed that the errors of countries using default factors are completely correlated ( $r = 1$ ), while errors of countries using country-specific factors are assumed uncorrelated ( $r = 0$ ). For countries using a mix of default and country-specific factors at the given subsector level, it is assumed that these errors are partially correlated ( $r = 0.5$ ) with one another and with the errors of countries using the default factors only.

Based on these correlation assumptions, the routine then aggregates CH<sub>4</sub> and N<sub>2</sub>O emissions and uncertainties for the specified subsector resolution at the EU27+UK level. Uncertainties at sector total level are then aggregated from the subsector estimates assuming no correlation between subsectors. However, for countries reporting very

1215 coarse resolution estimates (e.g. total sector CH<sub>4</sub> and N<sub>2</sub>O emissions) or where the sector has been partially or completely gap-filled, it is assumed that these uncertainties are partially correlated ( $r = 0.5$ ) with one another and with the other reported subsector level estimates. Level uncertainties on the total EU27+UK CH<sub>4</sub> and N<sub>2</sub>O emissions (with and without LULUCF) are then aggregated from the sector estimates assuming no error correlation between sectors.

## 1220 **EDGAR v6.0**

The Emissions Database for Global Atmospheric Research (EDGAR) is an independent global emission inventory of greenhouse gases (GHG) and air pollutants developed by the Joint Research Centre of the European Commission (<https://edgar.jrc.ec.europa.eu/index.php>). The first edition of the Emissions Database for Global Atmospheric Research was published in 1995. The dataset now includes almost all sources of fossil CO<sub>2</sub> emissions, is updated annually, and reports data for 1970 to n-1. Estimates are provided by sector. Emissions are estimated fully based on statistical data from 1970 till 2018 <https://data.jrc.ec.europa.eu/dataset/97a67d67-c62e-4826-b873-9d972c4f670b>. For complete description see Andrew (2020).

**Uncertainties:** EDGAR uses emission factors (EFs) and activity data (AD) to estimate emissions. Both EFs and AD are uncertain to some degree, and when combined, their uncertainties need to be combined too. To estimate EDGAR's uncertainties (stemming from lack of knowledge of the true value of the EF and AD), the methodology devised by IPCC (2006, Chapter 3) is adopted, that is the sum of squares of the uncertainty of the EF and AD (uncertainty of the product of two variables). A log-normal probability distribution function is assumed to avoid negative values, and uncertainties are reported as 95 % confidence interval according to IPCC (2006, chapter 3, equation 3.7). For emission uncertainty in the range 50 % to 230% a correction factor is adopted as suggested by Frey et al (2003) and IPCC (2006, chapter 3, equation 3.4). Uncertainties are published in Solazzo et al., 2021.

## **CAPRI**

CAPRI is an economic, partial equilibrium model for the agricultural sector, focused on the EU (Britz and Witzke, 2014<sup>12</sup>; Weiss and Leip, 2012<sup>13</sup>). CAPRI stands for 'Common Agricultural Policy Regionalised Impact analysis', and the name hints at the main objective of the system: assessing the effect of CAP policy instruments not only at the EU or Member State level but at sub-national level too. The model is calibrated for the base year (currently 2012) and then baseline projections are built, allowing the ex-ante evaluation of agricultural policies and trade policies on production, income, markets, trade and the environment.

Among other environmental indicators, CAPRI simulates CH<sub>4</sub> emissions from agricultural production activities (enteric fermentation, manure management, rice cultivation, agricultural soils). Activity data is mainly based on FAOSTAT and EUROSTAT statistics and estimation of emissions follows IPCC 2006 methodologies, with a higher or lower level of detail depending on the importance of the emission source. Details on CAPRI methodology

---

<sup>12</sup> [https://www.capri-model.org/docs/CAPRI\\_documentation.pdf](https://www.capri-model.org/docs/CAPRI_documentation.pdf)

<sup>13</sup> <https://www.sciencedirect.com/science/article/pii/S0167880911004415>

for emissions calculations is referenced in the Annex Table A1. For this study CAPRI updated emissions for three years: 2014, 2016 and 2018.

1250 **Uncertainties** were calculated for the updated years, 2014, 2016 and 2018. The uncertainty of the spatial allocation of emissions for CH<sub>4</sub> and N<sub>2</sub>O has been calculated by taking into account the uncertainty of the spatial disaggregation and the uncertainty of the emission sources, assuming:

- the disaggregation having an uncertainty of 50% for N<sub>2</sub>O and 20% for CH<sub>4</sub>.
- the emission processes have uncertainty of:

1255

- 50%: N<sub>2</sub>O soil processes;
- 30%: N<sub>2</sub>O manure processes;
- 30%: CH<sub>4</sub> manure and enteric, and
- 10%: rice.

1260 Then, for each cell, the uncertainty of the disaggregation and that of the process are combined as they are independent (sum of squares, see Solazzo et al., 2021) and then the total uncertainty for the grid cell is aggregated using emission weighted sum of squares.

## **GAINS**

1265 Specific sectors and abatement technologies in GAINS vary by the specific emitted compound, with source sector definition and emission factors largely following the IPCC methodology at the Tier 1 or Tier 2 level. GAINS includes in general all anthropogenic emissions to air, but does not cover emissions from forest fires, savannah burning and land use / land use change. Emissions are estimated for 174 countries/regions, with the possibility to aggregate to a global emission estimate, and spanning a timeframe from 1990 to 2050 in five-year intervals. Activity drivers for macroeconomic development, energy supply and demand, and agricultural activities are entered externally, GAINS extends with knowledge required to estimate “default” emissions (emissions occurring due to an economic activity without emission abatement) and emissions and costs of situations under emission control (see Amann et al., 2001).

1270 The GAINS model covers all source sectors of anthropogenic methane (CH<sub>4</sub>) emissions; agricultural sector emissions from livestock, rice cultivation and agricultural waste burning, energy sector emissions from upstream and downstream sources in fossil fuel extraction and use, and emissions from handling and treatment of solid waste and wastewater source sectors. A description of the modelling of CH<sub>4</sub> emissions in GAINS is presented in Höglund-Isaksson (2020). Generation of solid waste and the carbon content of wastewater are derived within the model in consistency with the relevant macroeconomic scenario. The starting point for estimations of anthropogenic CH<sub>4</sub> is the methodology recommended in the IPCC (2006 and revision in 2019) guidelines, for most source sectors using country-specific information to allow for deriving country- and sector/technology- specific emission factors at a Tier 2 level. Consistent methodologies were further developed to estimate emissions from oil and gas systems (Höglund-Isaksson, 2017) and solid waste (Höglund-Isaksson, 2018; Gómez-Sanabria et al., 2018). Emission factors are specified in a consistent manner across countries for given sets of technology and with past implementation of emission abatement measures reflected as changes in technology structures. The resulting emission estimates are well comparable across geographic and temporal scales. The GAINS approach to calculate waste emissions is developed in consistency with

the First-Order-Decay method recommended by IPCC (2006 and 2019 revision), applying different decay periods when estimating emissions from flows of different types of organic waste, i.e., food & garden, paper, wood, textile and other. Data on waste generation, composition and treatment are taken from EUROSTAT (2019) and complemented with national information from the UNFCCC (2019) Common Reporting Format tables on the amounts of waste diverted to landfills of various management levels and to treatment e.g., recycling, composting, biodigestion and incineration.

**Uncertainties:** Uncertainty is prevalent among many different dimensions both in the estimations of emissions, abatement potentials and costs. When constructing global bottom-up emission inventories at a detailed country and source level, it is inevitable that some information gaps will be bridged using default assumptions. As it is difficult to speculate about how such sources of uncertainty affect resulting historical and future emission estimates, we instead address uncertainty in historical emissions by making comparisons to estimates by other publicly available and independently developed bottom-up inventories and various top-down estimates consistent with atmospheric measurements and inverse model results. Although existing publicly available global bottom-up inventories adhere to the recommended guidelines of the IPCC (2006), the flexibility in these is large and results will depend on the availability and quality of gathered source information. There is accordingly a wide range of possible sources of uncertainty built into estimations in such comprehensive efforts. Having a pool of independently developed inventories, each with its own strengths and weaknesses, can improve the understanding of the scope for uncertainty, in particular when compared against top-down atmospheric measurements.

### ***FAOSTAT***

FAOSTAT: The Food and Agricultural Organization of the United Nations (FAO), provides CH<sub>4</sub> emissions totals or per gas/activity from agriculture and LULUCF available at: <https://www.fao.org/faostat/en/#data/GT>. The FAOSTAT emissions database is computed following Tier 1 IPCC 2006 Guidelines for National GHG Inventories (<http://www.ipcc-nggip.iges.or.jp/public/2006gl/index.html>). Country reports to FAO on crops, livestock and agriculture use of fertilizers are the source of activity data. Geospatial data are the source of AD for the estimates from cultivation of organic soils, biomass and peat fires. GHG emissions are provided by country, regions and special groups, with global coverage, relative to the period 1961-present (with annual updates, currently to 2019) and with projections for 2030 and 2050, expressed as CO<sub>2</sub>e for CH<sub>4</sub>, by underlying agricultural emission sub-domain and by aggregate (agriculture total, agriculture total plus energy, agricultural soils). LULUCF emissions consist of CH<sub>4</sub> (methane) associated with biomass and peat fires. Comparison to the UNFCCC submissions is also provided.

**Uncertainties** were computed by Tubiello et al., 2013 but are not available in the FAOSTAT database.

### ***Top-down anthropogenic CH<sub>4</sub> emission estimates***

#### ***FLEXPART – FLExKF***

FLExKF applies an Extended Kalman Filter (Brunner et al. 2012) in combination with backward Lagrangian transport simulations using the model FLEXPART (Stohl et al. 2005; Pisso et al. 2019). It optimizes surface-atmosphere fluxes by assimilating atmospheric observations in a sequential manner, which allows for an analytical solution for relatively large inversion problems (long time periods, number stations O(100)). Since model-observation

residuals typically follow a log-normal distribution, the method optimizes log-transformed emissions, which also guarantees a positive solution. Source-Receptor Matrices (Seibert and Frank, 2004) were computed at  $0.25^\circ \times 0.25^\circ$  resolution with FLEXPART driven by ECMWF Era Interim meteorological fields in the same way as for FlexInvert. Backward simulations were limited to 10 days prior to each observation and to the domain  $15^\circ\text{W} - 35^\circ\text{E}$ ,  $30^\circ\text{N} - 75^\circ\text{N}$ . Fluxes were estimated for this domain on a monthly basis at  $0.5^\circ \times 0.5^\circ$  resolution. For the version used in this study, FLExKF-CAMsv19r\_EMPA, the background mole fraction was taken from CAMsv19r which is based on the global TM5-4DVAR assimilation run (Bergamaschi et al. 2018a) where the above domain was cut out following the two-step approach of Rödenbeck et al. (2009).

**Uncertainties:** The uncertainty in the posterior fluxes is composed of random and systematic errors. The random uncertainties are represented by the posterior error covariance matrix provided by the Kalman Filter, which combines errors in the prior fluxes with errors in the observations and model representation. Systematic uncertainties primarily arise from systematic errors in modelled atmospheric transport and in background mole fractions, but also include aggregation errors, i.e. errors arising from the way the flux variables are discretized in space and time.

### ***FLEXINVERT***

The FlexInvert framework is based on Bayesian statistics and optimizes surface-atmosphere fluxes using the maximum probability solution (Rodgers, 2000). Atmospheric transport is modelled using the Lagrangian model FLEXPART (Stohl et al., 2005; Pisso et al., 2019) run in the backwards time mode to generate a so-called Source-Receptor Matrix (SRM). The SRM describes the relationship between the change in mole fraction and the fluxes discretized in space and time (Seibert and Frank, 2004) and was calculated for 8 days prior to each observation. For use in the inversions, FLEXPART was driven using ECMWF operational analysis wind fields. The state vector consisted of prior fluxes discretized on an irregular grid based on the SRMs (Thompson et al. 2014). This grid has finer resolution (in this case the finest was  $0.25^\circ \times 0.25^\circ$ ) where the fluxes have a strong influence on the observations and coarser resolution where the influence is only weak (the coarsest was  $2^\circ \times 2^\circ$ ). The fluxes were solved at 10-days temporal resolution. The state vector also included scalars for the background contribution. The background mixing ratio, i.e., the contribution to the mixing ratio that is not accounted for in the 8-day SRMs, was estimated by coupling the termination points of backwards trajectories (modelled using virtual particles) to initial fields of methane simulated with the Lagrangian FLEXPART-CTM model, which was developed at Empa based on FLEXPART (Stohl et al., 2005; Pisso et al., 2019). Data assimilation method described by Groot Zwaaftink et al. (2018) that constrains modelled fields with surface observations through nudging was applied for current simulations.

**Uncertainties:** The posterior fluxes are subject to systematic errors primarily from: 1) errors in the modelled atmospheric transport; 2) aggregation errors, i.e. errors arising from the way the flux variables are discretized in space and time; 3) errors in the background methane fields; and 4) the incomplete information from the observations and hence the dependence on the prior fluxes. In addition, there is, to a smaller extent, some error due to calibration offsets between observing instruments. Uncertainties in the observation space were inflated to take into account the model representation errors



### *InGOS and TM5-4DVAR*

The atmospheric models used within the European FP7 project InGOS (Integrated non-CO<sub>2</sub> Greenhouse gas Observing System) are described by Bergamaschi et al., 2018a and Supplement (<https://www.atmos-chem-phys.net/18/901/2018/acp-18-901-2018-supplement.pdf>). The models include global Eulerian models with a zoom over Europe (TM5-4DVAR, TM5-CTE, LMDZ), regional Eulerian models (CHIMERE), and Lagrangian dispersion models (STILT, NAME, COMET). The horizontal resolutions over Europe are  $\sim 1.0\text{--}1.2^\circ$  (longitude)  $\times$   $\sim 0.8\text{--}1.0^\circ$  (latitude) for the global models (zoom) and  $\sim 0.17\text{--}0.56^\circ$  (longitude)  $\times$   $\sim 0.17\text{--}0.5^\circ$  (latitude) for the regional models. Most models are driven by meteorological fields from the European Centre for Medium-Range Weather Forecasts (ECMWF) ERA-Interim reanalysis (Dee et al., 2011). In the case of STILT, the operational ECMWF analyses were used, while for NAME meteorological analyses of the Met Office Unified Model (UM) were employed. The regional models use boundary conditions (background CH<sub>4</sub> mole fractions) from inversions of the global models (STILT from TM3, COMET from TM5-4DVAR, CHIMERE from LMDZ) or estimate the boundary conditions in the inversions (NAME) using baseline observations at MaceHead as prior estimates. In the case of NAME and CHIMERE, the boundary conditions are further optimised in the inversion. The inverse modelling systems applied in this study use different inversion techniques. TM5-4DVAR, LMDZ, and TM3-STILT use 4DVAR variational techniques, which allow optimisation of emissions of individual grid cells. These 4DVAR techniques employ an adjoint model in order to iteratively minimise the cost function using a quasi-Newton (Gilbert and Lemaréchal, 1989) or conjugate gradient (Rödenbeck, 2005) algorithm. The NAME model applies a simulated annealing technique, a probabilistic technique for approximating the global minimum of the cost function. In CHIMERE and COMET, the inversions are performed analytically after reducing the number of parameters to be optimised by aggregating individual grid cells before the inversion. TM5-CTE applies an ensemble Kalman filter (EnKF) (Evensen, 2003), with a fixed-lag smoother (Peters et al., 2005).

**Uncertainty:** In general, the estimated model uncertainties depend on the type of station and for some models (TM5-4DVAR and NAME) also on the specific synoptic situation. In InGOS the uncertainty of the ensemble was calculated as  $1\sigma$  estimate. Bergamaschi et al. (2015) showed that the range of the derived total CH<sub>4</sub> emissions from north-western and eastern Europe using four different inverse modelling systems was considerably larger than the uncertainty estimates of the individual models because the latter typically use Bayes' theorem to calculate the reduction of assumed a prior emission uncertainties by assimilating measurements (propagating estimated observation and model errors to the estimated emissions). An ensemble of inverse models may provide more realistic overall uncertainty estimates, since estimates of model errors are often based on strongly simplified assumptions and do not represent the total uncertainty.

### *InTEM – NAME*

The Inverse Technique for Emission Modelling (InTEM) (Arnold et al., 2018) uses the NAME (Numerical Atmospheric dispersion Modelling Environment) (Jones et al, 2007) atmospheric Lagrangian transport model. NAME is driven by analysis 3-D meteorology from the UK Met Office Unified Model (Cullen, 1993). The horizontal and vertical resolution of the meteorology has improved over the modelled period from 40 km to 12 km (1.5 km over the UK). InTEM is a Bayesian system that minimises the mismatch between the model and the atmospheric observations

given the constraints imposed by the observation and model uncertainties and prior information with its associated uncertainties. The direction (latitude and longitude) and altitude varying background concentration and observation station bias are solved for within the inverse system along with the spatial distribution and magnitude of the emissions. The time-varying prior background concentration for the DECC network stations is derived from the MHD observations when they are very largely sensitive only to Northern Canada (Arnold et al., 2018). The prior bias (that can be positive or negative) for each station is set to zero with an uncertainty of 1 ppb. The observations from each station are assumed to have an exponentially decreasing 12-hr time correlation coefficient and, between stations, a 200 km spatial correlation coefficient. The observations are averaged into 2-hr periods. The uncertainty of the observations is derived from the variability of the observations within each 2-hr period. The modelling uncertainty for each 2-hr period at each station varies and is defined as the larger of; the median pollution events in that year at that station, or 16.5% of the magnitude of the pollution event. These values have been derived from analysis of the observations of methane at multiple heights at each station across the DECC network. Each inversion is repeated 24 times, each time 10% of the observations per year per station are randomly removed in 5-day intervals and the results and uncertainty averaged.

**Uncertainty:** This random removal of observations allows a greater exploration of the uncertainty, given the potential for some of the emission sources to be intermittent within the time-period of the inversion.

#### ***CTE-CH<sub>4</sub> Europe, CTE-SURF and CTE-GOSAT***

CarbonTracker Europe CH<sub>4</sub> (CTE-CH<sub>4</sub>) (Tsuruta et al., 2017) applies an ensemble Kalman filter (Peters et al. 2005) in combination with the Eulerian transport model TM5 (Krol et al. 2005). It optimizes surface fluxes weekly, and assimilates atmospheric CH<sub>4</sub> observations. TM5 was run at 1° x 1° resolution over Europe and 6° x 4° resolution globally, constrained by 3-hourly ECMWF ERA-Interim meteorological data. The photochemical sink of CH<sub>4</sub> due to tropospheric and stratospheric OH, and stratospheric Cl and O(<sup>1</sup>D) was pre-calculated based on Houweling et al. (2014) and Brühl and Crutzen (1993) and not adjusted in the optimization scheme.

Three experiments were conducted, which differ in (1) sets of prior fluxes, (2) sets of assimilated observations, and (3) optimization resolution over the Northern Hemisphere.

In Petrescu et al., 2021a study, CTE-FMI used sets of prior fluxes from LPX-Bern DYPTOP (Stocker et al., 2014) for biospheric, EDGAR v4.2 FT2010 (Janssens-Maenhout et al., 2013) for anthropogenic, GFED v4 (Giglio et al., 2013) for biomass-burning, Ito and Inatomi (2012) for termites and Tsuruta et al. (2017) for ocean sources. CTE-SURF and CTE-GOSAT use sets of prior fluxes from Global Carbon Project (Saunois et al., 2020). CTE-FMI and CTE-SURF assimilated ground-based surface CH<sub>4</sub> observations, while CTE-GOSAT assimilated GOSAT XCH<sub>4</sub> retrievals from NIES v2.72. CTE-FMI optimized fluxes at 1° x 1° resolution over Northern Europe, northeast Russia and southeast Canada, 6° x 4° resolution over other parts of the Northern Hemisphere land, and region-wise (combined TransCom regions and soil-type) over the Southern Hemisphere and ocean. CTE-SURF and CTE-GOSAT fluxes were optimized at 1° x 1° resolution over Europe and region-wise elsewhere globally. For the current study, CTE-FMI S5 simulations updated priors as described in Table B2.4.

**Uncertainty:** The prior uncertainty is assumed to be a Gaussian probability distribution function, where the error covariance matrix includes errors in prior fluxes, observations and transport model representations. The uncertainty

for the prior fluxes were assumed to be 80 % of the fluxes over land and 20 % over ocean, with correlation between grid cells or regions to be 100-500 km over land and 900 km over ocean. The uncertainty for observations and transport model representations vary between observations, with min. aggregated uncertainty to be 7.5 ppb for surface observations and 15 ppb for GOSAT data. The posterior uncertainty is calculated as standard deviation of the ensemble members, where the posterior error covariance matrix is driven by the ensemble Kalman filter.

### ***VERIFY Community Inversion Framework (CIF)***

In the current study, new CIF results are presented (Berchet et al., 2021). For CH<sub>4</sub>, inversions were run with CHIMERE, FLEXPART (NILU) and FLEXPART-EMPA. The results from CHIMERE differed somewhat from the two FLEXPART models in where the posterior fluxes departed from the prior estimates, but were reasonably comparable in terms of the annual emissions at regional scales. The models were run for EU27 plus Norway, Switzerland and UK, with annual mean emissions for 2005-2018.

**CHIMERE** (see <https://www.lmd.polytechnique.fr/chimere/>) is a non-hydrostatic Eulerian chemistry-transport model. Its area-limited domains can be designed to cover the hemispheric to the urban scales, with horizontal resolutions from several degrees to one kilometer. The time-steps usually cover a few minutes, depending on the CFL and choices made by the user for minimizing computation costs. For the purpose of flux inversions, the tangent-linear and the adjoint codes have been developed and parallelized, only for trace-gases (see (Fortems-Cheiney et al., 2021), their Section 3.2 for more details). The required input data are meteorological 3D and 2D fields (e.g. temperature, wind speed), boundary conditions for concentrations at the four sides and at the top of the domain and emission fluxes. The comparison to surface measurements is done by extracting from the model the simulated concentrations in the grid cell matching the stations' locations for the time-steps matching the measurement date and time. If the measurement covers a longer time (e.g. hourly means), the simulated concentrations for the matching time-steps are averaged. For this deliverable, CHIMERE was run using meteorological data from the ECMWF's IFS operational forecast (every three hours) retrieved at  $0.25^\circ \times 0.25^\circ$  and interpolated onto the model's grid ( $0.5^\circ \times 0.5^\circ$ ). CHIMERE extends from the surface to 200 hPa with 17 sigma-pressure levels.

For the inversions provided by NILU, FLEXPART-v10.4 was run using ECMWF's operational IFS forecast with backward trajectory lengths of 10 days for CH<sub>4</sub>. The footprints were saved at  $0.25^\circ \times 0.25^\circ$  for CH<sub>4</sub> inversions. For the inversions provided by EMPA, FLEXPART-v9.2 was run using ECMWF's ERA-Interim (up to 2018) and ERA5 for 2019 with backward trajectory lengths of 10 days and footprints were saved at  $0.25^\circ \times 0.25^\circ$ . For CH<sub>4</sub>, prior anthropogenic emissions come from (EDGAR-v6) and for fluxes from natural soils (JSBACH-HIMMELI) and inland waters (CSLM-CH<sub>4</sub> model), and were supplemented by estimates from previous studies for geological, ocean and termite emissions (Etiope et al., 2019, Weber et al., 2019 and Saunois et al., 2020 (GCP-CH<sub>4</sub>)). The EDGAR estimates were updated to include new activity data for 2016 to 2018, whereas in the previous version emissions for these years were based on a so-called fast-track estimation using proxies. The new estimate for lakes combines an empirical estimate, which provides only an annual climatology, with a monthly-resolved estimate from a mechanistic-stochastic modelling approach (MSM) accounting for nutrient (N and P) loads delivered to each lake and control of CH<sub>4</sub> emission by the lake trophic status.

**Uncertainties:** In the CIF, the uncertainties are described by matrices, with variances on the diagonal and covariances on the off-diagonal. They are called respectively the prior error (for the error statistics on the prior controlled variables) and the observation error (for the error statistics on the difference between the observed and modelled mixing ratios). Observations errors were assumed to be independent from each other in all inversions, i.e., the observation error covariance matrix is diagonal. For CHIMERE, measurement errors were combined with the transport, representation, and aggregation errors calculated for each station following (Szénási et al., 2021) using simulations based on the TNO emission inventory. For FLEXPART (NILU), the observations errors were taken from the observation files, but set to a minimum of 9 ppb. In addition, 50% of the contribution to from the fluxes outside the inversion domain (used in the calculation of the background mixing ratio) was added to the observation error. For FLEXPART-EMPA measurement errors were composed of an observation error and a model error, which are summed quadratically to obtain the total error. Observation errors were taken from the observation files and an average model error was determined for each station separately by an iterative procedure, following Koohkan and Bocquet (2012): An initial value was computed from the root-mean-square-differences between a priori simulated values and the observations. With this initial value, an inversion was performed. The model error was then scaled using the Eq. (20) of Koohkan and Bocquet (2012) until convergence.

#### ***MIROC4-ACTM:***

The MIROC4-ACTM time dependent inversions solve for emissions from 53 regions for CH<sub>4</sub> and 84 regions for N<sub>2</sub>O. The inversion framework is based on Bayesian statistics and optimizes surface-atmosphere fluxes using the maximum probability solution. Atmospheric transport is modelled using the JAMSTEC's Model for Interdisciplinary Research on climate, version 4 based atmospheric chemistry-transport model (MIROC4-ACTM) (Watanabe et al. 2008; Patra et al. 2018). The Source-Receptor Matrix (SRM) is calculated by simulating unitary emissions from 53 or 84 basis regions, for which the fluxes are optimised. The SRM describes the relationship between the change in mole fraction at the measurement locations for the unitary basis region fluxes. The MIROC4-ACTM meteorology was nudged to the JMA 55-year reanalysis (JRA55) horizontal wind fields and temperature. The calculation of photochemical losses is performed online. The hydroxyl (OH) radical concentration for reaction with CH<sub>4</sub> vary monthly but without any interannual variations. The simulated mole fractions for the total a priori fluxes are subtracted from the observed concentrations before running the inversion calculation (as in Patra et al., 2016 for CH<sub>4</sub> inversion). Both the inversion results are contributed to the GCP-CH<sub>4</sub> and GCP-N<sub>2</sub>O activities (Saunois et al., 2020; Thompson et al., 2019; Tian et al., 2020).

**Uncertainties:** The posterior fluxes are subject to systematic errors primarily from: 1) errors in the modelled atmospheric transport; 2) aggregation errors, i.e. errors arising from the way the flux variables are discretized in space (84 regions) and time (monthly-means); 3) errors in the background mole fractions (assumed to be a minor factor); and 4) the incomplete information from the sparse observational network and hence the dependence on the prior fluxes. In addition, there is, to a much smaller extent, some error due to calibration offsets between observing instruments, which is more pertinent for N<sub>2</sub>O than for other GHGs. We have validated model transport in troposphere using SF<sub>6</sub> for the inter-hemispheric exchange time, and the using SF<sub>6</sub> and CO<sub>2</sub> for the age of air in the stratosphere. The simulated

1505 N<sub>2</sub>O concentrations are also compared with aircraft measurements in the upper troposphere and lower stratosphere for  
evaluating the stratosphere-troposphere exchange rates. Comparisons with ACE-FTS vertical profiles in the  
stratosphere and mesosphere indicate good parameterisation of N<sub>2</sub>O loss by photolysis and chemical reactions, and  
thus the lifetime, which affect the global total N<sub>2</sub>O budgets. Random uncertainties are calculated by the inverse model  
depending on the prior flux uncertainties and the observational data density and data uncertainty. Only 37 sites are  
1510 used in the inversion and thus the reduction in priori flux uncertainties have been minimal. The net fluxes from the  
inversion from individual basis regions are less reliable compared to the anomalies in the estimated fluxes over a  
period of time.

### ***Global Carbon Project – Global Methane Budget (GMB)***

1515 GMB uses an ensemble of 22 top-down global inversions for anthropogenic CH<sub>4</sub> emissions presented in  
Saunois et al. (2020) for the Global Methane Budget. These inversions were simulated by nine atmospheric inversion  
systems based on various chemistry transport models, differing in vertical and horizontal resolutions, meteorological  
forcing, advection and convection schemes, and boundary layer mixing. Surface-based inversions were performed  
over the period 2000-2017 while satellite-based inversions cover the GOSAT data availability 2010-2017. The  
1520 protocol established for these simulations was not stringent as the prior emission flux data set was not mandatory, and  
each group selected their constraining observations. More information can be found in Saunois et al. (2020) in  
particular in their Table 6 and S6.

**Uncertainties:** currently there are no uncertainties reported for the GMB models. This study uses the median and the  
min/max as uncertainty range estimation from the 22 models ensemble. In general uncertainties might be due to factors  
1525 like: different transport models, physical parametrizations, prior fluxes, observation data sets etc.

## **A2: Natural CH<sub>4</sub> emissions**

### ***Bottom-up natural CH<sub>4</sub> emissions estimates***

#### ***CH<sub>4</sub> emissions from inland waters***

The CH<sub>4</sub> estimate from inland waters represents a climatology of diffusive and ebullitive CH<sub>4</sub> emissions from  
rivers, lakes and reservoirs. It is based on two approaches. The first approach synthesizes average annual CH<sub>4</sub>  
emissions fluxes for Europe that were rescaled to a consistent set of inland water surface area (Lauerwald et al., in  
rev. GBC) and corrected for the effect of seasonal ice cover. To obtain fluxes for the EU27+UK domain, the median  
1535 and first interquartile range values are scaled down by a factor 0.75 based on the surface area of the two domains. The  
second approach provides a spatially-resolved climatology of inland water fluxes at the resolution of 0.1°. The river  
estimate relies on the 0.1°x0.1° river water surface area of Lauerwald et al. (2015) and 3 observation-based  
assessments (Bastviken et al., 2011; Stanley et al., 2016; Rosentreter et al., 2021) of mean CH<sub>4</sub> flux densities for  
European rivers. Note the very large range encompassed by the 3 studies (0.07-0.66 Tg CH<sub>4</sub> yr<sup>-1</sup> for EU27+UK),  
1540 reflecting high uncertainty in the assessment of the river CH<sub>4</sub> flux. The lake estimate not only resolves the spatial  
variability, but also the temporal variability in CH<sub>4</sub> emissions. To do so, the mechanistic-stochastic-modeling (MSM)

approach of Maavara et al. (2017, 2019) and Lauerwald et al. (2019) was expanded to resolve the lake seasonal dynamics and the biogeochemical processes of the CH<sub>4</sub> and O<sub>2</sub> cycles occurring in the water column and sediments. To constrain the lake physics, the Canadian Small Lake Model (CSLM) was used (MacKay, 2012). CSLM represents lake stratification and mixing events by simulating vertical temperature profiles, thermocline and light penetration depths, and lake ice dynamics. For carbon, the MSM simulates a lake-mean trophic state from the balance between Net Primary Production (limited by light and nutrient inputs from the watershed) and heterotrophic decomposition of organic matter. It was upgraded to simulate vertical profiles of O<sub>2</sub> and CH<sub>4</sub> by accounting for eddy-diffusive transport and the set of consumption/production processes of the O<sub>2</sub>-CH<sub>4</sub> cycles at the (sub)-daily resolution with a vertical resolution of less than one meter (Maisonnier et al., in prep.). In the sediment, net CH<sub>4</sub> production was split into diffusive and ebullitive pathways using an approach modified from Langenegger et al. (2019). The new process-based model was then applied to the European domain, using a lake clustering approach whereby within each grid of the simulation domain (2.5°x2.5°), lakes are binned into different classes as a function of the key drivers of CH<sub>4</sub> fluxes that are lake-size and depth (Messenger et al., 2016), and lake trophic status. Then, for each grid and each class, a representative simulation forced by high-resolution local climate forcings extracted from the lake sector of ISIMIP was performed. To carry out the spatial upscaling, the resulting diffusive and ebullitive areal CH<sub>4</sub> fluxes through the water-air interface were multiplied by the surface area of each lake class in each grid of the domain, extracted from the HydroLAKES database (Messenger et al., 2016).

### ***JSBACH-HIMMELI***

The model framework, JSBACH-HIMMELI (Raivonen et al., 2017; Susiluoto et al., 2018) is used to estimate wetland and mineral soil emissions, and an empirical model is used to estimate the emissions from inland water bodies.

JSBACH-HIMMELI is a combination of two models, JSBACH, that is the land-surface model of MPI-ESM (Reick et al., 2013), and HIMMELI, that is a specific model for northern peatland emissions of CH<sub>4</sub> (Raivonen et al., 2017). HIMMELI (Helsinki Model of Methane build-up and emission for peatlands) has been developed especially for estimating CH<sub>4</sub> production and transport in northern peatlands. It simulates both CH<sub>4</sub> and CO<sub>2</sub> fluxes and can be used as a module within different modelling environments (Raivonen et al., 2017; Susiluoto et al., 2018). HIMMELI is driven with soil temperature, water table depth, the leaf area index and anoxic respiration. These parameters are provided to HIMMELI from JSBACH, which models hydrology, vegetation and soil carbon input from litter and root exudates. CH<sub>4</sub> emission and uptake of mineral soils are calculated applying the method by Spahni et al. (2011) based on soil moisture estimated by JSBACH.

The distribution of terrestrial vegetation types in JSBACH-HIMMELI is adopted from CORINE land cover data and from native JSBACH land cover for the areas that CORINE does not cover. The HIMMELI methane model is applied for peatlands and the mineral soil approach for the rest. The map of inland water CH<sub>4</sub> emissions has been combined with JSBACH-HIMMELI land use map so that the map of inland waters is preserved and JSBACH grid-based fractions of different land use categories adjusted accordingly. In order to avoid double-counting the terrestrial CH<sub>4</sub> flux estimates have been normalized by the ratio of the two inland water body distributions.

**Uncertainties:** As in any process modeling the uncertainties of the bottom up modeling of CH<sub>4</sub> arise from three primary sources: parameters, forcing data (including spatial and temporal resolution), and model structure. An important source of uncertainty in the case of terrestrial CH<sub>4</sub> flux modeling is the spatial distribution of peatlands.

1580 The uncertainties of JSBACH-HIMMELI peatland emissions were estimated by comparing the annual totals of measured and simulated methane fluxes at five European observation sites. Two of the sites are located in Finnish Lapland, one in middle Sweden, one in southern Finland and one in Poland.

For the sensitivity of mineral soil fluxes Spahni et al. (2011) tested two soil moisture thresholds, 85% or 95% of water holding capacity, below which mineral soils were assumed to be only CH<sub>4</sub> sinks, above which sources. We  
1585 used the higher value, 95% of water holding capacity. The uncertainty was estimated using CH<sub>4</sub> flux simulations of one year (2005). We did two new model runs, using moisture thresholds 95±15%, and derived the uncertainty from the resulting range in the annual emission sum.

### *Geological fluxes*

#### 1590 *Framework and previous works*

Geological methane emissions to the atmosphere, including natural gas seepage in petroliferous sedimentary basins and geothermal exhalations, were estimated at the global scale by multiple authors, based on bottom-up and top-down procedures (see review, including discussions on conflicting estimates, in Etiope and Schwietzke, 2019; Thornton et al. 2021 and references therein), and accounting for about 40-50 Tg CH<sub>4</sub> yr<sup>-1</sup>.

1595 For the European continent, a first geo-methane emission estimate was proposed by Simpson et al. (1999) with “a best guess” of 0.01 Tg yr<sup>-1</sup> and a speculative upper limit of 3 Tg yr<sup>-1</sup>, only on the basis of an extrapolation of a few submarine emission data. At the time of the Simpson’s work, very few data on geological methane fluxes on land were available, and emission factors were basically unknown. Bottom-up emission estimates at European level including onshore seepage and geothermal exhalations were proposed ten years later, by Etiope (2009), on the basis  
1600 of published regional emission estimates, suggesting around 3 Tg yr<sup>-1</sup> for geographic, onshore and offshore, Europe (including Azerbaijan; practically corresponding to present EU49).

Again ten years later, thanks to a wider data-set of CH<sub>4</sub> seepage flux from different geological environments in different countries and global inventories of geo-CH<sub>4</sub> emission sites, a process-based model using statistically derived emission factors and activity (areas) was developed to derive a global grid map of geo-CH<sub>4</sub> emissions (Etiope  
1605 et al. 2019). The global grid model, developed by ArcGIS at 1°x1° resolution, can be, in theory, used to derive (scale-up) geo-CH<sub>4</sub> emissions at continental or regional scale.

This exercise was done, for Europe (EU27+UK) by Petrescu et al. (2021a), obtaining a value of 8.8 Tg yr<sup>-1</sup>. The authors wished, however, to scale-down this value taking into account a global top-down estimate based on radiocarbon-free CH<sub>4</sub> in ice cores by Hmiel et al. (2020), who suggested, for the entire planet, 1.6 Tg yr<sup>-1</sup>. This global  
1610 estimate has more recently been contextualized and questioned by Thornton et al. (2021); in fact, the Hmiel et al. (2020) estimate has the same order of magnitude of emissions estimated by multiple authors for single local and regional seepage areas, so that the global emission must be considerable higher.

Petrescu et al. (2021) used however the upper limit of Hmiel et al. (2020), 5.4 Tg yr<sup>-1</sup>, to scale-down the global gridded emission of Etiope et al. (2019), i.e. 37.4 Tg yr<sup>-1</sup>, which is not the estimated global emission (43-50 Tg yr<sup>-1</sup>, which included some factors that could not be considered in the grid model). From the 8.8 Tg yr<sup>-1</sup> (EU27 + UK), Petrescu et al. (2021) obtained then 1.3 Tg yr<sup>-1</sup> (for marine and land geological emissions) as follows:

$$8.8 \times 5.4/37.4 = 1.3 \text{ Tg CH}_4 \text{ yr}^{-1} \quad (1)$$

Besides the subjective use of the upper limit of Hmiel et al. (2020) and of the gridded (not the estimated global) value of Etiope et al. (2019), it is important to note that the initial gridded value derived for EU27+UK, 8.8 yr<sup>-1</sup>, is affected by the relatively low precision, at the European scale, of the input data used for the global grid model. The global model was, in fact, developed on the basis of a global, large scale distribution of geological factors (for example the area of petroleum fields which determines the microseepage area), which lack the necessary precision for lower (continental and country) scale application. The main purpose of the global gridding was to offer a global spatial distribution of geo-CH<sub>4</sub> sources, with emission potential and methane isotopic values; it could not provide locally precise geo-CH<sub>4</sub> emissions because the datasets, developed for gridding purposes, was not complete and did not contain all the information necessary for improving previous estimates. A refinement of bottom-up estimates was possible only for mud volcanoes and microseepage because their gridding implied a more careful assessment of the spatial distribution and emission factors.

### ***Re-assessment of geo-CH<sub>4</sub> emissions in Europe***

For the current study, the global grid model of Etiope et al. (2019) was applied, using more detailed input data for Europe, with reference to the potential area of microseepage (activity) derivable by a more precise estimate of the continental oil-gas field area. The same microseepage emission factors statistically derived on global scale were used. For the other categories of geo-CH<sub>4</sub> sources (mud volcanoes, onshore seeps, submarine seepage and geothermal manifestations) European country masks from VERIFY (relative to EU27+UK and EU49) for the calculation of the onshore emission, and related EEZ (Exclusive Economic Zone) for the calculation of the sub-marine seepage were applied, to derive the global emission grid.

In the global microseepage emission model, the area where microseepage can potentially exist (named EMA - effective microseepage area) was estimated taking into account the distribution of microseepage observed by direct measurements in several oil-gas fields: statistical analysis of available data (summarized in Etiope et al. 2019) suggested that microseepage fluxes occur in about 57% of the petroleum field area (PFA). In theory, microseepage is expected also in the regions where seepage phenomena, manifested by macro-seeps (oil and gas seeps), exist. In Etiope et al. (2019) the global PFA was derived from Petrodata (Lujala et al. 2007), based on an oil-gas field digital map of USGS (Pawlewicz et al. 1997), which considered for each oil-gas field center point a buffer area of 30 km radius. The reason for this radius was not explained in Lujala et al. (2007).

In this work, the PFA of Europe (EU49) was derived by digitising all petroleum field center points from the USGS map (Pawlewicz et al. 1997). The microseepage CH<sub>4</sub> emission related to EMA is then derived by using the



same emission factors (four levels of microseepage; Table 2) established on global scale in Etiope et al. (2019). The results of the gridding, integrating activity (EMA) and emission factors, for EU49 are reported in Table A2.1.

1650

*Table A2.1: Results of microseepage gridding (0.05°x0.05°) for EU49*

	N. cell	Area (km <sup>2</sup> )	MS (t km <sup>-2</sup> yr <sup>-1</sup> )	Total output (t yr <sup>-1</sup> )
Gridded EMA	9457	199,703		2,985,570
Gridded Level 1	6843	143,307	0.474	67,927
Gridded Level 2	1899	40,094	11.366	455,708
Gridded Level 3	134	2959	40.15	118,804
Gridded Level 4	581	13,008	180.13	2,343,131

*MS: Microseepage emission factor statistically derived as described in Etiope et al. (2019).*

The EMA and related microseepage emission for EU27+UK are derived by applying the related mask on EU49, resulting in:

1655

EU27+UK EMA= 177,439 km<sup>2</sup> and microseepage EU27+UK = 2,161,060 t yr<sup>-1</sup>.

The total microseepage emission is quite sensitive to the activity (area); This estimate can be improved by increasing the number of measurements worldwide and related spatial (activity) and emission factor statistics.

For the other geological sources categories, i.e., onshore seeps (OS; including mud volcanoes), geothermal manifestations (GM) and submarine seepage (SS), the masks of the European territories (for EU27+UK and EU49, and the EEZ for the marine areas) on the global 1°x1° emission grid of Etiope et al. (2019) were applied. The result is summarised in Table A2.2.

1660

*Table A2.2: Gridded European geo-CH<sub>4</sub> emissions (t yr<sup>-1</sup>).*

	Microseepage (MS)	Onshore seeps (OS)	Geothermal (GM)	Submarine Seeps (SS)	TOTAL
EU49	2,985,570	2,162,539	404,205	1,653,049	7,205,363
EU27+UK	2,183,733	69,618	206,705	863,368	3,323,424

Table A2.3 compares the new results with previous European estimates (Etiope, 2009; Petrescu et al. 2021a).

1665

*Table A2.3: European geo-CH<sub>4</sub> emission estimates (Tg yr<sup>-1</sup>)*

	Etiope (2009)	Petrescu et al. (2021a)	This work

Geographic Europe (onshore+ offshore, including Azerbaijan)	3		
EU27+UK onshore		8.8 (from global grid model) 1.3 (scaled-down as Hmiel, 2020)	2.4
EU27+UK onshore + offshore			3.3
EU49 onshore			5.5
EU49 onshore + offshore			7.2

The overall uncertainties of the spatial distribution of the geo-CH<sub>4</sub> sources and CH<sub>4</sub> emissions depend on individual uncertainties of the four categories of seepage, which are discussed in Etiope et al. (2019). Compared to the global grid model, the uncertainty of the microseepage at European scale by refining the activity (microseepage area) has been reduced.

The new EU27+UK geo-CH<sub>4</sub> emission estimate is lower than the one derived by Petrescu et al. (2021a) using the global gridding, but higher than the scaled-down value (eq. 1). The EU49 (onshore+offshore) emission is higher than, but of the same order of magnitude of, the preliminary, rough estimate of geographic Europe, which included Azerbaijan, by Etiope (2009). Onshore geo-CH<sub>4</sub> emissions occur mostly in Azerbaijan, Italy, Romania, which are actually the EU49 countries with major onshore oil-gas reserves and production (BP, 2020), and thus with greater natural seepage potential. Offshore emissions are dominated by the large estimates published for the UK shelf (Judd et al, 1997, revised by Tizzard, 2008). These estimates need to be verified and improved. Beyond the emission values, our gridding provides, however, the first detailed map of natural geological methane emission in Europe, which can be used for continental scale methane budget modelling.

### ***Top-down natural CH<sub>4</sub> emissions estimates***

#### ***Global Carbon Project - Global Methane Budget (Saunois et al., 2020)***

For this study, none of the global inversions were updated.

GMB uses an ensemble of thirteen monthly gridded estimates of wetland emissions based on different land surface models as calculated for Saunois et al. (2020). Each model conducted a 30-year spin-up and then simulated net methane emissions from wetland ecosystems over 2000-2017. The models were forced by CRU-JRA reconstructed climate fields (Harris, 2019), and by the remote sensing-based wetland dynamical area dataset WAD2M (Wetland Area Dynamics for Methane Modeling). This data set provides monthly global areas over 2000-2017 based on a combination of microwave remote sensing data from Schroeder et al. (2015) and various regional inventory data sets.

More information is available in Saunio et al. (2020) and more details will be presented in a future publication led by Poulter et al., 2017 and colleagues.

**Uncertainty:** As described by Saunio et al. (2020) uncertainties are reported as minimum and maximum values of the available studies, in brackets. They do not take into account the uncertainty of the individual estimates, but rather express the uncertainty as the range of available mean estimates, i.e., the standard error across measurements/methodologies considered.

### **A3: Anthropogenic and natural N<sub>2</sub>O emissions**

#### ***Bottom-up N<sub>2</sub>O emission estimates***

**UNFCCC NGHGI (2019), EDGAR v6.0 and CAPRI:** descriptions are found in Appendix A1.

#### ***ECOSSE***

ECOSSE is a biogeochemical model that is based on the carbon model ROTH-C (Jenkinson and Rayner, 1977; Jenkinson et al. 1987; Coleman and Jenkinson, 1996) and the nitrogen-model SUNDIAL (Bradbury et al. 1993; Smith et al. 1996). All processes of the carbon and nitrogen dynamics are considered (Smith et al., 2010a,b). Additionally, in ECOSSE processes of minor relevance for mineral arable soils are implemented as well (e.g. methane emissions) to have a better representation of processes that are relevant for other soils (e.g. organic soils). ECOSSE can run in different modes and for different time steps. The two main modes are site specific and limited data. In the later version, basis assumptions/estimates for parameters can be provided by the model. This increases the uncertainty but makes ECOSSE a universal tool that can be applied for large scale simulations even if the data availability is limited. To increase the accuracy in the site-specific version of the model, detailed information about soil properties, plant input, nutrient application and management can be added as available.

During the decomposition process, material is exchanged between the SOM pools according to first order rate equations, characterised by a specific rate constant for each pool, and modified according to rate modifiers dependent on the temperature, moisture, crop cover and pH of the soil. The N content of the soil follows the decomposition of the SOM, with a stable C:N ratio defined for each pool at a given pH, and N being either mineralised or immobilised to maintain that ratio. Nitrogen released from decomposing SOM as ammonium (NH<sub>4</sub><sup>+</sup>) or added to the soil may be nitrified to nitrate (NO<sub>3</sub><sup>-</sup>).

For spatial simulations the model is implemented in a spatial model platform. This allows us to aggregate the input parameter for the needed resolution. ECOSSE is a one-dimensional model and the model platform provides the input data in a spatial distribution and aggregates the model outputs for further analysis. While climate data are interpolated, soil data are represented by the dominant soil type or by the proportional representation of the different soil types in the spatial simulation unit (this is in VERIFY a grid cell).

**Uncertainties** in ECOSSE arise from three primary sources: parameters, forcing data (including spatial and temporal resolution), and model structure.

### *DayCent*

DayCent was designed to simulate soil C dynamics, nutrient flows (N, P, S) and trace gas fluxes (CO<sub>2</sub>, CH<sub>4</sub>, N<sub>2</sub>O, NO<sub>x</sub>, N<sub>2</sub>) between soil, plants and the atmosphere at daily time-step. Submodels include soil water content and temperature by layer, plant production and allocation of net primary production (NPP), decomposition of litter and soil organic matter, mineralization of nutrients, N gas emissions from nitrification and denitrification, and CH<sub>4</sub> oxidation in non-saturated soils.

The DayCent modelling application at the EU level is a consolidated model framework running on LUCAS point (Orgiazzi, 2018) which was extensively explained in previous works (Lugato et al., 2017, 2018; Quemada et al., 2020) where a detailed description of numerical and geographical datasets and uncertainty estimations is reported.

Information directly derived from LUCAS (2009-2015) included the soil organic carbon content (SOC), particle size distribution and pH. Hydraulic properties and bulk density was also calculated with an empirically-derived pedotransfer. Management information was derived from official statistics (Eurostat, 2019) and included crop shares at NUTS2 level. The amount of mineral N was partitioned according to the regional crop rotations and agronomic crop requirements. Organic fertilization and irrigated areas were derived from the ‘Gridded Livestock of the World’ FAO dataset and the FAO-AQUASTAT product.

Meteorological data were downloaded from the E-OBS gridded dataset (<http://www.ecad.eu>) at 0.1° resolution. For the climatic projection, the gridded data from CORDEX database (<https://esgf-node.ipsl.upmc.fr/search/cordex-ipsi/>) were used. The average annual (2006-2010) atmospheric N deposition from the EMEP model (v4.5) were also implemented into the simulations. For current study, the results were updated and use the 2015-2019 mean.

**Uncertainty:** The starting year of the simulation was set in 2009 and projected in the future. The uncertainty analysis, based on the Montecarlo approach, was done running the model 52 times in each point and, contemporary, randomly sampling model inputs from probability density functions for: SOC pool partition, irrigation and both mineral and organic fertilization rates. The model outputs (including uncertainties) at point level were up-scaled regionally at 1 km resolution by a machine learning approach based on Random Forest regression.

### *N<sub>2</sub>O emissions from inland waters*

The N<sub>2</sub>O estimate represents a climatology of average annual N<sub>2</sub>O emissions from rivers, lakes, reservoirs and estuaries at the spatial resolution of 0.1°. Based on a spatially explicit representation of water bodies and point and non-point sources of N and P, this model quantifies the global scale spatial patterns in inland water N<sub>2</sub>O emissions in a consistent manner at 0.5° resolution, which were then downscaled to 0.1° using the spatial distribution of European inland water bodies. The procedure to calculate the cascading loads of N and P delivered to each water body along the river–reservoir–estuary continuum and to topologically connect 1.4 million lakes (extracted from the HYDROLAKES database) is described in Maavara et al., 2019 and Lauerwald et al., 2019. The methodology to quantify N<sub>2</sub>O emissions is based on the application of a mechanistic stochastic model (MSM) to estimate inland water C-N-P cycling as well as N<sub>2</sub>O production and emission generated by nitrification and denitrification. Using a Monte Carlo analysis, the MSM allows to generate relationships relating N processes and N<sub>2</sub>O emissions to N and P loads and water residence time

1765 from the mechanistic model outputs, which are subsequently applied for the spatially resolved upscaling. For the  
estimation of N<sub>2</sub>O emission, we ran two distinct model configurations relying on EFs scaling to denitrification and  
nitrification rates: one assuming that N<sub>2</sub>O production equals N<sub>2</sub>O emissions, the other taking into account the kinetic  
limitation on N<sub>2</sub>O gas transfer and progressive N<sub>2</sub>O reduction to N<sub>2</sub> during denitrification in water bodies with  
increasing residence time (Maavara et al., 2019). The model outputs from the two scenarios are used to constrain  
1770 uncertainties in N<sub>2</sub>O emission estimates. For this study, the upscaled RECCAP2 estimates were used (Lauerwald et  
al., in rev. GBC)

### **GAINS**

Specific sectors and abatement technologies in GAINS vary by the specific emitted compound, with source  
sector definition and emission factors largely following the IPCC methodology at the Tier 1 or Tier 2 level. GAINS  
1775 includes in general all anthropogenic emissions to air, but does not cover emissions from forest fires, savannah burning  
and land use / land use change. Emissions are estimated for 174 countries/regions, with the possibility to aggregate to  
a global emission estimate, and spanning a timeframe from 1990 to 2050 in five-year intervals. Activity drivers for  
macroeconomic development, energy supply and demand, and agricultural activities are entered externally, GAINS  
1780 extends with knowledge required to estimate “default” emissions (emissions occurring due to an economic activity  
without emission abatement) and emissions and costs of situations under emission control (Amann et al., 2001).

Emissions of nitrous oxide derive from energy, industry, agriculture, and waste. Land use change emissions  
are not included. In the energy sector, certain technologies implemented to improve air quality affect N<sub>2</sub>O emission  
factors (like catalytic converters in vehicles), sometimes also negatively. That is also the case for non-selective  
1785 catalytic reduction devices for NO<sub>x</sub> abatement in power plants, or for fluidized bed combustion. Relevant industrial  
processes cover nitric acid and adipic acid, with other processes (glyoxal, if relevant, or caprolactam) included. Both  
processes allow for two different levels of abatement technologies, which both are relatively easily accessible and low  
cost. The use of N<sub>2</sub>O in gaseous form, often as an anesthetic for medical purposes, is associated with population  
numbers and scaled by availability of hospital beds. Marked emission reductions (at low costs) as well as complete  
1790 phase out of emissions (high costs) are implemented as technologies. Agricultural emissions in part derive from  
manure handling, where different management strategies have repercussions on emissions. The larger fraction of  
emission is from application of nitrogen compounds in different forms to grassland, crops and rice, with rice using a  
different emission factor. Application of manure and of mineral fertilizer in GAINS can be reduced by advanced  
computer technology such as automatic steering and variable rate application, or by agrochemistry (nitrification  
1795 inhibitors). Costs of implementation are considered to depend on the size of a farm, hence farm size is an important  
parameter. In the waste sector, composting and wastewater treatment are considered relevant sources. For wastewater  
treatment, GAINS also considers a specific emission reduction option when optimizing processes towards N<sub>2</sub>O  
reduction (e.g. via favoring the anammox process). All details have been reported by Winiwarter et al. (2018) in their  
supplementary material.

1800 **Uncertainties:** The same paper provides full information on the uncertainty of N<sub>2</sub>O emissions in the GAINS model,  
which is a consequence of uncertainty provided in the activity data, in the emission factors, and in the actual structure

of the respective management strategies that also include the share of abatement technology already implemented. Further parameters also described (on uncertainty of future projections and on costs) are not relevant here.

## 1805 **FAOSTAT**

FAOSTAT: Statistics Division of the Food and Agricultural Organization of the United Nations, provides N<sub>2</sub>O emissions from agriculture: <https://www.fao.org/faostat/en/#data/GT> and its sub-domains, as well as N<sub>2</sub>O emissions from land use linked to biomass burning. The FAOSTAT emissions database is computed following Tier 1 IPCC 2006 Guidelines for National GHG Inventories (<http://www.ipcc-nggip.iges.or.jp/public/2006gl/index.html>). Country reports to FAO on crops, livestock and agriculture use of fertilizers are the source of activity data. Geospatial data are the source of AD for the estimates from cultivation of organic soils, biomass and peat fires. N<sub>2</sub>O emissions are provided by country, regions and special groups, with global coverage, relative to the period 1961-present (with annual updates, currently 2019) and with projections for 2030 and 2050 for agriculture only, expressed in both CO<sub>2</sub>e and N<sub>2</sub>O by underlying agricultural and land use emission sub-domain and by aggregate (agriculture total, agriculture total plus energy, agricultural soils). The main N<sub>2</sub>O emissions are reported for the following agricultural activities: manure management, synthetic fertilizers, manure applied to the soils, manure left in pasture, crop residues, cultivation of organic soils and burning crop residues. LULUCF emissions consist of N<sub>2</sub>O associated with burning biomass and peat fires, as well as from the drainage of organic soils. Comparison to the UNFCCC submissions is also provided.

**Uncertainties** were computed by Tubiello et al., 2013 but are not available in the FAOSTAT database.

## 1820 **Top-down N<sub>2</sub>O emission estimates**

### **FLEXINVERT**

The FlexInvert framework is based on Bayesian statistics and optimizes surface-atmosphere fluxes using the maximum probability solution (Rodgers 2000). Atmospheric transport is modelled using the Lagrangian model FLEXPART (Stohl et al. 2005; Pisso et al. 2019) run in the backwards time mode to generate a so-called Source-Receptor Matrix (SRM). The SRM describes the relationship between the change in mole fraction and the fluxes discretized in space and time (Seibert and Frank, 2004) and was calculated for 7 days prior to each observation. For use in the inversions, FLEXPART was driven using ECMWF Era Interim wind fields.

The state vector consisted of flux increments (i.e. offsets to the prior fluxes) discretized on an irregular grid based on the SRMs (Thompson et al. 2014). This grid has finer resolution (in this case the finest was 0.5°×0.5°) where the fluxes have a strong influence on the observations and coarser resolution where the influence is only weak (the coarsest was 2°×2°). The flux increments were solved at 2-weekly temporal resolution. The state vector also included scalars for the background mole fractions. The optimal (posterior) fluxes were found using the Conjugate Gradient method (e.g. Paige and Saunders, 1975).

The background mole fractions, i.e., the contribution to the modelled mole fractions that is not accounted for in the 7-day SRMs, was estimated by coupling the termination points of backwards trajectories (modelled using virtual particles) to initial fields of mole fractions from the optimized Eulerian model LMDz (i.e. the CAMS N<sub>2</sub>O mole fraction product v18r1) following the method of Thompson et al. 2014.

**Uncertainties:** The posterior fluxes are subject to systematic errors primarily from: 1) errors in the modelled atmospheric transport; 2) aggregation errors, i.e. errors arising from the way the flux variables are discretized in space and time; 3) errors in the background mole fractions; and 4) the incomplete information from the observations and hence the dependence on the prior fluxes. In addition, there is, to a smaller extent, some error due to calibration offsets between observing instruments, which is more pertinent for N<sub>2</sub>O than for other GHGs. Random uncertainties are calculated from a Monte Carlo ensemble of inversions following Chevallier et al. (2007) and uncertainties in the observation space were inflated to take into account the model representation errors.

#### ***VERIFY Community Inversion Framework (CIF)***

In the current study, new CIF results are presented (Berchet et al., 2021). For N<sub>2</sub>O, inversions were run with CHIMERE and FLEXPART (NILU). The results using the two models were very comparable at the level of EU27 plus Norway, Switzerland and UK, with annual mean emissions for 2005-2018.

**CHIMERE** (see <https://www.lmd.polytechnique.fr/chimere/>) is a non-hydrostatic Eulerian chemistry-transport model. Its area-limited domains can be designed to cover the hemispheric to the urban scales, with horizontal resolutions from several degrees to one kilometer. The time-steps usually cover a few minutes, depending on the CFL and choices made by the user for minimizing computation costs. For the purpose of flux inversions, the tangent-linear and the adjoint codes have been developed and parallelized, only for trace-gases (see (Fortems-Cheiney et al., 2021), their Section 3.2 for more details). The required input data are meteorological 3D and 2D fields (e.g. temperature, wind speed), boundary conditions for concentrations at the four sides and at the top of the domain and emission fluxes. The comparison to surface measurements is done by extracting from the model the simulated concentrations in the grid cell matching the stations' locations for the time-steps matching the measurement date and time. If the measurement covers a longer time (e.g. hourly means), the simulated concentrations for the matching time-steps are averaged. For this deliverable, CHIMERE was run using meteorological data from the ECMWF's IFS operational forecast (every three hours) retrieved at  $0.25^\circ \times 0.25^\circ$  and interpolated onto the model's grid ( $0.5^\circ \times 0.5^\circ$ ). CHIMERE extends from the surface to 200 hPa with 17 sigma-pressure levels.

For the inversions provided by NILU, FLEXPART-v10.4 was run using ECMWF's operational IFS forecast with backward trajectory lengths of 7 days for N<sub>2</sub>O. The footprints were saved at  $0.5^\circ \times 0.5^\circ$  for N<sub>2</sub>O inversions. For N<sub>2</sub>O anthropogenic emissions were taken from EDGAR-v6. An estimate for the natural N<sub>2</sub>O flux was provided by the O-CN land surface model – a monthly climatology of the pre-industrial (or baseline) fluxes (Zaehle et al., 2011) and an estimate for the ocean N<sub>2</sub>O flux was provided by the coupled ocean-biogeochemistry model, PlankTOM-v10 – also a monthly climatology (Buitenhuis et al., 2018).

**Uncertainties:** In the CIF, the uncertainties are described by matrices, with variances on the diagonal and covariances on the off-diagonal. They are called respectively the prior error (for the error statistics on the prior controlled variables) and the observation error (for the error statistics on the difference between the observed and modelled mixing ratios). Observations errors were assumed to be independent from each other in all inversions, i.e., the observation error covariance matrix is diagonal. For CHIMERE, measurement errors were provided from observation files. Transport,

representation and aggregation errors were deduced from the CH<sub>4</sub>-based errors. For FLEXPART (NILU), the observations errors were calculated in the same way as for CH<sub>4</sub> but a minimum error of 0.3 ppb was used.

### *Global N<sub>2</sub>O Budget – GCP (Tian et al., 2020)*

#### *CAMS-N<sub>2</sub>O*

Within the GCP 2019 results, N<sub>2</sub>O fluxes are estimated using the atmospheric inversion framework, CAMS-N<sub>2</sub>O. Atmospheric inversions use observations of atmospheric mixing ratios, in this case, of N<sub>2</sub>O, and provide the fluxes that best explain the observations while at the same time being guided by a prior estimate of the fluxes. In other words, the fluxes are optimized to fit the observations within the limits of the prior and observation uncertainties. To produce the optimized (*a posteriori*) fluxes a number of steps are involved: first, the observations are pre-processed, second, a prior flux estimate is prepared, third mixing ratios are simulated using the prior fluxes and are used to estimate the model representation error, and fourth, the inversion is performed. In total 140 ground-based sites, ship and aircraft transects are included in the inversion. The term “site” refers to locations where there is a long-term record of observations and includes ground-based measurements, both from discrete samples (or “flasks”) and quasi-continuous sampling by in-situ instruments, as well as aircraft measurements. A prior estimate of the total N<sub>2</sub>O flux with monthly resolution and inter-annually varying fluxes is prepared from a number of models and inventories. For the soil fluxes (including anthropogenic and natural) an estimate from the land surface model OCN-v1.2 is used, which is driven by observation-based climate data, N-fertilizer statistics and modelled N-deposition (Zaehle et al. 2011). For the ocean fluxes, an estimate from the ocean biogeochemistry model PlankTOM-v10.2 is used, which is a prognostic model (Buitenhuis et al. 2018). Atmospheric transport is modelled using an offline version of the Laboratoire de Meteorologie Dynamique model, LMDz5, which computes the evolution of atmospheric compounds using archived fields of winds, convection mass fluxes and planetary boundary layer (PBL) exchange coefficients that have been calculated using the online version nudged to ECMWF ERA interim winds.

CAMS-N<sub>2</sub>O uses the Bayesian inversion method to find the optimal fluxes of N<sub>2</sub>O given prior information about the fluxes and their uncertainty, and observations of atmospheric N<sub>2</sub>O mole fractions. The method is the same as that used in Thompson et al. (2014). For this study, inversions were not updated.

**Uncertainty:** Uncertainties in CAMS-N<sub>2</sub>O simulations pertain to observation space and to state space. Uncertainty in the observation space is calculated as the quadratic sum of the measurement and transport uncertainties. The measurement uncertainty is assumed to be 0.3 ppb (approximately 0.1%) based on the recommendations of data providers. The transport uncertainty includes estimates of uncertainties in advective transport (based on the method of Rödenbeck et al. (2003)) and from a lack of subgrid-scale variability (based on the method of Bergamaschi et al. (2010)). For the error in each land grid cell, the maximum magnitude of the flux in the cell of interest and its 8 neighbours is used, while for ocean grid cells the magnitude of the cell of interest only is used. Posterior flux uncertainties are calculated from a Monte Carlo ensemble of inversions, based on the method of Chevallier et al. (2005).



1910 ***TOMCAT-INVICAT***

TOMCAT-INVICAT (Wilson et al., 2014) is a variational inverse transport model, which is based on the global chemical transport model TOMCAT, and its adjoint. It uses a 4-D variational (4D-VAR) optimization framework based on Bayesian theory which seeks to minimize model-observation differences by altering surface fluxes, while allowing for prior knowledge of these fluxes to be retained. TOMCAT (Monks et al., 2017) is an offline chemical transport model, in which meteorological data is taken from ECMWF ERA-Interim reanalyses (Dee et al., (2011)). The model grid resolution, and therefore the optimised surface flux estimates, have a horizontal resolution of 5.6 x 5.6 degrees. The model has 60 vertical levels running from the surface to 0.1 hPa. For each individual year's fluxes, which are optimised on a monthly basis, 30 minimisation iterations are carried out. For this study, inversions were not updated.

1920 **Uncertainty:** Uncertainties in TOMCAT-INVICAT N<sub>2</sub>O inversions are described as follows and further in Thompson et al., (2019). Uncertainty in the observations is calculated as the quadratic sum of the measurement and transport uncertainties. The measurement uncertainty for each observation is assumed to be 0.4 ppb. For the transport error for each observation is assumed to be the mean difference between the observation grid cell and its 8 neighbours. Prior flux errors are assumed to be 100% or the prior estimate, and are uncorrelated in space and time. Posterior flux

1925 uncertainties are not currently able to be calculated.

***MIROC4-ACTM***

The MIROC4-ACTM time dependent inversion for 84 regions (TDI84) framework is based on Bayesian statistics and optimizes surface-atmosphere fluxes using the maximum probability solution (Rodgers 2000).

1930 Atmospheric transport is modelled using the JAMSTEC's Model for Interdisciplinary Research on climate, version 4 based atmospheric chemistry-transport model (MIROC4-ACTM) (Watanabe et al. 2008; Patra et al. 2018, 2022). The Source-Receptor Matrix (SRM) is calculated by simulating unitary emissions from 84 basis regions, for which the fluxes are optimised. The SRM describes the relationship between the change in mole fraction at the measurement locations for the unitary basis region fluxes (similar to Rayner et al., 1997). The MIROC4-ACTM meteorology was

1935 nudged to the JMA 55-year reanalysis (JRA55) horizontal wind fields and temperature. The simulated mole fractions for the total a priori fluxes are subtracted from the observed concentrations before running the inversion calculation (as in Patra et al., 2016 for CH<sub>4</sub> inversion).

In this study, the simulation have been updated to 2019 (Patra et al., 2022).

**Uncertainties:** The posterior fluxes are subject to systematic errors primarily from: 1) errors in the modelled atmospheric transport; 2) aggregation errors, i.e. errors arising from the way the flux variables are discretized in space (84 regions) and time (monthly-means); 3) errors in the background mole fractions (assumed to be a minor factor); and 4) the incomplete information from the sparse observational network and hence the dependence on the prior fluxes. In addition, there is, to a much smaller extent, some error due to calibration offsets between observing instruments, which is more pertinent for N<sub>2</sub>O than for other GHGs. We have validated model transport in the troposphere using

1940 SF<sub>6</sub> for the inter-hemispheric exchange time, and the using SF<sub>6</sub> and CO<sub>2</sub> for the age of air in the stratosphere. The

1945 simulated N<sub>2</sub>O concentrations are also compared with aircraft measurements in the upper troposphere and lower

stratosphere for evaluating the stratosphere-troposphere exchange rates. Comparisons with ACE-FTS vertical profiles in the stratosphere and mesosphere indicate good parameterisation of N<sub>2</sub>O loss by photolysis and chemical reactions, and thus the lifetime, which affect the global total N<sub>2</sub>O budgets.

1950                Random uncertainties are calculated by the inverse model depending on the prior flux uncertainties and the observational data density and data uncertainty. Only 37 sites are used in the inversion and thus the reduction in priori flux uncertainties have been minimal. The net fluxes from the inversion from individual basis regions are less reliable compared to the anomalies in the estimated fluxes over a period of time.

1955        **B1: Overview figures**

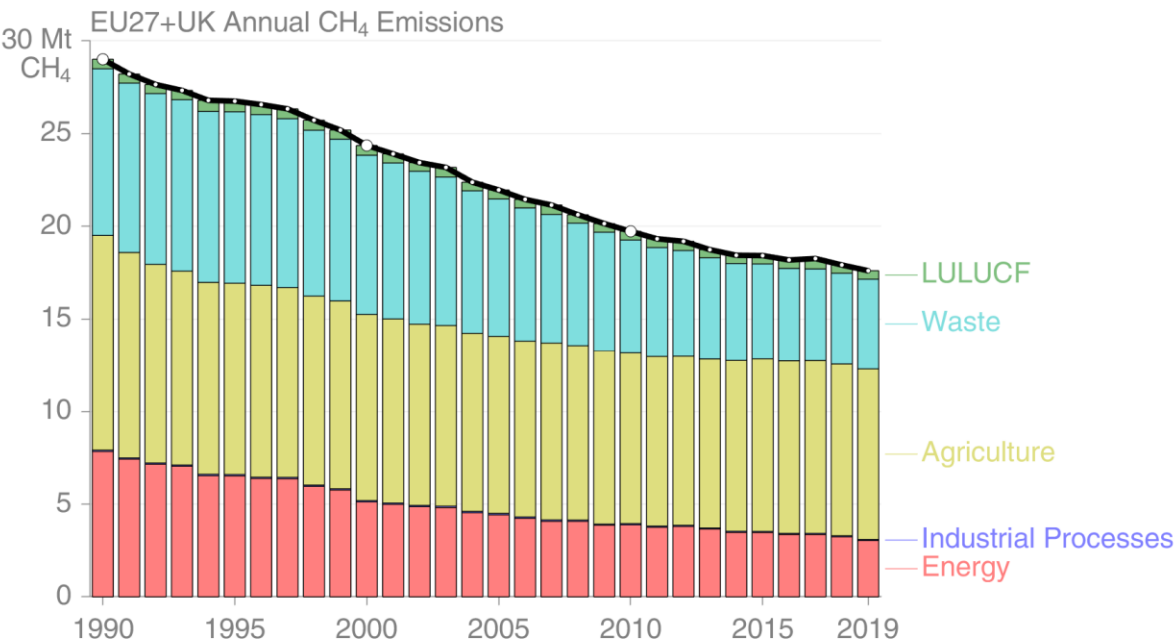


Figure B1a: EU27+UK total CH<sub>4</sub> emissions time series per sectors as reported by UNFCCC NGHGI (2021).

1960

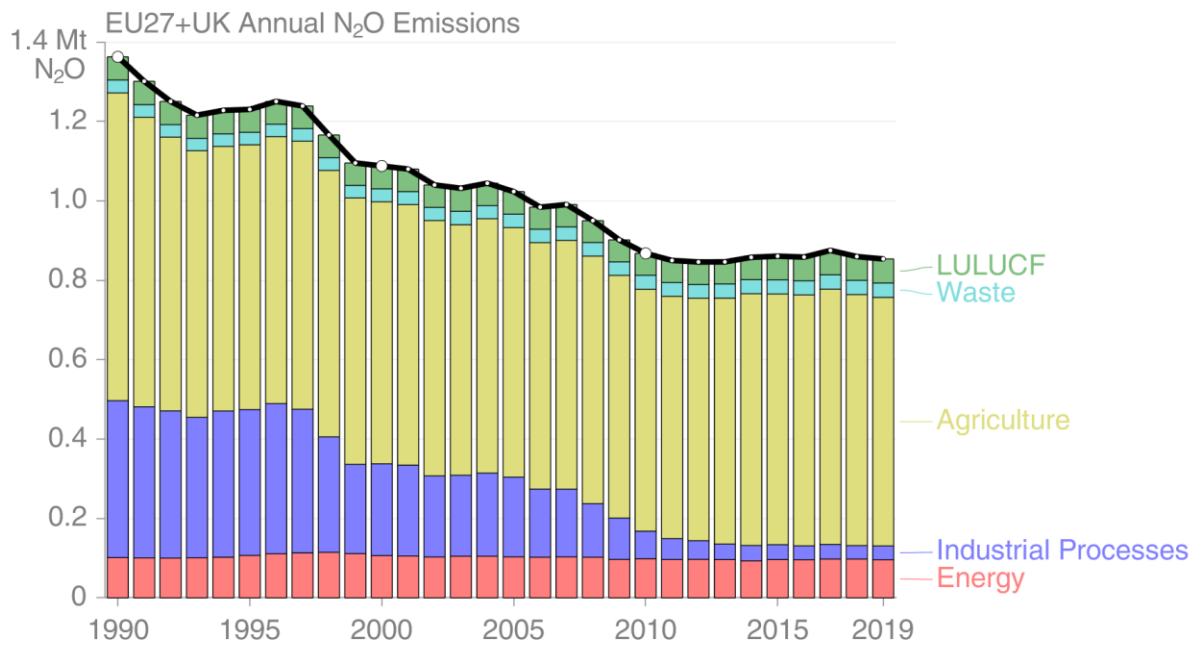
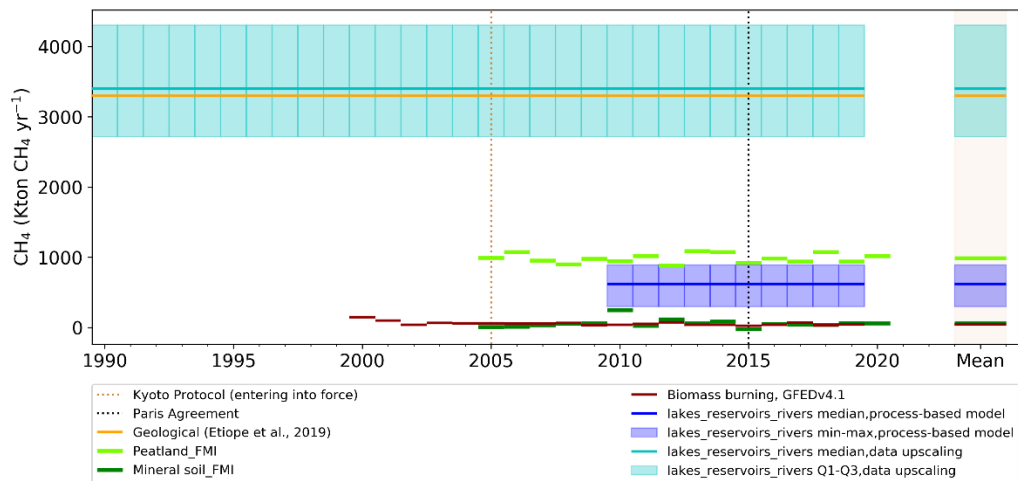


Figure B1b: EU27+UK total  $N_2O$  emissions time series per sectors as reported by UNFCCC NGHGI (2021).



1965 Figure B1c: EU27+UK natural  $CH_4$  emissions from Figure 4b, as following: two estimates for inland waters (lakes\_rivers\_reservoirs process-based models, blue and upscaled emissions, cyan), peatlands and mineral soils (from JSBACH-HIMMELI, light green and dark green), geological emissions (orange) and biomass burning, (from GFEDv4.1, brown).

1970

**B2: Source specific methodology: AD, EF and uncertainties**

Table B2.1: Source specific activity data (AD), emission factors (EF) and uncertainty methodology for all current VERIFY and non-VERIFY 2021 data product collection.

1975

CH <sub>4</sub> bottom-up anthropogenic emissions				
Data source	AD/Tier	EFs/Tier	Uncertainty assessment method	Emission data availability
<b>UNFCCC NGHGI (2021)</b>	Country-specific information consistent with the IPCC GLs.	IPCC GLs/country-specific information for higher tiers.	IPCC GLs ( <a href="https://www.ipcc-nggip.iges.or.jp/public/2006gl/">https://www.ipcc-nggip.iges.or.jp/public/2006gl/</a> , last access: December 2019) for calculating the uncertainty of emissions based on the uncertainty of AD and EF, two different approaches: (1) error propagation and (2) Monte Carlo simulation.  The EU GHG inventory team provided yearly harmonized and gap-filled uncertainties	NGHGI official data (CRFs) are found at <a href="https://unfccc.int/ghg-inventories-annex-i-parties/2021">https://unfccc.int/ghg-inventories-annex-i-parties/2021</a>
<b>EDGAR v6.0</b>	International Energy Agency (IEA) for fuel combustion Food and Agricultural Organisation (FAO) for agriculture US Geological Survey (USGS) for industrial processes (e.g. cement, lime, ammonia and ferroalloys) GGFR/NOAA for gas flaring World Steel Association for iron and steel production International Fertilisers Association (IFA) for urea consumption and production	IPCC 2006, Tier 1 or Tier 2 depending on the sector	Tier 1 with error propagation by sectors for CH <sub>4</sub>	<a href="https://edgar.jrc.ec.europa.eu/dataset_ghg60">https://edgar.jrc.ec.europa.eu/dataset_ghg60</a>

	Complete description of the data sources can be found in Janssens-Maenhout et al. 2019 and in Crippa et al. (2019b).			
<b>CAPRI</b>	Farm and market balances, economic parameters, crop areas, livestock population and yields from EUROSTAT, parameters for input-demand functions at regional level from FADN (EC), data on trade between world regions from FAOSTAT, policy variables from OECD.	IPCC 2006: Tier 2 for emissions from enteric fermentation of cattle and from manure management of cattle. Tier 1 for all other livestock types and emission categories. N-flows through agricultural systems (including N excretion) calculated endogenously.	Spatial uncertainties computed for 2014, 2016 and 2018	Detailed gridded data CH <sub>4</sub> and N <sub>2</sub> O emissions can be obtained by contacting the data provider: <a href="mailto:Adrian.Leip@ec.europa.eu">Adrian.Leip@ec.europa.eu</a>
<b>GAINS</b>	Livestock numbers by animal type (FAOSTAT, 2010; EUROSTAT, 2009; UNFCCC, 2010) Growth in livestock numbers from FAOSTAT (2003), CAPRI model (2009) Rice cultivation Land area for rice cultivation (FAOSTAT, 2010) Projections for EU are taken from the CAPRI Model	Country-specific information and: Livestock - Implied EFs reported to UNFCCC and IPCC Tier 1 (2006, Vol.4, Ch. 10) default factors Rice cultivation - IPCC Tier 1–2 (2006, Vol. 4, p. 5.49) Agricultural waste burning - IPCC Tier 1 (2006, Vol. 5, p. 520)	IPCC (2006, Vol.4, p.10.33) uncertainty range	Detailed gridded data CH <sub>4</sub> and N <sub>2</sub> O emissions can be obtained by contacting the data providers: for CH <sub>4</sub> , contact Lena Höglund Isaksson (hoglund@iiasa.ac.at); for N <sub>2</sub> O, contact Wilfried Winiwarter (winiwart@iiasa.ac.at).
<b>FAOSTAT</b>	FAOSTAT Crop and Livestock Production domains from country reporting; FAOSTAT	IPCC guidelines Tier 1	IPCC (2006, Vol.4, p.10.33) Uncertainties in estimates of GHG emissions are due to uncertainties in emission factors and activity data.	Agriculture total and subdomain specific GHG emissions are found for download at <a href="http://www.fao.org/faostat/en/#data/GT">http://www.fao.org/faostat/en/#data/GT</a> (last access: April 2022).

	Land Use Domain; Harmonized world soil; ESA CCI and Copernicus Global Land Cover Service (C3S) maps; MODIS MCD12Q1 v6; FAO Gridded Livestock of the World; MODIS MCD64A1.006 burned area products		They may be related to, inter alia, natural variability, partitioning fractions, lack of spatial or temporal coverage, or spatial aggregation.	
<b>CH<sub>4</sub> bottom-up natural emissions</b>				
<b>Data source</b>	<b>AD/Tier</b>	<b>EFs/Tier</b>	<b>Uncertainty assessment method</b>	<b>Emission data availability</b>
<b>Mechanistic Stochastic Model CH<sub>4</sub> emissions from inland waters</b>	Hydrosheds 15s (Lehner et al., 2008) and Hydro1K (USGS, 2000) for river network, HYDROLAKE S for lakes and reservoirs network and surface area (Messenger et al., 2016); Worldwide Typology of estuaries by Dürr et al. (2011)	N/A	Four model configurations for CH <sub>4</sub>	Detailed gridded data can be obtained by contacting the data providers: Ronny Lauerwald ronny.lauerwald@inrae.fr Pierre Regnier <a href="mailto:Pierre.Regnier@ulb.ac.be">Pierre.Regnier@ulb.ac.be</a>
<b>JSBACH-HIMMELI</b>	JSBACH vegetation and soil carbon and physical parameters provided to HIMMELI to simulate wetland methane fluxes HydroLAKES database (Messenger et al., 2016). CORINE land cover data VERIFY climate drivers 0.1° × 0.1°	CH <sub>4</sub> fluxes from peatlands and mineral soils	the standard deviation and the resulting range in the annual emission sum represents a measure of uncertainty.	Detailed gridded data CH <sub>4</sub> emissions can be obtained by contacting the data providers: <a href="mailto:Tuula.Aalto@fmi.fi">Tuula.Aalto@fmi.fi</a> <a href="mailto:tiina.markkanen@fmi.fi">tiina.markkanen@fmi.fi</a>

Geological emissions, including marine and land geological)	Areal distribution activity: $1^\circ \times 1^\circ$ maps include the four main categories of natural geo-CH <sub>4</sub> emission: (a) onshore hydrocarbon macro-seeps, including mud volcanoes, (b) submarine (offshore) seeps, (c) diffuse microseepage and (d) geothermal manifestations.	CH <sub>4</sub> fluxes, measurements and estimates based on size and activity	95% confidence interval of the median emission-weighted mean sum of individual regional values	Etioppe et al, 2019 with updated activity for current study) Detailed gridded data on geological CH <sub>4</sub> emissions can be obtained by contacting the data providers: Giuseppe Etioppe: <a href="mailto:giuseppe.etioppe@ingv.it">giuseppe.etioppe@ingv.it</a> Giancarlo Ciotoli <a href="mailto:giancarlo.ciotoli@gmail.com">giancarlo.ciotoli@gmail.com</a>
<b>CH<sub>4</sub> Top-down inversions</b>				
<b>Regional inversions over Europe ( high transport model resolution )</b>				
<b>Data source</b>	<b>AD/Tier</b>	<b>EFs/Tier</b>	<b>Uncertainty assessment method</b>	<b>Emission data availability</b>
<b>FLEXPART - FLExKF</b>	Extended Kalman Filter in combination with backward Lagrangian transport simulations using the model FLEXPART Atmospheric observations ECMWF Era Interim meteorological fields	FLExKF-CAMSv19r_EMPA specific background	The random uncertainties are represented by the posterior error covariance matrix provided by the Kalman Filter, which combines errors in the prior fluxes with errors in the observations and model representation (see description in Appendix A1)	Detailed gridded data can be obtained by contacting the data provider: Dominik.Brunner@empa.ch
<b>TM5-4DVAR</b>	Global Eulerian models with a zoom over Europe, ERA-Interim reanalysis	4DVAR variational techniques	Uncertainty was calculated as $1\sigma$ estimate. See descriptions in Appendix A1	Detailed gridded data can be obtained by contacting the data provider: Peter.BERGAMASCHI@ext.ec.europa.eu
<b>FLEXINVERT</b>	Bayesian statistics Atmospheric transport is modelled using the Lagrangian model FLEXPART	prior fluxes from LPX-Bern DYP TOP, EDGAR v4.2 FT2010 GFED v4 Termites and ocean fluxes ground-based surface CH <sub>4</sub> observations. Background fields based on nudged FLEXPART-CTM simulations (Groot Zwaafink et al., 2018)		Detailed gridded data CH <sub>4</sub> emissions can be obtained by contacting the data provider: Christine Groot Zwaafink cgz@nilu.no

<b>InTEM-NAME</b>	Atmospheric Lagrangian transport model analysis 3-D meteorology from the UK Met Office Unified Model.	(a) the UK National Atmospheric Emissions Inventory (NAEI) 2015 within the UK. (b) Outside the UK – EDGAR 2010 emissions distributed uniformly over land (excluding the UK).	Derived from the variability of the observations within each 2 h period: a) 40 %; b) 50 %.	Detailed gridded data can be obtained by contacting the data provider: Alistair Manning (alistair.manning@metoffice.gov.uk).
<b>CTE-FMI</b>	Ensemble Kalman filter Eulerian transport model TM5 ECMWF ERA-Interim meteorological data	prior fluxes from LPX-Bern DYPTOP, EDGAR v4.2 FT2010 GFED v4 Termites and ocean fluxes ground-based surface CH <sub>4</sub> observations GOSAT XCH <sub>4</sub> retrievals from NIES v2.72	The prior uncertainty is assumed to be a Gaussian probability distribution function The posterior uncertainty is calculated as standard deviation of the ensemble members, where the posterior error covariance matrix are driven by the ensemble Kalman filter.	Detailed gridded data can be obtained by contacting the data provider: aki.tsuruta@fmi.fi
<b>InGOS</b>	18 European monitoring stations EDGARv4.2FT-InGOS wetland inventory of J.Kaplan and LPX-Bern v1.0 ERA-Interim reanalysis Met Office Unified Model	For Priors please see Table B2.4	The uncertainty of the model ensemble was calculated as 1σ estimate. Individual models use Bayes' theorem to calculate the reduction of assumed a priori emission uncertainties by assimilating measurements.	Detailed gridded data can be obtained by contacting the data provider: Peter.BERGAMASCHI@ext.ec.europa.eu
<b>VERIFY Community Inversion Framework (CIF): CHIMERE, FLEXPARTv10.4 (NILU) and FELXPART (EMPA) (only CH<sub>4</sub>)</b>	Extended Kalman Filter in combination with backward Lagrangian transport simulations using the model FLEXPART Atmospheric observations ECMWF Era Interim meteorological fields CHIMERE is a non-hydrostatic Eulerian chemistry-transport model	For Priors please see Table B2.4	The uncertainty in each grid cell (0.25°x0.25° for CH <sub>4</sub> and 0.5°x0.5° for N <sub>2</sub> O) includes that due to the spatial disaggregation plus that due to emission-weighted uncertainty of a specific process.	Detailed gridded data can be obtained by contacting the data providers: Antoine Berchet <a href="mailto:antoine.berchet@lsce.ipsl.fr">antoine.berchet@lsce.ipsl.fr</a> Brunner, Dominik <a href="mailto:Dominik.Brunner@empa.ch">Dominik.Brunner@empa.ch</a> Rona Thompson <a href="mailto:rlt@nilu.no">rlt@nilu.no</a> Gregoire Broquet <a href="mailto:gregoire.broquet@lsce.ipsl.fr">gregoire.broquet@lsce.ipsl.fr</a>



Global inversions from the Global Carbon Project CH <sub>4</sub> budget (Saunois et al. 2020)				
<b>GCP-CH<sub>4</sub> 2019 anthropogenic and natural partitions from inversions</b>	ensemble of inversions gathering various chemistry transport models surface or satellite data	For Priors please see Table B4	Uncertainties are reported as minimum and maximum values of the available studies, as the range of available mean estimates, i.e., the standard error across measurements/met hodologies considered. Posterior uncertainty mostly use Monte Carlo methods	Detailed gridded data can be obtained by contacting the data provider: Marielle Saunois <a href="mailto:marielle.saunois@lsce.ipsl.fr">marielle.saunois@lsce.ipsl.fr</a>
N <sub>2</sub> O bottom-up anthropogenic emissions				
Data source	AD/Tier	EFs/Tier	Uncertainty assessment method	Emission data availability
UNFCCC NGHGI (2021), EDGAR v6.0, CAPRI, GAINS and FAOSTAT see above				
<b>ECOSSE</b>	The model is a point model, which provides spatial results by using spatial distributed input data (lateral fluxes are not considered). The model is a TIER 3 approach that is applied on grid map data, polygon organized input data or study sites.	IPCC 2006: Tier 3 The simulation results will be allocated due to the available information (size of spatial unit, representation of considered land use, etc.).	N/A	Detailed gridded data can be obtained by contacting the data provider: Kuhnert, Matthias <a href="mailto:matthias.kuhnert@abdn.ac.uk">matthias.kuhnert@abdn.ac.uk</a>
<b>DayCent</b>	Spatial explicit simulations at point level, up-scaled at 1km for agricultural areas.	Tier 3; Land management and input factors for the cropland remaining cropland category based on datasets covering the 2005-2015 period.	Monte Carlo	Detailed gridded data can be obtained by contacting the data provider: Emanuele.LUGATO@ec.europa.eu
N <sub>2</sub> O bottom-up natural emissions				
<b>Mechanistic Stochastic Model for N<sub>2</sub>O emissions from inland waters</b>	Hydrosheds 15s (Lehner et al., 2008) and Hydro1K (USGS, 2000) for river network, HYDROLAKE S for lakes and reservoirs network and surface area	EFs applied to denitrification and nitrification rates for N <sub>2</sub> O emissions. Values constrained from the range reported in Beaulieu et al., 2011.	Upscaled emission estimates from RECCAP2	Detailed gridded data can be obtained by contacting the data providers: Ronny Lauerwald <a href="mailto:ronny.lauerwald@inrae.fr">ronny.lauerwald@inrae.fr</a> Pierre Regnier <a href="mailto:Pierre.Regnier@ulb.ac.be">Pierre.Regnier@ulb.ac.be</a>

	(Messenger et al., 2016); Worldwide Typology of estuaries by Dürr et al. (2011); terrestrial N and P loads by Global-NEWS (Van Drecht et al., 2009; Bouwman et al., 2009), redistributed at 0.5° resolution by Maavara et al., 2019.			
<b>Regional N<sub>2</sub>O inversions over Europe ( high transport model resolution )</b>				
<b>FLEXINVERT</b>	Bayesian statistics Atmospheric transport is modelled using the Lagrangian model FLEXPART	background mole fractions	Random uncertainties are calculated from a Monte Carlo ensemble of inversions	Detailed gridded N <sub>2</sub> O data can be obtained by contacting the data provider: Rona Thompson rlt@nilu.no
<b>Global N<sub>2</sub>O inversions over Europe from GN<sub>2</sub>OB (Tian et al., 2020)</b>				
<b>CAMS-N<sub>2</sub>O</b>	Bayesian inversion method observations of atmospheric mixing ratios fluxes from ground-based sites, ship and aircraft transects soil fluxes OCN-v1.2 ocean biogeochemistry model PlankTOM-v10.2 GFED-v4.1s EDGAR-4.32 ECMWF ERA interim	Fires emission factors from Akagi et al., 2011	Uncertainty in the observation space is calculated as the quadratic sum of the measurement and transport uncertainties. For the error in each land grid cell, the maximum magnitude of the flux in the cell of interest and its 8 neighbours is used; for ocean grid cells the magnitude of the cell of interest only is used.	Detailed gridded N <sub>2</sub> O data can be obtained by contacting the data provider: Rona Thompson rlt@nilu.no
<b>TOMCAT-INVICAT</b>	Variational Bayesian inverse model assimilating surface flask observations of atmospheric mixing ratios. ECMWF ERA-Interim	Prior emissions estimates are from OCN-v1.1 model (soils), EDGARv4.2FT2010 (anthro. non-soil), PlankTOM5 (oceans) and GFEDv4.1s (biomass burning).	Uncertainty in the observation space is calculated as the quadratic sum of the measurement and transport uncertainties. For the error in each land grid cell, the maximum	Detailed gridded N <sub>2</sub> O data can be obtained by contacting the data provider: Christopher Wilson [GEO] C.Wilson@leeds.ac.uk

	meteorological driving data.		magnitude of the flux in the cell of interest and its 8 neighbours is used. Prior emission uncertainties are 100% and uncorrelated.	
<b>MIROC4-ACTM</b>	Matrix inversion for calculation of fluxes from 53 and 84 partitions of the globe for CH <sub>4</sub> and N <sub>2</sub> O, respectively. Forward model transport is nudged to JRA-55 horizontal winds and temperature.	Fire emissions for CH <sub>4</sub> are taken from GFEDv4s	A posteriori uncertainties are obtained from the Bayesian statistics model. A priori emissions uncertainties are uncorrelated.	Detailed gridded data can be obtained by contacting the data provider: Prabir Patra prabir@jamstec.go.jp

*Table B2.2: Biogeochemical models that computed wetland emissions used in this study. Runs were performed for the whole period 2000-2017. Models run with prognostic (using their own calculation of wetland areas) and/or diagnostic (using WAD2M) wetland surface areas (see Sect 3.2.1) From Saunio et al., 2020.*

1980

Model	Institution	Prognostic	Diagnostic	References
CLASS-CTEM	Environment and Climate Change Canada	y	y	Arora, Melton and Plummer (2018) Melton and Arora (2016)
DLEM	Auburn University	n	y	Tian et al., (2010;2015)
ELM	Lawrence Berkeley National Laboratory	y	y	Riley et al. (2011)
JSBACH	MPI	n	y	Kleinen et al. (2019)
JULES	UKMO	y	y	Hayman et al. (2014)
LPJ GUESS	Lund University	n	y	McGuire et al. (2012)
LPJ MPI	MPI	n	y	Kleinen et al. (2012)
LPJ-WSL	NASA GSFC	y	y	Zhang et al. (2016b)
LPX-Bern	University of Bern	y	y	Spahni et al. (2011)

ORCHIDEE	LSCE	y	y	Ringeval et al. (2011)
TEM-MDM	Purdue University	n	y	Zhuang et al. (2004)
TRIPLEX_GHG	UQAM	n	y	Zhu et al., (2014;2015)
VISIT	NIES	y	y	Ito and Inatomi (2012)

*Table B2.3: Top-down studies used in our new analysis, with their contribution to the decadal and yearly estimates noted. For decadal means, top down studies have to provide at least 8 years of data over the decade to contribute to the estimate, from Saunio et al., 2020*

Model	Institution	Observation used	Time period	Number of inversions	References
Carbon Tracker-Europe CH <sub>4</sub>	FMI	Surface stations	2000-2017	1	Tsuruta et al. (2017)
Carbon Tracker-Europe CH <sub>4</sub>	FMI	GOSAT NIES L2 v2.72	2010-2017	1	Tsuruta et al. (2017)
GELCA	NIES	Surface stations	2000-2015	1	Ishizawa et al. (2016)
LMDz-PYVAR	LSCE/CEA	Surface stations	2010-2016	2	Yin et al. (2019)
LMDz-PYVAR	LSCE/CEA	GOSAT Leicester v7.2	2010-2016	4	Yin et al. (2019)
LMDz-PYVAR	LSCE/CEA	GOSAT Leicester v7.2	2010-2017	2	Zheng et al. (2018a, 2018b)
MIROC4-ACTM	JAMSTEC	Surface stations	2000-2016	1	Patra et al. (2016; 2018)
NICAM-TM	NIES	Surface stations	2000-2017	1	Niwa et al. (2017a; 2017b)
NIES-TM-FLEXPART-VAR (NTFVAR)	NIES	Surface stations	2000-2017	1	Maksyutov et al. (2020); Wang et al. (2019b)
NIES-TM-FLEXPART-VAR (NTFVAR)	NIES	GOSAT NIES L2 v2.72	2010-2017	1	Maksyutov et al. (2020); Wang et al., (2019b)
TM5-CAMS	TNO/VU	Surface stations	2000-2017	1	Segers and Houweling (2018); Bergamaschi et al. (2010; 2013), Pandey et al. (2016)
TM5-CAMS	TNO/VU	GOSAT ESA/CCI	2010-2017	1	Segers and Houweling (2018,report); Bergamaschi

		v2.3.8 (combined with surface observations)			et al. (2010; 2013), Pandey et al. (2016)
TM5-4DVAR	EC-JRC	Surface stations	2000-2017	2	Bergamaschi et al. (2013, 2018)
TM5-4DVAR	EC-JRC	GOSAT OCPR v7.2 (combined with surface observations)	2010-2017	2	Bergamaschi et al. (2013, 2018)
TOMCAT	Uni. of Leeds	Surface stations	2003-2015	1	McNorton et al. (2018)

1985

Table B2.4: List of prior datasets for natural CH<sub>4</sub> and N<sub>2</sub>O emissions used by all inverse models

Project	Model	Prior						
		Wetlands	Geological	Fire	Termites	Soil sink	Ocean/Lakes	Wild animals
VERIFY	CTE_FMI S5	JSBACH-HIMMELI	GCP_CH4 Etiopie et al., 2019	RCO plus GFED4s.1	Castaldi as GCP_CH4	LPX-Bern DYPTOP (Stocker et al., 2014)	Weber et al., 2019 for oceans and ULB for lakes in Europe, 0 for the rest of the world	
VERIFY	FLEXPART(F LExKF- CAMsv19r)_E MPA	JSBACH-HIMMELI			GCP	Ridgwell /GCP	GCP/ULB	
VERIFY	FLEXINVERT	LPX-Bern DYPTOP (Stocker et al., 2014)		GFED4s	Ito and Inatomi, 2012	LPX-Bern DYPTOP (Stocker et al., 2014)	(Tsuruta et al., 2017)	
VERIFY	TM5_4DVAR JRC	GCP_CH4_2019	GCP_CH4 2019 (global total: 15 Tg CH <sub>4</sub> yr <sup>-1</sup> )		GCP_CH4_2019	GCP_CH4_ 2019	GCP_CH4_ 2019	
VERIFY-CIF	FLEXPART-NILU FLEXPART-EMPA CHIMERE	JSBACH-HIMMELI	Etiopie, 2019	EDGAR-v6 (biofuel) and GFED-v41s (biomass)	Saunois et al., 2020 (GCP-CH <sub>4</sub> )		Weber et al. 2019	

InGOS	INGOS-CTE-S4_EC	LPX-Bern v1.0 (Spahni et al., 2013)		GFED	Ito and Inatomi 2012	LPX-Bern v1.0 (Spahni et al., 2013)	Tsuruta et al., 2015	
InGOS	INGOS-LMDZEU-S4_EC	wetland inventory of J. Kaplan (Bergamaschi et al., 2007)						
InGOS	INGOS-TM3STILT-S4_EC	wetland inventory of J. Kaplan (Bergamaschi et al., 2007)						
InGOS	INGOS-TM5VAR-S4_EC	wetland inventory of J. Kaplan (Bergamaschi et al., 2007)			Sanderson /GCP	Ridgwell /GCP	Lambert /GCP	Osilon climatology
InGOS	INGOS-NAME-S4_EC	wetland inventory of J. Kaplan (Bergamaschi et al., 2007)						
GCP	GELCA-SURF_NIES	VISIT (Ito and Inatomi, 2012)	n/a	GFEDv3.1 then GFAS v1.2 after 2011	Sanderson (TransCom-CH <sub>4</sub> / GCP)	VISIT (Ito and Inatomi, 2012)	n/a	
GCP	MIROCv4-SURF_JAMA STEC	VISIT (Ito and Inatomi, 2012) (global total range : 173-197 Tg CH <sub>4</sub> yr <sup>-1</sup> )	Etiopie and Milkov, 2004 (global total: 7.5 Tg CH <sub>4</sub> yr <sup>-1</sup> )	GFEDv4s (global total range : 14-35 Tg CH <sub>4</sub> yr <sup>-1</sup> )	Sanderson (TransCom-CH <sub>4</sub> ) (global total: 20.5 Tg CH <sub>4</sub> yr <sup>-1</sup> )	VISIT (Ito and Inatomi, 2012)	Lambert/Houweling (TransCom-CH <sub>4</sub> ) (global total: 18.5 Tg CH <sub>4</sub> yr <sup>-1</sup> )	
GCP	NICAM-SURF_NIES	VISIT (Ito and Inatomi, 2012)	GCP based on Etiopie 2015	GFEDv4s / GCP	Sanderson (TransCom-CH <sub>4</sub> / GCP)	VISIT (Ito and Inatomi, 2012)	Lambert/Houweling (TransCom-CH <sub>4</sub> / GCP)	
GCP	TOMCAT-SURF_ECMWF	JULES emissions from Mc Norton 2016a	Tomcat 2006	GFED V4	Matthews and Fung 2006	Patra et al. 2011	Tomcat 2006 Matthews	

							and Fung 1987 - all emissions total rescaled to Schwietzke et al. 2016	
GCP	NTFVAR- GOSAT_NIES	VISIT (Ito and Inatomi, 2012)	Etiopie and Milkov, 2004	GFAS v1.2	Ito and Inatomi 2012	VISIT (Ito and Inatomi, 2012)	TransCom- CH4	
GCP	NTFVAR- SURF_NIES	VISIT (Ito and Inatomi, 2012)	Etiopie and Milkov, 2004	GFAS v1.2	Ito and Inatomi 2012	VISIT (Ito and Inatomi, 2012)	TransCom- CH4	
GCP	LMDZ- GOSAT1_LSC E	Bloom 2017	n/a	GFED V41s	Sanderson /GCP	Ridgwell /GCP	Lambert /GCP	
GCP	LMDZ- GOSAT2_LSC E	GCP - ensemble mean ESSD Saunois et al . 2016	GCP based on Etiopie 2015	GFED V41s	Sanderson /GCP	Ridgwell /GCP	Lambert /GCP	
GCP	LMDZ-GOSAT1 LMDZ-GOSAT1 LMDZ-GOSAT1 LMDZ-GOSAT1 LMDZ-SURF1 LMDZ-SURF2	Kaplan 2002 rescaled by Bergamaschi 2007	n/a	GFED V41	Sanderson 1996 /GCP	Ridgwell /GCP	Lambert and Schmidt 1993	
GCP	TM5-CAMS- GOSAT_TNO	Kaplan climatology	n/a	GFED V31 climatology after 2011	Sanderson /GCP	Ridgwell /GCP	Lambert /GCP	Osmon climatology
GCP	TM5- GOSAT1_EC	WETCHIMP ensemble mean;	GCP_CH4 2019 (global total: 15 Tg CH4 yr <sup>-1</sup> )		Sanderson /GCP	Ridgwell /GCP	Lambert /GCP	Osmon climatology
GCP	TM5- GOSAT2_EC	GCP_CH4_2019	GCP_CH4 2019 (global total: 15 Tg CH4 yr <sup>-1</sup> )	GCP_CH4_2019	GCP_CH4_2019	GCP_CH4 _2019	GCP_CH4_ 2019	

GCP	TM5-SURF1_EC	WETCHIMP ensemble mean;	GCP_CH4 2019 (global total: 15 Tg CH4 yr <sup>-1</sup> )		Sanderson /GCP	Ridgwell /GCP	Lambert /GCP	Osmon climatology
GCP	TM5-SURF2_EC	GCP_CH4_2019	GCP_CH4 2019 (global total: 15 Tg CH4 yr <sup>-1</sup> )	GCP_CH4_2019	GCP_CH4_2019	GCP_CH4_2019	GCP_CH4_2019	
GCP	CTE-GOSAT_FMI	GCP_CH4_2019	Etiopie 2015	GCP_CH4_2019 (=GFED4s)	GCP_CH4_2019	GCP_CH4_2019	GCP_CH4_2019	
GCP	CTE-SURF_FMI	GCP_CH4_2019	Etiopie 2015	GCP_CH4_2019 (=GFED4s)	GCP_CH4_2019	GCP_CH4_2019	GCP_CH4_2019	
	NAME-SURF_MetOff ice							
N <sub>2</sub> O VERIFY CIF	FLEXPART-NILU CHIMERE			GFED-v41s		O-CN	PlankTom-v10	

#### Author contributions:

AMRP designed this research and led the discussions with all co-authors, AMRP wrote the initial draft of the paper and edited all the following versions; CQ made the figures, PPe, MJM, V B processed the original data submitted to the VERIFY portal, MJM, PPe and PB designed and are managing the VERIFY web portal, BM provided the new gap-filled yearly UNFCCC NGHGI Member States uncertainty calculations and checked language and content of the final reviewed version, GPP provided the figures B1a and B1b in Appendix B1 and checked language and content of the final version, AB provided the figures 5 and 14, DBr provided the figure 7, AT provided the data for the figures 8 and 9 in section 3.1.5. and AMRP made the figures 8 and 9, AT and CQ provided input to the review answers, PPa, OT, RLT, CQ, GE, MK, LH-J, PR, RL, DBa, WW, provided in depth advice and commented/edited the initial versions of the manuscript, MB, RLT, AT, DBr, MK, PGE, GC, PR, RL, LH-J, WW, TA, AB, GC, MC, FD, CDGZ, AL, EL, AJM, MMa, TM, GDO, PKP, MS, AJJ, ES, HT, FNT, SZ. are data providers.

#### Competing interests

The authors declare that they have no conflict of interest.

#### Acknowledgements

We thank Aurélie Paquirissamy, Géraud Moulas and all ARTTIC team, for the great managerial support offered during the project. FAOSTAT statistics are produced and disseminated with the support of its member countries to the FAO regular budget. Annual, gap-filled and harmonized NGHGI uncertainty estimates for the EU and its Member States



2005 were provided by the EU GHG inventory team (European Environment Agency and its European Topic Centre on Climate change mitigation). The views expressed in this publication are those of the author(s) and do not necessarily reflect the views or policies of FAO. We acknowledge the work of other members of the EDGAR group (Edwin Schaaf, Jos Olivier) and the outstanding scientific contribution to the VERIFY project of Peter Bergamaschi. Timo Vesala thanks the ICOS-Finland, University of Helsinki. The TM5-CAMS inversions are available from  
 2010 <https://atmosphere.copernicus.eu>; Arjo Segers acknowledges the support from the Copernicus Atmosphere Monitoring Service, implemented by the European Centre for Medium-Range Weather Forecasts on behalf of the European Commission (grant no. CAMS2\_55).

### Financial support

2015 This research has been supported by the European Commission, Horizon 2020 Framework Programme (VERIFY, grant no. 776810).  
 Ronny Lauerwald thanks the CLand Convergence Institute. Prabir Patra acknowledges support of the Environment Research and Technology Development Fund (JPMEERF20182002) of the Environmental Restoration and Conservation Agency of Japan. Pierre Regnier acknowledges the ESM 2025. David Basviken acknowledges support  
 2020 of the European Research Council (ERC) under the European Union's Horizon 2020 research and innovation programme (grant agreement No 725546 METLAKE). Greet Janssens-Maenhout acknowledges the European Union's Horizon 2020 research and innovation programme (CoCO2, grant no. 958927). Tuula Aalto acknowledges support from the Finnish Academy grants no. 351311, 345531. Sonke Zhaele acknowledges support from the ERC consolidator grant QUINCY (grant no. 647204).

2025

### References

- Amann, M., Bertok, I., Borken-Kleefeld, J., Cofala, J., Heyes, C., Höglund-Isaksson, L., Klimont, Z., Nguyen, B., Posch, M., Rafaj, P., Sandler, R., Schöpp, W., Wagner, F., Winiwarter, W. Cost-effective control of air quality and greenhouse gases in Europe: modeling and policy applications. *Environmental Modelling and Software* 26, 1489-1501, 2011.
- 2030 Arnold, T., Manning, A. J., Kim, J., Li, S., Webster, H., Thomson, D., Mühle, J., Weiss, R. F., Park, S., and O'Doherty, S.: Inverse modelling of CF<sub>4</sub> and NF<sub>3</sub> emissions in East Asia, *Atmos. Chem. Phys.*, 18, 13305-13320, 10.5194/acp-18-13305-2018, 2018.
- 2035 Arora, V. K., Melton, J. R., and Plummer, D.: An assessment of natural methane fluxes simulated by the CLASS-CTEM model, *Biogeosciences*, 15, 4683-4709, <https://doi.org/10.5194/bg-15-4683-2018>, 2018.
- Bastviken, D., L. J. Tranvik, J. A. Downing, P. M. Crill, and A. Enrich-Prast: Freshwater methane emissions offset the continental Carbon Sink, *Science*, 331(6013), 50–50, doi:10.1126/science.1196808, 2011.
- Beaulieu, J.J., DelSontro, T. & Downing, J.A.: Eutrophication will increase methane emissions from lakes and impoundments during the 21st century. *Nat Commun* 10, 1375, <https://doi.org/10.1038/s41467-019-09100-5>, 2019.
- 2040

- Berchet, A., Pison, I., Chevallier, F., Bousquet, P., Bonne, J.-L., and Paris, J.-D.: Objectified quantification of uncertainties in Bayesian atmospheric inversions, *Geosci. Model Dev.*, *Geosci. Model Dev.*, 8, 1525–1546, doi: 10.5194/gmd-8-1525-2015, 5 2015a.
- 2045 Berchet, A., Pison, I., Chevallier, F., Paris, J.-D., Bousquet, P., Bonne, J.-L., Arshinov, M. Y., Belan, B. D., Cressot, C., Davydov, D. K., Dlugokencky, E. J., Fofonov, A. V., Galanin, A., Lavric, J. V., Machida, T., Parker, R., Sasakawa, M., Spahni, R., Stocker, B. D., and Winderlich, J.: Natural and anthropogenic methane fluxes in Eurasia: a mesoscale quantification by generalized atmospheric inversion, *Biogeosciences*, 12, 5393–5414, doi: 10.5194/bg-12-5393-2015, 2015b.
- 2050 Berchet, A., Sollum, E., Thompson, R. L., Pison, I., Thanwerdas, J., Broquet, G., Chevallier, F., Aalto, T., Berchet, A., Bergamaschi, P., Brunner, D., Engelen, R., Fortems-Cheiney, A., Gerbig, C., Groot Zwaafink, C. D., Haussaire, J.-M., Henne, S., Houweling, S., Karstens, U., Kutsch, W. L., Luijkx, I. T., Monteil, G., Palmer, P. I., van Peet, J. C. A., Peters, W., Peylin, P., Potier, E., Rödenbeck, C., Saunio, M., Scholze, M., Tsuruta, A., and Zhao, Y.: The Community Inversion Framework v1.0: a unified system for atmospheric inversion studies, *Geosci. Model Dev.*, 14, 5331–5354, <https://doi.org/10.5194/gmd-14-5331-2021>, 2021.
- 2055 Bergamaschi, P., Corazza, M., Karstens, U., Athanassiadou, M., Thompson, R. L., Pison, I., Manning, A. J., Bousquet, P., Segers, A., Vermeulen, A. T., Janssens-Maenhout, G., Schmidt, M., Ramonet, M., Meinhardt, F., Aalto, T., Haszpra, L., Moncrieff, J., Popa, M. E., Lowry, D., Steinbacher, M., Jordan, A., O'Doherty, S., Piacentino, S., and Dlugokencky, E.: Top-down estimates of European CH<sub>4</sub> and N<sub>2</sub>O emissions based on four different inverse models, *Atmos. Chem. Phys.*, 15, 715–736, <https://doi.org/10.5194/acp-15-715-2015>, 2015.
- 2060 Bergamaschi, P., Danila, A. M., Weiss, R., Ciais, P., Thompson, R. L., Brunner, D., Levin, I., Meijer, Y., Chevallier, F., Janssens-Maenhout, G., Bovensmann, H., Crisp, D., Basu, S., Dlugokencky, E., Engelen, R., Gerbig, C., Günther, D., Hammer, S., Henne, S., Houweling, S., Karstens, U., Kort, E., Maione, M., Manning, A., Miller, J., Montzka, S., Pandey, S., Peters, W., Peylin, P., Pinty, B., Ramonet, M., Reimann, S., Röckmann, T., Schmidt, M., Strogies, M., Sussams, J., Tarasova, O., Van Aardenne, J., Vermeulen, A., and Vogel F.: Atmospheric monitoring and inverse modelling for verification of greenhouse gas inventories, JRC report, <https://doi.org/10.2760/759928>, 2018b.
- 2065 Bergamaschi, P., Houweling, S., Segers, A., Krol, M., Frankenberg, C., Scheepmaker, R. A., Dlugokencky, E., Ofsy, S. C., Kort, E. A., Sweeney, C., Schuck, T., Brenninkmeijer, C., Chen, H., Beck, V., and Gerbig, C.: Atmospheric CH<sub>4</sub> in the first decade of the 21st century: Inverse modeling analysis using SCIAMACHY satellite retrievals and NOAA surface measurements, *J. Geophys. Res.-Atmos.*, 118, 7350–7369, <https://doi.org/10.1002/jgrd.50480>, 2013.
- 2070 Bergamaschi, P., Karstens, U., Manning, A. J., Saunio, M., Tsuruta, A., Berchet, A., Vermeulen, A. T., Arnold, T., Janssens-Maenhout, G., Hammer, S., Levin, I., Schmidt, M., Ramonet, M., Lopez, M., Lavric, J., Aalto, T., Chen, H., Feist, D. G., Gerbig, C., Haszpra, L., Hermansen, O., Manca, G., Moncrieff, J., Meinhardt, F., Necki, J., Galkowski, M., O'Doherty, S., Paramonova, N., Scheeren, H. A., Steinbacher, M., and Dlugokencky, E.: Inverse modelling of European CH<sub>4</sub> emissions during 2006–2012 using different inverse models and reassessed atmospheric observations, *Atmos. Chem. Phys.*, 18, 901–920, <https://doi.org/10.5194/acp-18-901-2018>, 2018a.
- 2075 Bergamaschi, P., Krol, M., Meirink, J. F., Dentener, F., Segers, A., van Aardenne, J., Monni, S., Vermeulen, A., Schmidt, M., Ramonet, M., Yver, C., Meinhardt, F., Nisbet, E. G., Fisher, R., O'Doherty, S., and Dlugokencky, E. J.: Inverse modeling of European CH<sub>4</sub> emissions 2001–2006, *J. Geophys. Res.*, 115, D22309, <https://doi.org/10.1029/2010JD014180>, 2010.
- 2080 Bousquet, P., Ringeval, B., Pison, I., Dlugokencky, E. J., Brunke, E.-G., Carouge, C., Chevallier, F., Fortems-Cheiney, A., Frankenberg, C., Hauglustaine, D. A., Krummel, P. B., Langenfelds, R. L., Ramonet, M., Schmidt, M., Steele, L. P., Szopa, S., Yver, C., Viovy, N., and Ciais, P.: Source attribution of the changes in atmospheric methane for 2006–2008, *Atmos. Chem. Phys.*, 11, 3689–3700, doi: 10.5194/acp-11-3689-2011, 2011.
- 2085 BP (2020). Statistical review of world energy. 2020, 69<sup>th</sup> edition. [bp.com/statisticalreview](https://www.bp.com/statisticalreview).

- Bradbury, N.J., Whitmore, A.P., Hart, P.B.S., Jenkinson, D.S.: Modelling the fate of nitrogen in crop and soil in the years following application of <sup>15</sup>N-labelled fertilizer to winter wheat, *J Agr Sci* 121: 363-379, 1993.
- Britz, W. and Witzke, P.: CAPRI model documentation 2014, available at: [https://www.capri-model.org/docs/capri\\_documentation.pdf](https://www.capri-model.org/docs/capri_documentation.pdf) (last access: September 2020), 2014.
- 2090 Brunner D. 2022: Internal VERIFY deliverable report available at [https://projectworkspace.eu/sites/VERIFY/Deliverables/WP4/VERIFY\\_D4.15\\_CH4%20fluxes%20at%20very%20high%20resolution\\_v1.pdf](https://projectworkspace.eu/sites/VERIFY/Deliverables/WP4/VERIFY_D4.15_CH4%20fluxes%20at%20very%20high%20resolution_v1.pdf), 2011, last access June, 2022.
- 2095 Brunner, D., Arnold, T., Henne, S., Manning, A., Thompson, R. L., Maione, M., O'Doherty, S., and Reimann, S.: Comparison of four inverse modelling systems applied to the estimation of HFC-125, HFC-134a, and SF<sub>6</sub> emissions over Europe, *Atmos. Chem. Phys.*, 17, 10651–10674, <https://doi.org/10.5194/acp-17-10651-2017>, 2017.
- Brunner, D., Henne, S., Keller, C. A., Reimann, S., Vollmer, M. K., O'Doherty, S., & Maione, M.: An extended Kalman-filter for regional scale inverse emission estimation. *Atmospheric Chemistry and Physics*, 12(7), 3455-3478. <https://doi.org/10.5194/acp-12-3455-2012>, 2012.
- Brühl, C. and Crutzen, P. J.: MPIC Two-dimensional model, *NASA Ref. Publ.*, 1292, 103–104, 1993.
- 2100 Buitenhuis, E. T., Suntharalingam, P., & Le Quéré, C.: Constraints on global oceanic emissions of N<sub>2</sub>O from observations and models, *Biogeosciences*, 15(7), 2161–2175, [doi:10.5194/bg-15-2161-2018](https://doi.org/10.5194/bg-15-2161-2018), 2018.
- Carlson, D. and Oda, T.: Editorial: Data publication – ESSD goals, practices and recommendations, *Earth Syst. Sci. Data*, 10, 2275–2278, <https://doi.org/10.5194/essd-10-2275-2018>, 2018.
- 2105 Chevallier, F., Bréon, F. -M., and Rayner, P. J.: Contribution of the Orbiting Carbon Observatory to the estimation of CO<sub>2</sub> sources and sinks: Theoretical study in a variational data assimilation framework, *J. Geophys. Res.*, 112(D9), [doi:10.1029/2006jd007375](https://doi.org/10.1029/2006jd007375), 2007.
- Chevallier, F., Fisher, M., Peylin, P., Serrar, S., Bousquet, P., Bréon, F. M., Chédin, A. and Ciais, P.: Inferring CO<sub>2</sub> sources and sinks from satellite observations: Method and application to TOVS data, *J. Geophys. Res.*, 110(D24309), [doi:10.1029/2005jd006390](https://doi.org/10.1029/2005jd006390), 2005.
- 2110 Coleman, K., Jenkinson, D.S.: RothC-26.3 - A model the turnover of carbon in soil. In: Powlson DS, Smith P, Smith JU (ed) *Evaluation of soil organic matter models using existing long-term datasets*. NATO ASI Series I, vol. 38. Springer, Berlin, pp 237–246, 1996.
- 2115 COM(2020) 562, Stepping up Europe's 2030 climate ambition Investing in a climate-neutral future for the benefit of our people, [https://ec.europa.eu/clima/sites/clima/files/eu-climate-action/docs/com\\_2030\\_ctp\\_en.pdf](https://ec.europa.eu/clima/sites/clima/files/eu-climate-action/docs/com_2030_ctp_en.pdf), 2020, last access November 2020.
- COM(96) 557 Strategy for reducing methane emissions, <https://eur-lex.europa.eu/legal-content/EN/TXT/PDF/?uri=CELEX:51996DC0557&from=NL>, 1996, last access September 2020,.
- CORDEX: Coordinated Regional Climate Downscaling Experiment, available at: <https://esgf-node.ipsl.upmc.fr/search/cordex-ipsi/>, last access June 2020.
- 2120 Crippa, M., Oreggioni, G., Guizzardi, D., Muntean, M., Schaaf, E., Lo Vullo, E., Solazzo, E., Monforti-Ferrario, F., Olivier, J.G.J., Vignati, E., Fossil CO<sub>2</sub> and GHG emissions of all world countries - 2019 Report, EUR 29849 EN, Publications Office of the European Union, Luxembourg, ISBN 978-92-76-11100-9, [doi:10.2760/687800](https://doi.org/10.2760/687800), JRC117610, 2019.
- 2125 Crippa, M., Solazzo, E., Huang, G., Guizzardi, D., Koffi, E. N., Muntean, M., Schieberle, C., Friedrich, R., and Janssens-Maenhout, G.: Towards time varying emissions: development of high resolution temporal profiles in the Emissions Database for Global Atmospheric Research, *Nature Scientific Data*, in review, 2019a.

CSIRO <https://www.csiro.au/en/Research/OandA/Areas/Assessing-our-climate/Latest-greenhouse-gas-data>, last access October, 2020.

Cullen, M. J. P.: The unified forecast/climate model, *Meteorol. Mag.*, 122, 81–94, 1993.

- 2130 Dee, D. P., Källén, E., Simmons, A. J., Haimberger, L.: Comments on ‘Reanalyses suitable for characterizing long-term trends’, *Bull. Amer. Meteorol. Soc.*, 92: 65–70, 2011.

Deemer, B. R., Harrison, J. A., Li, S., Beaulieu, J. J., DelSontro, T., Barros, N., Bezerra-Neto, J. F., Powers, S. M., dos Santos, M. A. and Vonk, J. A.: Greenhouse Gas Emissions from Reservoir Water Surfaces: A New Global Synthesis, *Bioscience*, 66(11), 949–964, doi:10.1093/biosci/biw117, 2016.

- 2135 Del Sontro, T., Beaulieu, J. J. and Downing, J. A.: Greenhouse gas emissions from lakes and impoundments: Upscaling in the face of global change, *Limnol. Oceanogr. Lett.*, 3(3), 64–75, doi:10.1002/lol2.10073, 2018.

Directive 1999/31/EC, <https://eur-lex.europa.eu/legal-content/EN/TXT/PDF/?uri=CELEX:31999L0031&from=EN>, 1999, last access June 2020.

Ebdon D. (1985). *Statistics in geography*. Blackwell, Oxford, 232 pp.

- 2140 Eisma, R., Vermeulen, A., and Van der Borg, K.: 14CH<sub>4</sub> Emissions from Nuclear Power Plants in Northwestern Europe, *Radiocarbon*, 37(2), 475–483, 1995.

Etheridge, D. M., Steele, L. P., Francey, R. J., and Langenfelds, R. L.: Atmospheric methane between 1000 A.D. and present: Evidence of anthropogenic emissions and climatic variability, *Journal of Geophysical Research*, Vol. 103, no. D13, 15,979–15,993, 10.1029/98JD00923, 1998.

- 2145 Etiope G.: Natural emissions of methane from geological seepage in Europe. *Atm. Environm.*, 43, 1430–1443, doi:10.1016/j.atmosenv.2008.03.014, 2009.

Etiope, G., Ciotoli, G., Schwietzke, S., and Schoell, M.: Gridded maps of geological methane emissions and their isotopic signature, *Earth Syst. Sci. Data*, 11, 1–22, <https://doi.org/10.5194/essd-11-1-2019>, 2019.

- 2150 Etiope G., Schwietzke S.: Global geological methane emissions: an update of top-down and bottom-up estimates. *Elem. Sci. Anth.* 7, 47, <http://doi.org/10.1525/elementa.383>, 2019.

EUROSTAT. Waste generation and treatment. <https://ec.europa.eu/eurostat/web/waste/data/database>. 2020

Evensen, G.: The Ensemble Kalman Filter: theoretical formulation and practical implementation, *Ocean Dynam.*, 53, 343–367, <https://doi.org/10.1007/s10236-003-0036-9>, 2003.

- 2155 FAO: The State of Food and Agriculture: Social protection and agriculture: breaking the cycle of rural poverty, 2015, Rome, Italy, available at: <http://www.fao.org/3/a-i4910e.pdf> (last access: September 2020), 2015.

FAO: The State of Food Security and Nutrition in the World: Transforming food systems for affordable healthy diets, 2020, Rome, Italy, available at: <http://www.fao.org/3/ca9692en/CA9692EN.pdf> (last access: October 2020), 2020.

FAO-AQUASTAT: FAO's Global Information System on Water and Agriculture available at <http://www.fao.org/aquastat/en/>, last access September 2020.

- 2160 FAOSTAT: Statistics Division of the Food and Agricultural Organisation of the UN, Live animal numbers, crop production, total nitrogen fertiliser consumption statistics till 2016, available at: <http://www.fao.org/faostat/en/#home>, last access: December 2018.

Feng, L., Palmer, P.I., Zhu, S. et al. Tropical methane emissions explain large fraction of recent changes in global atmospheric methane growth rate. *Nature Comm* 13, 1378 (2022). <https://doi.org/10.1038/s41467-022-28989-z>

- 2165 Feng, L., Palmer, P. I., Parker, R. J., Lunt, M. F., and Boesch, H.: Methane emissions responsible for record-breaking

atmospheric methane growth rates in 2020 and 2021, *Atmos. Chem. Phys. Discuss.* [preprint], <https://doi.org/10.5194/acp-2022-425>, in review, 2022.

- 2170 Fortems-Cheiney, A., Pison, I., Broquet, G., Dufour, G., Berchet, A., Potier, E., Coman, A., Siour, G., and Costantino, L.: Variational regional inverse modeling of reactive species emissions with PYVAR-CHIMERE-v2019, *Geosci. Model Dev.*, 14, 2939–2957, <https://doi.org/10.5194/gmd-14-2939-2021>, 2021.
- 2175 Friedlingstein, P., Jones, M. W., O’Sullivan, M., Andrew, R. M., Hauck, J., Peters, G. P., Peters, W., Pongratz, J., Sitch, S., Le Quéré, C., Bakker, D. C. E., Canadell, J. G., Ciais, P., Jackson, R. B., Anthoni, P., Barbero, L., Bastos, A., Bastrikov, V., Becker, M., Bopp, L., Buitenhuis, E., Chandra, N., Chevallier, F., Chini, L. P., Currie, K. I., Feely, R. A., Gehlen, M., Gilfillan, D., Gkritzalis, T., Goll, D. S., Gruber, N., Gutekunst, S., Harris, I., Haverd, V., Houghton, R. A., Hurtt, G., Ilyina, T., Jain, A. K., Joetzjer, E., Kaplan, J. O., Kato, E., Klein Goldewijk, K., Korsbakken, J. I., Landschützer, P., Lauvset, S. K., Lefèvre, N., Lenton, A., Lienert, S., Lombardozzi, D., Marland, G., McGuire, P. C., Melton, J. R., Metzl, N., Munro, D. R., Nabel, J. E. M. S., Nakaoka, S.-I., Neill, C., Omar, A. M., Ono, T., Peregon, A., Pierrot, D., Poulter, B., Rehder, G., Resplandy, L., Robertson, E., Rödenbeck, C., Séférian, R., Schwinger, J., Smith, N., Tans, P. P., Tian, H., Tilbrook, B., Tubiello, F. N., van der Werf, G. R., Wiltshire, A. J., and Zaehle, S.: Global Carbon Budget 2019, *Earth Syst. Sci. Data*, 11, 1783–1838, <https://doi.org/10.5194/essd-11-1783-2019>, 2019.
- 2185 Fronzek, S., Pirttioja, N., Carter, T.R., Bindi, M., Hoffmann, H., Palosuo, T., Ruiz-Ramos, M., Tao, F., Trnka, M., Acutis, M., Asseng, S., Baranowski, P., Basso, B., Bodin, P., Buis, S., Cammarano, D., Deligios, P., Destain, M.-F., Dumont, B., Ewert, F., Ferrise, R., François, L., Gaiser, T., Hlavinka, P., Jacquemin, I., Kersebaum, K.C., Kollas, C., Krzyszczak, J., Lorite, I.J., Minet, J., Minguez, M.I., Montesino, M., Moriondo, M., Müller, C., Nendel, C., Öztürk, I., Perego, A., Rodríguez, A., Ruane, A.C., Ruget, F., Sanna, M., Semenov, M.A., Slawinski, C., Stratonovitch, P., Supit, I., Waha, K., Wang, E., Wu, L., Zhao, Z., Rötter, R.P.: Classifying multi-model wheat yield impact responses surfaces showing sensitivity to temperature and precipitation change. *Agric. Syst.* 159, 209–224, <https://doi.org/10.1016/j.agry.2017.08.004>, 2018.
- 2190 Gerbig, C., Lin, J. C., Wofsy, S. C., Daube, B. C., Andrews, A. E., Stephens, B. B., Bakwin, P. S., and Grainger, C. A.: Toward constraining regional-scale fluxes of CO<sub>2</sub> with atmospheric observations over a continent: 2. Analysis of COBRA data using a receptor-oriented framework, *J. Geophys. Res.*, 108, 4757, <https://doi.org/10.1029/2003JD003770>, 2003.
- 2195 Giglio, L., Randerson, J. T. and van der Werf, G. R.: Analysis of daily, monthly, and annual burned area using the fourth-generation global fire emissions database (GFED4), *J. Geophys. Res. Biogeosci.*, 118(1), 317–328, [doi:10.1002/jgrg.20042](https://doi.org/10.1002/jgrg.20042), 2013.
- 2200 Gilbert, J.C., and Lemaréchal, C.: Some numerical experiments with variable storage quasi-Newton algorithms,” IASA Working Paper WP-88, A-2361, Laxenburg, 1988.
- Gruber, W., Vilez, K., Kipf, M., Wunderlin, P., Siegrist, H., Vogt, L., Joss, A.: N<sub>2</sub>O emission in full-scale wastewater treatment: Proposing a refined monitoring strategy, *Science of The Total Environment*, Vol. 699, 134-157, ISSN 0048-9697, <https://doi.org/10.1016/j.scitotenv.2019.134157>, 2020.
- 2205 Hayman, G. D., O’Connor, F. M., Dalvi, M., Clark, D. B., Gedney, N., Huntingford, C., Prigent, C., Buchwitz, M., Schneising, O., Burrows, J. P., Wilson, C., Richards, N., and Chipperfield, M.: Comparison of the HadGEM2 climate-chemistry model against in situ and SCIAMACHY atmospheric methane data, *Atmospheric Chemistry and Physics*, 14, 13257-13280, [doi:10.5194/acp-14-13257-2014](https://doi.org/10.5194/acp-14-13257-2014), 2014.
- 2210 Heimann H., Körner S.: The global atmospheric tracer model TM3. Technical Reports - Max-Planck-Institut für Biogeochemie 5, pp. 131 Technical Report: (5.pdf), 2003.

- Hmiel, B., V. V. Petrenko, M. N. Dyonisius, C. Buizert, A. M. Smith, P. F. Place, C. Harth, R. Beaudette, Q. Hua, B. Yang, I. Vimont, S. E. Michel, J. P. Severinghaus, D. Etheridge, T. Bromley, J. Schmitt, X. Fäin, R. F. Weiss & E. Dlugokencky: Preindustrial  $^{14}\text{CH}_4$  indicates greater anthropogenic fossil  $\text{CH}_4$  emissions, *Nature* 578, 409–412, 2020.
- 2215 Höglund-Isaksson L., Winiwarter, W., Purohit, P., Gomez-Sanabria, A., Rafaj, P., Schopp, W., Borken-Kleefeld, J.: Non- $\text{CO}_2$  greenhouse gas emissions in the EU-28 from 2005 to 2070 with mitigation potentials and costs -GAINS model methodology. Report prepared by IIASA for DG-CLIMA under Service contract 340201/2017/766154/SER/CLIMA.C1, October 2018.
- 2220 Höglund-Isaksson, L., Gómez-Sanabria, A., Klimont, Z., Rafaj, P., Schöpp, W.: Technical potentials and costs for reducing global anthropogenic methane emissions in the 2050 timeframe - results from the GAINS model, forthcoming, Feb 2020.
- Höglund-Isaksson, L.: Bottom-up simulations of methane and ethane from global oil and gas systems, *Environmental Research Letters*, 12(2), doi:10.1088/1748-9326/aa583e, 2017.
- Hourdin, F., Armengaud, A.: The use of finite-volume methods for atmospheric advection of trace species. Part I: test of various formulations in a general circulation model, *Mon Wea Rev* 127:822–837, 1999.
- 2225 Hourdin, F., Musat, I., Bony, S., Braconnot, P., Codron, F., Dufresne, J.L., Fairhead, L., Filiberti, M.A., Friedlingstein, P., Grandpeix, J.Y., Krinner, G., LeVan, P., Lott, F.: The LMDZ4 general circulation model: climate performance and sensitivity to parametrized physics with emphasis on tropical convection, *Clim Dyn* 27(7–8):787–813. doi:10.1007/s00382-006-0158-0, 2006.
- 2230 Houweling, S., Krol, M., Bergamaschi, P., Frankenberg, C., Dlugokencky, E. J., Morino, I., Notholt, J., Sherlock, V., Wunch, D., Beck, V., Gerbig, C., Chen, H., Kort, E. A., Röckmann, T. and Aben, I.: A multi-year methane inversion using SCIAMACHY, accounting for systematic errors using TCCON measurements, *Atmos. Chem. Phys.*, 14(8), 3991–4012, doi:10.5194/acp-14-3991-2014, 2014.
- IEA energy balance statistics for 1970-2015, <http://www.iea.org/>, 2017, last access March 2020.
- 2235 IPCC 2019 Refinement to Guidelines for National Greenhouse Gas Inventories. Volume 5: Waste, Chapter 3: Solid Waste disposal. Towprayoon S, Ishigaki T, Chiemchaisri C, Abdel-Aziz A O, 2019a.
- IPCC Guidelines for National Greenhouse Gas Inventories (NGHGI): <https://www.ipcc-nggip.iges.or.jp/public/2006gl/> 2006 last access: January 2022.
- 2240 IPCC, 2006, Vol. 1, Chap. 3, [https://www.ipcc-nggip.iges.or.jp/public/2006gl/pdf/1\\_Volume1/V1\\_3\\_Ch3\\_Uncertainties.pdf](https://www.ipcc-nggip.iges.or.jp/public/2006gl/pdf/1_Volume1/V1_3_Ch3_Uncertainties.pdf), last access June 2022.
- IPCC: Special Report on climate change, desertification, land degradation, sustainable land management, food security, and greenhouse gas fluxes in terrestrial ecosystems (SRCCL), IPCC report, available at: <https://www.ipcc.ch/report/srccl/>, last access: January 2022.
- 2245 IPCC: Supplement to the 2006 IPCC Guidelines for National Greenhouse Gas Inventories: Wetlands, edited by: Hiraishi, T., Krug, T., Tanabe, K., Srivastava, N., Baasansuren, J., Fukuda, M., and Troxler, T. G., IPCC, Switzerland, 2014.
- Ishizawa, M., Mabuchi, K., Shirai, T., Inoue, M., Morino, I., Uchino, O., Yoshida, Y., Maksyutov, S., and Belikov, D.: Inter-annual variability of  $\text{CO}_2$  exchange in Northern Eurasia inferred from GOSAT XCO<sub>2</sub>, *Environ. Res. Lett.*, 11, 105001, doi:10.1088/1748-9326/11/10/105001, 2016.
- 2250 Ito, A. and Inatomi, M.: Use of a process-based model for assessing the methane budgets of global terrestrial ecosystems and evaluation of uncertainty, *Biogeosciences*, 9(2), 759–773, doi:10.5194/bg-9-759-2012, 2012.

- Jansen, J., Woolway, R. I., Kraemer, B. M., Albergel, C., Bastviken, D., Weyhenmeyer, G. A., Marcé, R., Sharma, S., Sobek, S., Tranvik, L. J., Perroud, M., Golub, M., Moore, T. N., Vinnå, L. R., La Fuente, S., Grant, L., Pierson, D. C., Thiery, W., and Jennings, E.: Global increase in methane production under future warming of lake bottom waters, *Glob. Change Biol.*, 28, 5427–5440, <https://doi.org/10.1111/gcb.16298>, 2022.
- Janssens-Maenhout, G., Crippa, M., Guizzardi, D., Muntean, M., Schaaf, E., Dentener, F., Bergamaschi, P., Pagliari, V., Olivier, J. G. J., Peters, J. A. H. W., van Aardenne, J. A., Monni, S., Doering, U., Petrescu, A. M. R., Solazzo, E., and Oreggioni, G. D.: EDGAR v4.3.2 Global Atlas of the three major greenhouse gas emissions for the period 1970–2012, *Earth Syst. Sci. Data*, 11, 959–1002, <https://doi.org/10.5194/essd-11-959-2019>, 2019.
- Janssens-Maenhout, G., Pagliari, V., Guizzardi, D. and Muntean, M.: Global emission inventories in the Emission Database for Global Atmospheric Research (EDGAR) – Manual (I) I. Gridding: EDGAR emissions distribution on global gridmaps, EUR - Scientific and Technical Research Reports, Publications Office of the European Union. [online] Available from: [http://publications.jrc.ec.europa.eu/repository/bitstream/JRC78261/edgarv4\\_manual\\_i\\_gridding\\_pubsy\\_final.pdf](http://publications.jrc.ec.europa.eu/repository/bitstream/JRC78261/edgarv4_manual_i_gridding_pubsy_final.pdf) (Accessed 7 February 2018), 2013.
- Jenkinson, D.S., Hart, P.B.S., Rayner, J.H., Parry, L.C.: Modelling the turnover of organic matter in long-term experiments at Rothamste, *INTECOL Bulletin* 15:1-8, 1987.
- Jenkinson, D.S., Rayner, J.H.: The turnover of organic matter in some of the Rothamsted classical experiments, *Soil Sci* 123: 298–305, 1977.
- Jones, A., Thomson, D., Hort, M., and Devenish, B.: The UK Met Office’s next-generation atmospheric dispersion model, NAME III, *Air Pollution Modeling and Its Applications Xvii*, edited by: Borrego, C. and Norman, A. L., 580–589, 2007.
- Judd, A.G., Davies, J., Wilson, J., Holmes, R., Baron, G., and Bryden, I.: Contributions to atmospheric methane by natural seepages on the UK continental shelf, *Mar. Geol.*, 137, 165–189, 1997.
- Kleinen, T., Brovkin, V., and Schuldt, R. J.: A dynamic model of wetland extent and peat accumulation: results for the Holocene, *Biogeosciences*, 9, 235–248, doi:10.5194/bg-9-235-2012, 2012.
- Kleinen, T., Mikolajewicz, U., and Brovkin, V.: Terrestrial methane emissions from the Last Glacial Maximum to the preindustrial period, *Clim. Past*, 16, 575–595, <https://doi.org/10.5194/cp-16-575-2020>, 2020.
- Koohkan, M. R. and Bocquet, M.: Accounting for representativeness errors in the inversion of atmospheric constituent emissions: Application to the retrieval of regional carbon monoxide 20 fluxes., *Tellus B*, 64, 19 047, 2012.
- Krol, M., Houweling, S., Bregman, B., Broek, M. van den, Segers, A., Velthoven, P. van, Peters, W., Dentener, F. and Bergamaschi, P.: The two-way nested global chemistry-transport zoom model TM5: algorithm and applications, *Atmospheric Chemistry and Physics*, 5(2), 417–432, doi:<https://doi.org/10.5194/acp-5-417-2005>, 2005.
- Langenegger, T., Vachon, D., Donis, D., & McGinnis, D. F.: What the bubble knows: Lake methane dynamics revealed by sediment gas bubble composition. *Limnology and Oceanography*, 64, 1526– 1544, <https://doi.org/10.1002/lno.11133>, 2019.
- Lauerwald, R., Regnier, P., Figueiredo, V., Enrich-Prast, A., Bastviken, D., Lehner, B., Maavara, T., Raymond, P.: Natural lakes are a minor global source of N<sub>2</sub>O to the atmosphere. *Global Biogeochemical Cycles*, 33. <https://doi.org/10.1029/2019GB006261>, 2019.
- Lauerwald et al., in rev. GBC
- Leip A.: VERIFY deliverable report available at: [https://projectworkspace.eu/sites/VERIFY/Deliverables/WP4/VERIFY\\_D4.1\\_First%20CH4%20and%20N2O%20fluxes%20from%20anthropogenic%20sources%20from%20BU%20models.pdf](https://projectworkspace.eu/sites/VERIFY/Deliverables/WP4/VERIFY_D4.1_First%20CH4%20and%20N2O%20fluxes%20from%20anthropogenic%20sources%20from%20BU%20models.pdf), 2019, last access June, 2022.



- 2295 Lin, J. C., Gerbig, C., Wofsy, S. C., Andrews, A. E., Daube, B. C., Davis, K. J., and Grainger, C. A.: A near-field tool for simulating the upstream influence of atmospheric observations: The Stochastic Time-Inverted Lagrangian Transport (STILT) model, *J. Geophys. Res.*, 108(D16), 4493, doi:10.1029/2002JD003161, 2003.
- Li, Y., Shang, J., Zhang, C., Zhang, W., Niu, L., Wang, L., Zhang, H.: The role of freshwater eutrophication in greenhouse gas emissions: A review, *Sci. Total Environ.*, 768 (2021), article 144582, [10.1016/j.scitotenv.2020.144582](https://doi.org/10.1016/j.scitotenv.2020.144582), 2021.
- 2300 Lugato, E., Leip, A., Jones, A.: Mitigation potential of soil carbon management overestimated by neglecting N<sub>2</sub>O emissions. *Nat. Clim. Chang.* <https://doi.org/10.1038/s41558-018-0087-z>, 2018.
- Lugato, E., Paniagua, L., Jones, A., De Vries, W., Leip, A.: Complementing the topsoil information of the Land Use/Land Cover Area Frame Survey (LUCAS) with modelled N<sub>2</sub>O emissions. *PLoS One* 12. <https://doi.org/10.1371/journal.pone.0176111>, 2017.
- 2305 Lujala, Päivi; Jan Ketil Rød & Nadja Thieme, 2007. 'Fighting over Oil: Introducing a New Dataset', *Conflict Management and Peace Science*. 24(3): 239–256.
- Maavara, T., Lauerwald, R., Laruelle, G., Akbarzadeh, Z., Bouskill, N., Van Cappellen, P. and Regnier, P.: Nitrous oxide emissions from inland waters: Are IPCC estimates too high?, *Glob. Chang. Biol.*, 25(2), 473–488, doi:10.1111/gcb.14504, 2019.
- 2310 Maavara, T., Lauerwald, R., Regnier, P., & Van Cappellen, P.: Global perturbation of organic carbon cycling by river damming, *Nature Communications*, 8. <https://doi.org/10.1038/ncomms15347>, 2017.
- MacKay, M. D.: A Process-Oriented Small Lake Scheme for Coupled Climate Modeling Applications. *Journal of Hydrometeorology*, 13(6), 1911–1924. <https://doi.org/10.1175/JHM-D-11-0116.1>, 2012.
- Maisonnier et al., in prep.
- 2315 Maksyutov, S., Oda, T., Saito, M., Janardanan, R., Belikov, D., Kaiser, J. W., Zhuravlev, R., Ganshin, A., Valsala, V. K., Andrews, A., Chmura, L., Dlugokencky, E., Haszpra, L., Langenfelds, R. L., Machida, T., Nakazawa, T., Ramonet, M., Sweeney, C., and Worthy, D.: Technical note: A high-resolution inverse modelling technique for estimating surface CO<sub>2</sub> fluxes based on the NIES-TM – FLEXPART coupled transport model and its adjoint, *Atmos. Chem. Phys. Discuss.*, <https://doi.org/10.5194/acp-2020-251>, in review, 2020.
- 2320 Manning, A. J., O'Doherty, S., Jones, A. R., Simmonds, P. G., and Derwent, R. G.: Estimating UK methane and nitrous oxide emissions from 1990 to 2007 using an inversion modeling approach, *J. Geophys. Res.-Atmos.*, 116(D2), doi:10.1029/2010jd014763, 2011.
- McCauley, E., Downing, J. A. and Watson, S.: Sigmoid Relationships between Nutrients and Chlorophyll among Lakes, *Can. J. Fish. Aquat. Sci.*, 46(7), 1171–1175, doi:10.1139/f89-152, 1989.
- 2325 McCauley, E., Downing, J. A., & Watson, S.: Sigmoid relationships between nutrients and chlorophyll among lakes, *Canadian Journal of Fisheries and Aquatic Sciences*, 46, 1171– 1175, 1989.
- McGuire, A. D., Christensen, T. R., Hayes, D., Herault, A., Euskirchen, E., Kimball, J. S., Koven, C., Lafleur, P., Miller, P. A., Oechel, W., Peylin, P., Williams, M., and Yi, Y.: An assessment of the carbon balance of Arctic tundra: comparisons among observations, process models, and atmospheric inversions, *Biogeosciences*, 9, 3185–3204, doi:10.5194/bg-9-3185- 2012, 2012.
- 2330 McNorton, J., Wilson, C., Gloor, M., Parker, R. J., Boesch, H., Feng, W., Hossaini, R., and Chipperfield, M. P.: Attribution of recent increases in atmospheric methane through 3- D inverse modelling, *Atmos. Chem. Phys.*, 18, 18149–18168, <https://doi.org/10.5194/acp-18-18149-2018>, 2018.



- 2335 Meirink, J. F., Bergamaschi, P., and Krol, M. C.: Four-dimensional variational data assimilation for inverse modelling of atmospheric methane emissions: method and comparison with synthesis inversion, *Atmos. Chem. Phys.*, 8, 6341–6353, <https://doi.org/10.5194/acp-8-6341-2008>, 2008.
- Melton, J. R., and Arora, V. K.: Competition between plant functional types in the Canadian Terrestrial Ecosystem Model (CTEM) v. 2.0, *Geoscientific Model Development*, 9, 323–361, doi:10.5194/gmd-9-323-2016, 2016.
- 2340 Menut, L., B. Bessagnet, D. Khvorostyanov, M. Beekmann, N. Blond, A. Colette, I. Coll, G. Curci, G. Foret, A. Hodzic, S. Mailler, F. Meleux, J.-L. Monge, I. Pison, G. Siour, S. Turquety, M. Valari, R. Vautard, and M. G. Vivanco, CHIMERE 2013: a model for regional atmospheric composition modelling, *Geosci. Model Dev.*, 6, 981–1028, doi: 10.5194/gmd-6-30981-2013, 2013.
- Messenger, M. L., Lehner, B., Grill, G., Nedeva, I. and Schmitt, O.: Estimating the volume and age of water stored in global lakes using a geo-statistical approach, *Nat. Commun.*, 7, 13603, doi:10.1038/ncomms13603, 2016.
- 2345 Monks, S. A., Arnold, S. R., Hollaway, M. J., Pope, R. J., Wilson, C., Feng, W., Emmerson, K. M., Kerridge, B. J., Latter, B. L., Miles, G. M., Siddans, R., and Chipperfield, M. P.: The TOMCAT global chemical transport model v1.6: description of chemical mechanism and model evaluation, *Geosci. Model Dev.*, 10, 3025–3057, <https://doi.org/10.5194/gmd-10-3025-2017>, 2017.
- 2350 Near Real Time, EEA 2019 EEA Report, Approximated EU GHG inventory: proxy GHG estimates for 2018, <https://www.eea.europa.eu/publications/approximated-eu-ghg-inventory-proxy>, 2019.
- Nisbet, E.G., Dlugokencky, E.J., Manning, M.R., Lowry, D., Fisher, R.E., France, J.L., Michel, S.E., Miller, J.B., White, J.W.C., Vaughn, B., Bousquet, P., Pyle, J.A., Warwick, N.J., Cain, M., Brownlow, R., Zazzeri, G., Lanoisellé, M., Manning, A.C., Gloor, E., Worthy, D.E.J., Brunke, E.-G., Labuschagne, C., Wolff, E.W. & Ganesan, A.L.: Rising atmospheric methane: 2007–2014 growth and isotopic shift, *Global Biogeochemical Cycles*, 30, 1356–1370, 2016.
- 2355 Niwa, Y., Tomita, H., Satoh, M., Imasu, R., Sawa, Y., Tsuboi, K., Matsueda, H., Machida, T., Sasakawa, M., Belan, B., and Saigusa, N.: A 4D-Var inversion system based on the icosahedral grid model (NICAM-TM 4D-Var v1.0) – Part 1: Offline forward and adjoint transport models, *Geosci. Model Dev.*, 10, 1157–1174, <https://doi.org/10.5194/gmd-10-1157-2017>, 2017a.
- NOAA atmospheric data ([https://www.esrl.noaa.gov/gmd/ccgg/trends\\_ch4/](https://www.esrl.noaa.gov/gmd/ccgg/trends_ch4/), last access June 2020).
- 2360 Olczak, M. and Piebalgs, A.: How far should the new EU Methane Strategy go? [https://cadmus.eui.eu/bitstream/handle/1814/62188/PB\\_2019\\_07\\_FSR\\_Energy.pdf?sequence=1](https://cadmus.eui.eu/bitstream/handle/1814/62188/PB_2019_07_FSR_Energy.pdf?sequence=1), last access September 2020, doi:10.2870/621991, 2019.
- 2365 Olhoff A, Rocha Romero J, Hans F, Kuramochi T, Höhne N, Peters GP, et al.: The impact of COVID-19 and recovery packages on emission pathways to 2030: Inputs to the UNEP Emissions Gap Report 2021 Final project report [Internet]. Copenhagen: Nordisk Ministerråd; 2022. 55 p. (TemaNord). Available from: <http://urn.kb.se/resolve?urn=urn:nbn:se:norden:org:diva-12467>
- Orgiazzi, A., Ballabio, C., Panagos, P., Jones, A., Fernández-Ugalde, O.: LUCAS Soil, the largest expandable soil dataset for Europe: a review. *Eur. J. Soil Sci.*, 2018.
- 2370 Paige, C. C., & Saunders, M. A. (1975). Solution of Sparse Indefinite Systems of Linear Equations. *SIAM Journal on Numerical Analysis*, 12(4), 617–629. <http://www.jstor.org/stable/2156178>
- Pandey, S., Houweling, S., Krol, M., Aben, I., Chevallier, F., Dlugokencky, E. J., Gatti, L. V., Gloor, E., Miller, J. B., Detmers, R., Machida, T., and Röckmann, T.: Inverse modeling of GOSAT-retrieved ratios of total column CH<sub>4</sub> and CO<sub>2</sub> for 2009 and 2010, *Atmos. Chem. Phys.*, 16, 5043–5062, <https://doi.org/10.5194/acp-16-5043-2016>, 2016.
- 2375 Patra, P. K., Saeki, T., Dlugokencky, E. J., Ishijima, K., Umezawa, T., Ito, A., Aoki, S., Morimoto, S., Kort, E. A., Crotwell, A., Ravikumar, K., Nakazawa, T.: Regional methane emission estimation based on observed atmospheric concentrations (2002–2012), *J. Meteorol. Soc. Jpn.*, 94, 91–113, 2016.

- Patra, P. K., Takigawa, M., Watanabe, S., Chandra, N., Ishijima, K., Yamashita, Y.: Improved Chemical Tracer Simulation by MIROC4.0-based Atmospheric Chemistry-Transport Model (MIROC4-ACTM), SOLA, 14, 91-96, 2018.
- 2380 Patra, P. K., E. J. Dlugokencky, J. W. Elkins, G. S. Dutton., Y. Tohjima, M. Sasakawa, A. Ito, R. F. Weiss, M. Manizza, P. B. Krummel, R. G. Prinn, S. O'Doherty, D. Bianchi, C. Nevison, E. Solazzo, H. Lee, S. Joo, E. A. Kort, S. Maity, and M. Takigawa: Forward and inverse modelling of atmospheric nitrous oxide using MIROC4-atmospheric chemistry-transport model. J. Meteor. Soc. Japan, 100, <https://doi.org/10.2151/jmsj.2022-018>, 2022.
- 2385 Pawlewicz, M. J., Steinshouer, D. W., & Gautier, D. L.: Map showing geology, oil and gas fields, and geologic provinces of Europe including Turkey (No. 97-470-I), US Geological Survey, 1997.
- Peters, W., Miller, J. B., Whitaker, J., Denning, A. S., Hirsch, A., Krol, M. C., Zupanski, D., Bruhwiler, L., and Tans, P. P.: An ensemble data assimilation system to estimate CO<sub>2</sub> surface fluxes from atmospheric trace gas observations, J. Geophys. Res., 110, D24304, <https://doi.org/10.1029/2005JD006157>, 2005.
- 2390 Petrescu, A. M. R., Peters, G. P., Janssens-Maenhout, G., Ciais, P., Tubiello, F. N., Grassi, G., Nabuurs, G.-J., Leip, A., Carmona-Garcia, G., Winiwarter, W., Höglund-Isaksson, L., Günther, D., Solazzo, E., Kiesow, A., Bastos, A., Pongratz, J., Nabel, J. E. M. S., Conchedda, G., Pilli, R., Andrew, R. M., Schelhaas, M.-J., and Dolman, A. J.: European anthropogenic AFOLU greenhouse gas emissions: a review and benchmark data, Earth Syst. Sci. Data, 12, 961–1001, <https://doi.org/10.5194/essd-12-961-2020>, 2020.
- 2395 Petrescu, A. M. R., Qiu, C., Ciais, P., Thompson, R. L., Peylin, P., McGrath, M. J., Solazzo, E., Janssens-Maenhout, G., Tubiello, F. N., Bergamaschi, P., Brunner, D., Peters, G. P., Höglund-Isaksson, L., Regnier, P., Lauerwald, R., Bastviken, D., Tsuruta, A., Winiwarter, W., Patra, P. K., Kuhnert, M., Oreggioni, G. D., Crippa, M., Saunio, M., Perugini, L., Markkanen, T., Aalto, T., Groot Zwaftink, C. D., Tian, H., Yao, Y., Wilson, C., Conchedda, G., Günther, D., Leip, A., Smith, P., Haussaire, J.-M., Leppänen, A., Manning, A. J., McNorton, J., Brockmann, P., and Dolman, A. J.: The consolidated European synthesis of CH<sub>4</sub> and N<sub>2</sub>O emissions for the European Union and United Kingdom: 1990–2017, Earth Syst. Sci. Data, 13, 2307–2362, <https://doi.org/10.5194/essd-13-2307-2021>, 2021a.
- 2400 Petrescu, A. M. R., McGrath, M. J., Andrew, R. M., Peylin, P., Peters, G. P., Ciais, P., Broquet, G., Tubiello, F. N., Gerbig, C., Pongratz, J., Janssens-Maenhout, G., Grassi, G., Nabuurs, G.-J., Regnier, P., Lauerwald, R., Kuhnert, M., Balkovič, J., Schelhaas, M.-J., Denier van der Gon, H. A. C., Solazzo, E., Qiu, C., Pilli, R., Konovalov, I. B., Houghton, R. A., Günther, D., Perugini, L., Crippa, M., Ganzenmüller, R., Luijkx, I. T., Smith, P., Munassar, S., Thompson, R. L., Conchedda, G., Monteil, G., Scholze, M., Karstens, U., Brockmann, P., and Dolman, A. J.: The consolidated European synthesis of CO<sub>2</sub> emissions and removals for the European Union and United Kingdom: 1990–2018, Earth Syst. Sci. Data, 13, 2363–2406, <https://doi.org/10.5194/essd-13-2363-2021>, 2021b.
- 2410 Petrescu, A. M. R., Qiu, C., McGrath, M. J., Peylin, P., Peters, G. P., Ciais, P., Thompson, R. L., Tsuruta, A., Brunner, D., Kuhnert, M., Matthews, B., Palmer, P.I., Tarasova, O., Regnier, P., Lauerwald, R., Bastviken, D., Höglund-Isaksson, L., Winiwarter, W., Etiope, G., Aalto, T., Balsamo, G., Bastrikov, V., Berchet, A., Brockmann, P., Ciotoli, G., Conchedda, G., Crippa, M., Dentener, F., Groot Zwaftink, C. D., Guizzardi, D., Günther, D., Haussaire, J.-M., Houweling, S., Janssens-Maenhout, G., Kouyate, M., Leip, A., Leppänen, A., Lugato, E., Maisonnier, M., Manning A. J., Markkanen, T., McNorton, J., Muntean, M., Orregioni, G. D., Patra, P. K., Perugini, L., Pison, I., Raivonen, M.
- 2415 T., Saunio, M., Segers, A. J., Smith, P., Solazzo, E., Tian, H., Tubiello, F. N., Vesala, T., Wilson, C., Zaehle, S.: The consolidated European synthesis of CH<sub>4</sub> and N<sub>2</sub>O emissions for EU27 and UK: 1990–2020, version 2, Zenodo, <https://doi.org/10.5281/zenodo.7553800>, 2023.
- Pisso, I., Sollum, E., Grythe, H., Kristiansen, N., Cassiani, M., Eckhardt, S., Arnold, D., Morton, D., Thompson, R. L., Groot Zwaftink, C. D., Evangeliou, N., Sodemann, H., Haimberger, L., Henne, S., Brunner, D., Burkhart, J. F., Fouilloux, A., Brioude, J., Philipp, A., Seibert, P., and Stohl, A.: The Lagrangian particle dispersion model FLEXPART version 10.3, Geosci. Model Dev., 12, 4955–499, 2019.
- 2420

- Poulter, B., Bousquet, P., Canadell, J. G., Ciais, P., Peregon, A., Saunois, M., Arora, V. K., Beerling, D. J., Brovkin, V., Jones, C. D., Joos, F., Gedney, N., Ito, A., Kleinen, T., Koven, C. D., McDonald, K., Melton, J. R., Peng, C., Prigent, C., Schroeder, R., Riley, W. J., Saito, M., Spahni, R., Tian, H., Taylor, L., Viovy, N., Wilton, D., Wiltshire, A., Xu, X., Zhang, B., Zhang, Z., and Zhu, Q.: Global wetland contribution to 2000–2012 atmospheric methane growth rate dynamics, *Environ. Res. Lett.*, 12, 094013, <https://doi.org/10.1088/1748-9326/aa8391>, 2017.
- 2425 Quemada, M., Lassaletta, L., Leip, A., Jones, A., Lugato, E.: Integrated management for sustainable cropping systems: looking beyond the greenhouse balance at the field scale. *Glob. Chang. Biol.* gcb.14989, 2020.
- Raivonen, M., Smolander, S., Backman, L., Susiluoto, J., Aalto, T., Markkanen, T., Mäkelä, J., Rinne, J., Peltola, O., Aurela, M., Tomasic, M., Li, X., Larmola, T., Juutinen, S., Tuittila, E.-S., Heimann, M., Sevanto, S., Kleinen, T., Brovkin, V., and Vesala, T.: HIMMELI v1.0: Helsinki Model of Methane build-up and emission for peatlands, *Geosci. Model Devel.*, 10, 4665–4691, 2017.
- 2430 Rayner, P. J., Enting, I. G., Francey, R. J., and Langenfelds, R.: Reconstructing the recent carbon cycle from atmospheric CO<sub>2</sub>, δ<sup>13</sup>C and O<sub>2</sub>/N<sub>2</sub> observations, *Tellus B*, 51, 213–232, 1999.
- 2435 Regulation (EU) 2018/1999 (European Climate Law) amended proposal for a regulation of the European parliament and of the council on establishing the framework for achieving climate neutrality [https://ec.europa.eu/clima/sites/clima/files/eu-climate-action/docs/prop\\_reg\\_ecl\\_en.pdf](https://ec.europa.eu/clima/sites/clima/files/eu-climate-action/docs/prop_reg_ecl_en.pdf), last access October 2020.
- Regulation (EU) 525/2013 of the European Parliament and of the Council, <https://eur-lex.europa.eu/legal-content/EN/TXT/PDF/?uri=CELEX:32013R0525&from=EN>, last access November 2020.
- 2440 Reick, C., Raddatz, T., Brovkin, V. & Gayler, V.: Representation of natural and anthropogenic land cover change in MPI-ESM. *Journal of Advances in Modeling Earth Systems*, 5, 459–482, <https://doi.org/10.1002/jame.20022>, 2013.
- Riley, W. J., Subin, Z. M., Lawrence, D. M., Swenson, S. C., Torn, M. S., Meng, L., Mahowald, N. M., and Hess, P.: Barriers to predicting changes in global terrestrial methane fluxes: analyses using CLM4Me, a methane biogeochemistry model integrated in CESM, *Biogeosciences*, 8, 1925–1953, doi:10.5194/bg-8-1925-2011, 2011.
- 2445 Ringeval, B., Friedlingstein, P., Koven, C., Ciais, P., de Noblet-Ducoudre, N., Decharme, B., and Cadule, P.: Climate-CH<sub>4</sub> feedback from wetlands and its interaction with the climate-CO<sub>2</sub> feedback, *Biogeosciences*, 8, 2137–2157, doi:10.5194/bg-8-2137-2011, 2011.
- Rinta, P., Bastviken, D., Schilder, J., Van Hardenbroek, M., Stotter, T., and Heiri, O.: Higher late summer methane emission from central than northern European lakes. *J. Limnol.* 76, 52–67. doi: 10.4081/jlimnol.2016.1475, 2017.
- 2450 Rodgers, C. D.: *Inverse Methods for Atmospheric Sounding: Theory and Practice*, Series on Atmospheric, Oceanic and Planetary Physics – Vol. 2, World Scientific Publishing Co. Pte. Ltd., Singapore, <https://doi.org/10.1142/3171>, 2000.
- Rosentreter, J.A., Borges, A.V., Deemer, B.R. et al. Half of global methane emissions come from highly variable aquatic ecosystem sources. *Nat. Geosci.* 14, 225–230 (2021). <https://doi.org/10.1038/s41561-021-00715-2>
- 2455 Rödenbeck, C., C. Gerbig, K. Trusilova, and M. Heimann, A two-step scheme for high-resolution regional atmospheric trace gas inversions based on independent models, *Atmos. Chem. Phys.*, 9, 5331–5342, doi: 10.5194/acp-9-5331-2009, 2009.
- Rödenbeck, C., Estimating CO<sub>2</sub> sources and sinks from atmospheric mixing ratio measurements using a global inversion of atmospheric transport, Tech. Rep. 6, Max-Planck-Institut für Biogeochemie, Jena, [http://www.bgcjena.mpg.de/mpg/website/Biogeochemie/Publikationen/TechnicalReports/tech\\_report6.pdf](http://www.bgcjena.mpg.de/mpg/website/Biogeochemie/Publikationen/TechnicalReports/tech_report6.pdf), [http://www.bgcjena.mpg.de/uploads/Publications/TechnicalReports/tech\\_report6.pdf](http://www.bgcjena.mpg.de/uploads/Publications/TechnicalReports/tech_report6.pdf), 2005.
- 2460 Rödenbeck, C., Houweling, S., Gloor, M., and Heimann, M.: CO<sub>2</sub> flux history 1982–2001 inferred from atmospheric data using a global inversion of atmospheric transport, *Atmos. Chem. Phys.*, 3, 1919–1964, <https://doi.org/10.5194/acp-3-1919-2003>, 2003.

- 2465 Rutherford JS, Sherwin ED, Ravikumar AP, Heath GA, Englander J, Cooley D, Lyon D, Omara M, Langfitt Q, Brandt AR. 2021. Closing the methane gap in US oil and natural gas production emissions inventories. *Nature Communications* 12:4715.
- 2470 Saunio, M., Stavert, A. R., Poulter, B., Bousquet, P., Canadell, J. G., Jackson, R. B., Raymond, P. A., Dlugokencky, E. J., Houweling, S., Patra, P. K., Ciais, P., Arora, V. K., Bastviken, D., Bergamaschi, P., Blake, D. R., Brailsford, G., Bruhwiler, L., Carlson, K. M., Carrol, M., Castaldi, S., Chandra, N., Crevoisier, C., Crill, P. M., Covey, K., Curry, C. L., Etiope, G., Frankenberg, C., Gedney, N., Hegglin, M. I., Höglund-Isaksson, L., Hugelius, G., Ishizawa, M., Ito, A., Janssens-Maenhout, G., Jensen, K. M., Joos, F., Kleinen, T., Krummel, P. B., Langenfelds, R. L., Laruelle, G. G.,
- 2475 Liu, L., Machida, T., Maksyutov, S., McDonald, K. C., McNorton, J., Miller, P. A., Melton, J. R., Morino, I., Müller, J., Murguía-Flores, F., Naik, V., Niwa, Y., Noce, S., O'Doherty, S., Parker, R. J., Peng, C., Peng, S., Peters, G. P., Prigent, C., Prinn, R., Ramonet, M., Regnier, P., Riley, W. J., Rosentreter, J. A., Segers, A., Simpson, I. J., Shi, H., Smith, S. J., Steele, L. P., Thornton, B. F., Tian, H., Tohjima, Y., Tubiello, F. N., Tsuruta, A., Viovy, N., Voulgarakis, A., Weber, T. S., van Weele, M., van der Werf, G. R., Weiss, R. F., Worthy, D., Wunch, D., Yin, Y., Yoshida, Y.,
- 2480 Zhang, W., Zhang, Z., Zhao, Y., Zheng, B., Zhu, Q., Zhu, Q., and Zhuang, Q.: The Global Methane Budget 2000–2017, *Earth Syst. Sci. Data*, 12, 1561–1623, <https://doi.org/10.5194/essd-12-1561-2020>, 2020.
- Segers, .: Validation of the CH<sub>4</sub> surface flux inversion - reanalysis 1990-2019, [Document Title \(copernicus.eu\)](https://www.copernicus.eu/publications/document/titles/camsw73_2018sc2_d73.2.4.1-2019_202012_validation_ch4_1990-2019_v2), CAMS73\_2018SC2\_D73.2.4.1-2019\_202012\_validation\_CH4\_1990-2019\_v2, 2020, last access: June 2022.
- Segers, A. and Houweling, S.: Description of the CH<sub>4</sub> Inversion Production Chain, CAMS (Copernicus Atmospheric Monitoring Service) Report, available at: [https://atmosphere.copernicus.eu/sites/default/files/2018-11/CAMS73\\_2015SC3\\_D73.2.5.5-2018\\_201811\\_production\\_chain\\_v1\\_0.pdf](https://atmosphere.copernicus.eu/sites/default/files/2018-11/CAMS73_2015SC3_D73.2.5.5-2018_201811_production_chain_v1_0.pdf), 2018, last access: March 2020.
- Seibert, P. and Frank, A.: Source-receptor matrix calculation with a Lagrangian particle dispersion model in backward mode, *Atmos. Chem. Phys.*, 4, 51–63, <https://doi.org/10.5194/acp-4-51-2004>, 2004.
- 2490 Silpa, K., Yao, L. C., Bhada-Tata, P., Van Woerden, F.: What a Waste 2.0 : A Global Snapshot of Solid Waste Management to 2050. Urban Development;. Washington, DC: World Bank. © World Bank. <https://openknowledge.worldbank.org/handle/10986/30317> License: CC BY 3.0 IGO, 2018.
- Simpson, D., Winiwarter, W., Borjesson, G., Cinderby, S., Ferreira, A., Guenther, A., Nicjolas Hewitt, C., Janson, R., Aslam, M., Khalil, K., Owen, S., Pierce, T.E., Puxbaum, H., Shearer, M., Skiba, U., Steinbrecher, R., Tarrason, L., Oquist, M.G.: Inventorying emissions from nature in Europe. *J. Geoph. Res.* 104 (D7), 8113-8152, 1999.
- 2495 Smith, J.U., Bradbury, N.J., Addiscott, T.M.: SUNDIAL: A PC-based system for simulating nitrogen dynamics in arable land. *Agron J* 88:38-43,1996.
- Smith, J.U., Gottschalk, P., Bellarby, J., Chapman, S., Lilly, A., Towers, W., Bell, J., Coleman, K., Nayak, D.R., Richards, M.I., Hillier, J., Flynn, H.C., Wattenbach, M., Aitkenhead, M., Yeluripurti, J.B., Farmer, J., Milne, R., Thomson, A., Evans, C., Whitmore, A.P., Falloon, P. & Smith, P.: Estimating changes in national soil carbon stocks using ECOSSE – a new model that includes upland organic soils. Part I. Model description and uncertainty in national scale simulations of Scotland. *Climate Research* 45, 179-192. doi: 10.3354/cr00899, 2010a..
- 2500 Smith, J.U., Gottschalk, P., Bellarby, J., Chapman, S., Lilly, A., Towers, W., Bell, J., Coleman, K., Nayak, D.R., Richards, M.I., Hillier, J., Flynn, H.C., Wattenbach, M., Aitkenhead, M., Yeluripurti, J.B., Farmer, J., Milne, R., Thomson, A., Evans, C., Whitmore, A.P., Falloon, P. & Smith, P. Estimating changes in national soil carbon stocks using ECOSSE – a new model that includes upland organic soils. Part II. Application in Scotland. *Climate Research* 45, 193-205. doi: 10.3354/cr00902, 2010b.
- 2505 Solazzo, E., Crippa, M., Guizzardi, D., Muntean, M., Choulga, M., and Janssens-Maenhout, G.: Uncertainties in the Emissions Database for Global Atmospheric Research (EDGAR) emission inventory of greenhouse gases. *Atmos.Chem. Phys.*, <https://doi.org/10.5194/acp-21-1-2021>, 2021.

- 2510 Spahni, R., Wania, R., Neef, L., van Weele, M., Pison, I., Bousquet, P., Frankenberg, C., Foster, P. N., Joos, F., Prentice, I. C., and van Velthoven, P.: Constraining global methane emissions and uptake by ecosystems, *Biogeosciences*, 8, 1643–1665, <https://doi.org/10.5194/bg-8-1643-2011>, 2011.
- Spahni, R., Wania, R., Neef, L., van Weele, M., Pison, I., Bousquet, P., Frankenberg, C., Foster, P. N., Joos, F., Prentice, I. C., and van Velthoven, P.: Constraining global methane emissions and uptake by ecosystems, *Biogeosciences*, 8, 1643–1665, <https://doi.org/10.5194/bg-8-1643-2011>, 2011.
- 2515 Stanley, E. H., N. J. Casson, S. T. Christel, J. T. Crawford, L. C. Loken, and S. K. Oliver: The ecology of methane in streams and rivers: Patterns, controls, and global significance, *Ecol. Monogr.*, 86, 146–171, 2016.
- Stocker, B. D., Spahni, R. and Joos, F.: DYPTOP: a cost-efficient TOPMODEL implementation to simulate sub-grid spatio-temporal dynamics of global wetlands and peatlands, *Geosci. Model Dev.*, 7(6), 3089–3110, doi:10.5194/gmd-7-3089-2014, 2014.
- 2520 Stohl, A., Forster, C., Frank, A., Seibert, P., and Wotawa, G.: Technical note: The Lagrangian particle dispersion model FLEXPART version 6.2, *Atmos. Chem. Phys.*, 5, 2461–2474, doi:10.5194/acp-5-2461-2005, 2005.
- Susiluoto, J., Raivonen, M., Backman, L., Laine, M., Mäkelä, J., Peltola, O., Vesala, T., and Aalto, T.: Calibrating a wetland methane emission model with hierarchical modeling and adaptive MCMC, *Geosci. Model Dev.*, 11, 1199–1228, <https://doi.org/10.5194/gmd-11-1199-2018>, 2018.
- 2525 Szénási, B., Berchet, A., Broquet, G., Segers, A., Gon, H. D. van der, Krol, M., Hullegie, J. J. S., Kiesow, A., Günther, D., Petrescu, A. M. R., Saunio, M., Bousquet, P., and Pison, I.: A pragmatic protocol for characterising errors in atmospheric inversions of methane emissions over Europe, *Tellus B Chem Phys Meteorology*, 73, 1–23, <https://doi.org/10.1080/16000889.2021.1914989>, 2021.
- 2530 Thompson, R. L. and Stohl, A.: FLEXINVERT: an atmospheric Bayesian inversion framework for determining surface fluxes of trace species using an optimized grid, *Geosci. Model Devel.*, 7, 2223–2242, doi:10.5194/gmd-7-2223-2014, 2014.
- Thompson, R. L., Nisbet, E. G., Pisso, I., Stohl, A., Blake, D., Dlugokencky, E. J., Helmig, D. & White, J. W. C. Variability in Atmospheric Methane From Fossil Fuel and Microbial Sources Over the Last Three Decades. *Geophys. Res. Lett.* 112, D04306–10. (doi:10.1029/2018GL078127), 2018.
- 2535 Thompson, R.L., Lassaletta, L., Patra, P.K., Wilson, C., Wells, K. C., Gressent, A., Koffi, E. N., Chipperfield, M. P., Winiwarter, W., Davidson, E. A., Tian, H. & Canadell, J. G. : Acceleration of global N<sub>2</sub>O emissions seen from two decades of atmospheric inversion. *Nat. Clim. Chang.* 9, 993–998, <https://doi.org/10.1038/s41558-019-0613-7>, 2019.
- Thompson R. L., Groot Zwaafink, C.D., Brunner, D., A. Tsuruta, A., Aalto, T., Raivonen, M., Crippa, M., Solazzo, E., Guizzardi, D., Regnier, P. and Maisonnier, M: Effects of extreme meteorological conditions in 2018 on European methane emissions estimated using atmospheric inversions, *Phil. Trans. R. Soc. A380*: 20200443. <https://doi.org/10.1098/rsta.2020.0443>, 2021.
- 2540 Thornton B.F., Etiope G., Schwietzke S., Milkov A.V., Klusman R.W., Judd A., Oehler D.Z.: Conflicting estimates of natural geologic methane emissions. *Elem. Sci. Anth.*, 9, 1, doi:<https://doi.org/10.1525/elementa.2021.00031>, 2021.
- Tian, H., Chen, G., Lu, C., Xu, X., Ren, W., Zhang, B., Banger, K., Tao, B., Pan, S., Liu, M., Zhang, C., Bruhwiler, L., and Wofsy, S.: Global methane and nitrous oxide emissions from terrestrial ecosystems 3735 due to multiple environmental changes, *Ecosystem Health and Sustainability*, 1, 1–20, doi:10.1890/ehs14-0015.1, 2015.
- 2550 Tian, H., Xu, R., Canadell, J. G., Thompson, R. L., Winiwarter, W., Suntharalingam, P., Davidson, E. A., Ciais, P., Jackson, R. B., Janssens-Maenhout, G., Prather, M. J., Regnier, P., Pan, N., Pan, S., Peters, G. P., Shi, H., Tubiello, F. N., Zaehle, S., Zhou, F., Arneth, A., Battaglia, G., Berthet, S., Bopp, L., Bouwman, A. F., Buitenhuis, E. T.; Chang, J., Chipperfield, M. P., Dangal, S. R. S., Dlugokencky, E., Elkins, J. W., Eyre, B. D., Fu, B., Hall, B. D., Ito, A., Joos,

- 2555 F., Krummel, P. B., Landolfi, A., Laruelle, G. G., Lauerwald, R., Li, W., Lienert, S., Maavara, T., Macleod, M., Millet, D. B., Olin, S., Patra, P. K., Prinn, R. G., Raymond, P. A., Ruiz, D. J., van der Werf, G. R., Vuichard, N., Wang, J., Weiss, R. F., Wells, K. C., Wilson, C., Yang, J., Yao, Y.: A comprehensive quantification of global nitrous oxide sources and sinks, *Nature*, vol. 586, 248–256, doi: 10.1038/s41586-020-2780-0, 2020.
- 2560 Tian, H., Xu, X., Liu, M., Ren, W., Zhang, C., Chen, G., and Lu, C.: Spatial and temporal patterns of CH<sub>4</sub> and N<sub>2</sub>O fluxes in terrestrial ecosystems of North America during 1979–2008: application of a global biogeochemistry model, *Biogeosciences*, 7, 2673–2694, doi:10.5194/bg-7-2673-2010, 2010.
- 2565 Tian, H., Yang, J., Xu, R., Lu, C., Canadell, J. G., Davidson, E. A., Jackson, R. B., Arneeth, A., Chang, J., Ciais, P., Gerber, S., Ito, A., Joos, F., Lienert, S., Messina, P., Olin, S., Pan, S., Peng, C., Saikawa, E., Thompson, R. L., Vuichard, N., Winiwarter, W., Zaehle, S., and Zhang, B.: Global soil nitrous oxide emissions since the preindustrial era estimated by an ensemble of terrestrial biosphere models: Magnitude, attribution, and uncertainty, *Glob. Change Biol.*, 25, 640–659, <https://doi.org/10.1111/gcb.14514>, 2019. Yuanzhi Yao<sup>1</sup>, Hanqin Tian, Hao Shi, Shufen Pan, Rongting Xu, Naiqing Pan and Josep G. Canadell: Increased global nitrous oxide emissions from streams and rivers in the Anthropocene, *Nat. Climate Change*, <https://doi.org/10.1038/s41558-019-0665-8>, 2020.
- 2570 Tizzard, L. H.: The Contribution to atmospheric methane from sub-seabed sources in the UK continental shelf, PhD thesis, University of Newcastle upon Tyne, <https://ethos.bl.uk/OrderDetails.do?uin=uk.bl.ethos.445613>, 2008
- 2575 Trusilova, K., Rödenbeck C., Gerbig C., and Heimann M.: Technical note: A new coupled system for global-to-regional downscaling of CO<sub>2</sub> concentration estimation, *Atmos. Chem. Phys.*, 10, 3205–3213, 2010.
- 2580 Tsuruta, A., Aalto, T., Backman, L., Hakkarainen, J., Laan-Luijckx, I. T. van der, Krol, M. C., Spahni, R., Houweling, S., Laine, M., Dlugokencky, E., Gomez-Pelaez, A. J., Schoot, M. van der, Langenfelds, R., Ellul, R., Arduini, J., Apadula, F., Gerbig, C., Feist, D. G., Kivi, R., Yoshida, Y. and Peters, W.: Global methane emission estimates for 2000–2012 from CarbonTracker Europe-CH<sub>4</sub> v1.0, *Geoscientific Model Development*, 10(3), 1261–1289, doi:doi:10.5194/gmd-10-1261-2017, 2017.
- 2585 Tsuruta, A., Aalto, T., Backman, L., Hakkarainen, J., van der Laan-Luijckx, I. T., Krol, M. C., Spahni, R., Houweling, S., Laine, M., Dlugokencky, E., Gomez-Pelaez, A. J., van der Schoot, M., Langenfelds, R., Ellul, R., Arduini, J., Apadula, F., Gerbig, C., Feist, D. G., Kivi, R., Yoshida, Y., and Peters, W.: Global methane emission estimates for 2000–2012 from CarbonTracker Europe-CH<sub>4</sub> v1.0, *Geosci. Model Dev.*, 10, 1261–1289, <https://doi.org/10.5194/gmd-10-1261-2017>, 2017.
- 2590 Tubiello, F. N., Salvatore, M., Rossi, S., Ferrara, A., Fitton, N., and Smith, P.: The FAOSTAT database of greenhouse gas emissions from agriculture, *Environ. Res. Lett.*, 8, 015009, <https://doi.org/10.1088/1748-3268/8/1/015009>, 2013.
- 2595 Tubiello, F. N.: Greenhouse Gas Emissions Due to Agriculture, *Enc. Food Security and Sustain.*, 1, 196–205, <https://doi.org/10.1016/B978-0-08-100596-5.21996-3>, 2019.
- UNFCCC UK NIR: <https://unfccc.int/documents/273439>
- 2590 UNEP United Nations Environment Programme (2021). Emissions Gap Report 2021, <https://www.unep.org/resources/emissions-gap-report-2021>, 2021, 2019, last access July 2022.
- 2595 UNFCCC Decision 24/CP.19 of the UNFCCC Conference of the Parties (COP). Revision of the UNFCCC reporting guidelines on annual inventories for Parties included in Annex I to the Convention. FCCC/CP/2013/10/Add.3, <https://unfccc.int/process-and-meetings/transparency-and-reporting/reporting-and-review-under-the-convention/greenhouse-gas-inventories-annex-i-parties/reporting-requirements>, 2014.
- UNFCCC: Kyoto Climate Change Decision, available at: <https://unfccc.int/process-and-meetings/conferences/past-conferences/kyoto-climate-change-conference-december-1997/decisions-kyoto-climate-change-conference-december-1997> (last access: October 2020), 1997.



- 2600 UNFCCC NGHGI 2022 NIR reports: UNFCCC: National Inventory Submissions 2022, available at: <https://unfccc.int/ghg-inventories-annex-i-parties/2022>, last access: May 2022, 2022.
- UNFCCC NGHGI 2021 CRFs: <https://unfccc.int/ghg-inventories-annex-i-parties/2021>, last access March 2022, 2022.
- 2605 van der Werf, G. R., Randerson, J. T., Giglio, L., van Leeuwen, T. T., Chen, Y., Rogers, B. M., Mu, M., van Marle, M. J. E., Morton, D. C., Collatz, G. J., Yokelson, R. J., and Kasibhatla, P. S.: Global fire emissions estimates during 1997–2016, *Earth Syst. Sci. Data*, 9, 697–720, <https://doi.org/10.5194/essd-9-697-2017>, 2017.
- VERIFY <http://webportals.ipsl.jussieu.fr/VERIFY/FactSheets/>
- 2610 Vermeulen, A. T., Eisma, R., Hensen, A., and Slanina, J.: Transport model calculations of NW-European methane emissions, *Environ. Sci. Policy*, 2, 315–324, 1999.
- 2615 Vermeulen, A. T., Pieterse, G., Hensen, A., van den Bulk, W. C. M., and Erisman, J. W.: COMET: a Lagrangian transport model for greenhouse gas emission estimation – forward model technique and performance for methane, *Atmos. Chem. Phys. Discuss.*, 6, 8727–8779, <https://doi.org/10.5194/acpd-6-8727-2006>, 2006.
- 2620 Wang, X., Jacob, D. J., Eastham, S. D., Sulprizio, M. P., Zhu, L., Chen, Q., Alexander, B., Sherwen, T., Evans, M. J., Lee, B. H., Haskins, J. D., Lopez-Hilfiker, F. D., Thornton, J. A., Huey, G. L., and Liao, H.: The role of chlorine in global tropospheric chemistry, *Atmos. Chem. Phys.*, 19, 3981–4003, <https://doi.org/10.5194/acp-19-3981-2019>, 2019b.
- Watanabe, S., H. Miura, M. Sekiguchi, T. Nagashima, K. Sudo, S. Emori, and M. Kawamiya, Development of an atmospheric general circulation model for integrated Earth system modeling on the Earth Simulator, *J. Earth Simulator*, 9, 27–35, 2008.
- 2625 Weber, T., Wiseman, N.A. & Kock, A.: Global ocean methane emissions dominated by shallow coastal waters, *Nat Commun* 10, 4584, <https://doi.org/10.1038/s41467-019-12541-7>, 2019.
- Weiss, F. and Leip, A.: Greenhouse gas emissions from the EU livestock sector: A life cycle assessment carried out with the CAPRI model, *Agriculture, Ecosyst. Environ.*, 149, 124–134, 2012.
- 2630 Wilson, C., Chipperfeld, M. P., Gloor, M. & Chevallier, F.: Development of a variational flux inversion system (INVICAT v1.0) using the TOMCAT chemical transport model. *Geosci. Model Dev.* 7, 2485–2500, 2014.
- Winiwarter, W., Höglund-Isaksson, L., Klimont, Z., Schöpp, W., and Amann, M.: Technical opportunities to reduce global anthropogenic emissions of nitrous oxide, *Environ. Res. Lett.*, 13, 014011, <https://doi.org/10.1088/1748-9326/aa9ec9>, 2018.
- 2635 WMO: United in Science Report, available at: <https://public.wmo.int/en/our-mandate/climate/wmo-statement-state-of-global-climate> (last access: January 2022), 2021.
- Yin, Y., Chevallier, F., Frankenberg, C., Ciais, P., Bousuquet, P., Saunois, M., Zheng, B., Worden, J. R., Bloom, A. A., Parker, R., Jacob, D. J., and Dlugokencky, E. J.: Sources from tropical wetlands and China accelerate methane growth rate since 2010, submitted to PNAS, 2019.
- 2640 Zaehle, S., Ciais, P., Friend, A. D., and Prieur, V.: Carbon benefits of anthropogenic reactive nitrogen offset by nitrous oxide emissions, *Nature*, 4, 601–605, 2011.
- Zhang, Z., Zimmermann, N. E., Kaplan, J. O., and Poulter, B.: Modeling spatiotemporal dynamics of global wetlands: comprehensive evaluation of a new sub-grid TOPMODEL parameterization and uncertainties, *Biogeosciences*, 13, 1387–1408, <https://doi.org/10.5194/bg-13-1387-2016>, 2016b.

- 2645 Zheng, B., Chevallier, F., Ciais, P., Yin, Y., and Wang, Y.: On the role of the flaming to smoldering transition in the seasonal cycle of African fire emissions, *Geophys. Res. Lett.*, doi: 10.1029/2018GL079092, 2018a.
- Zheng, B., Chevallier, F., Ciais, P., Yin, Y., Deeter, M., Worden, H., Wang, Y. L., Zhang, Q., and He, K. B.: Rapid decline in carbon monoxide emissions and export from East Asia between years 2005 and 2016, *Environ. Res. Lett.*, 13, 044007, doi: 10.1088/1748-9326/aab2b3, 2018b.
- 2650 Zhu, Q., Liu, J., Peng, C., Chen, H., Fang, X., Jiang, H., Yang, G., Zhu, D., Wang, W., and Zhou, X.: Modelling methane emissions from natural wetlands by development and application of the TRIPLEXGHG model, *Geoscientific Model Development*, 7, 981-999, doi:10.5194/gmd-7-981-2014, 2014.
- Zhu, Q., Peng, C., Chen, H., Fang, X., Liu, J., Jiang, H., Yang, Y., and Yang, G.: Estimating global natural wetland methane emissions using process modelling: spatio-temporal patterns and contributions to atmospheric methane fluctuations, *Global Ecology and Biogeography*, 24, 959-972, 2015.
- 2655 Zhuang, Q., J. M. Melillo, D. W. Kicklighter, R. G. Prinn, D. A. McGuire, P. A. Steudler, B. S. Felzer, S. Hu.: Methane fluxes between terrestrial ecosystems and the atmosphere at northern high latitudes during the past century: A retrospective analysis with a process-based biogeochemistry model, *Global Biogeochemical Cycles*, 18, GB3010, doi:10.1029/2004GB002239, 2004.